Dissertation
submitted to the
Combined Faculty for the Natural Sciences and Mathematics
of the Ruperto Carola University Heidelberg, Germany
for the degree of
Doctor of Natural Sciences

Presented by
M. Sc. Clara Becker
born in: Heidelberg
Oral examination: 22.11.2019

Mechanisms of growth control in the postembryonic medaka retina

Referees: Prof. Dr. Joachim Wittbrodt
Prof. Dr. Jan Lohmann

Abstract

Postembryonic stem cell niches are present throughout the vertebrate clade to facilitate development, homeostasis, regeneration and growth. While teleosts and amphibians display sustained stem cell activity in most organs after embryogenesis, higher vertebrates retain stem cell activity only in specific tissues. Despite these differences, similar challenges are imposed on all vertebrate organisms: new tissue has to be generated to expand or replace existent one while simultaneously ensuring integrity and functionality of the organ. Tight control of stem and progenitor cell proliferation is necessary to avoid aberrant growth such as in cancer. In the retina of the teleost medaka (*Oryzias latipes)*, retinal stem (RSC) and progenitor (RPC) cells are located in the ciliary marginal zone (CMZ) and mediate postembryonic growth and neurogenesis. Since function and shape of the eye are intimately linked, the activity of RSCs and RPCs is tightly coordinated to establish proper cell type composition and number. In this thesis I addressed intrinsic and extrinsic regulation mechanisms of the RSC niche. I hypothesised that retinal growth underlies intrinsically active growth factor signaling, and that immune cells safeguard the RSC niche in homeostasis and injury.

To analyse intrinsic regulation of RSC proliferation, I assessed the function of insulin-like growth factor (Igf) signaling in the CMZ using gain- and loss-of-function approaches. I found that Igf1 receptor over-activation increased cell cycle speed, RPC number and consequently retinal size, while simultaneously preserving the stereotypical retinal architecture. Strikingly, RSCs were not susceptible to mitogenic stimuli, indicating that RPC amplification is the determinant of retinal size and composition. To understand the extrinsic regulation of the RSC niche, I examined the interplay of immune cells and RSCs. I found that Ccl25b-positive RSCs are phagocytosed by Ccr9a-positive immune cells located in the CMZ. *Ccl25b* mutation abrogates reactivation of immune cells upon RSC injury, implicating Ccl25b–Ccr9a signaling in the immune–stem cell interaction during homeostatic surveillance and injury response.

In summary, my results propose that accurate postembryonic growth and tissue integrity depend on both cell intrinsic and extrinsic mechanisms of growth control in the RSC niche of medaka.

Zusammenfassung

Postembryonale Stammzellnischen sind in der ganzen Wirbeltierklade vorhanden um Entwicklung, Homöostase, Regeneration und Wachstum zu ermöglichen. Während Knochenfische und Amphibien nach der Embryogenese durchgehend weiterwachsen, wird die Stammzellaktivität in höheren Wirbeltieren nur in speziellen Geweben erhalten. Trotz dieser Unterschiede stehen alle Wirbeltiere vor ähnlichen Herausforderungen: neues Gewebe für Wachstum oder Ersatz von vorhandenem Gewebe muss gebildet werden während zeitgleich die Intaktheit und Funktionalität des Organs sichergestellt werden muss. Um abnormales Wachstum wie Krebs zu vermeiden muss die Zellteilung von Stamm- und Vorläuferzellen deshalb strikter Kontrolle unterliegen. In der Netzhaut des Knochenfischs Medaka (*Oryzias latipes*) befinden sich Stamm- und -vorläuferzellen in der ziliären Randzone, die postembryonales Wachstum und Neurogenese ausführen. Die Stamm- und Vorläuferzellaktivität ist streng koordiniert um die richtige Anzahl und Zusammensetzung der Zelltypen zu erhalten, da die Funktion mit der Form des Auges einhergeht. In dieser Doktorarbeit habe ich mich mit intrinsischen und extrinsischen Regulierungsmechanismen der Netzhautstammzellnische befasst. Ich stellte folgende Hypothesen auf: Intrinsisch aktive Wachstumsfaktorsignalwege liegen dem Netzhautwachstum zugrunde; Immunzellen bewachen die Netzhautstammzellnische in Homöostase und bei Beschädigung.

Zur Analyse der intrinsischen Stammzellteilungsregulierung adressierte ich die Funktion des Insulin-ähnlichen Wachstumsfaktors (Igf) in der ziliären Randzone durch Funktionsverlust- und -gewinnstudien. Ich fand heraus, dass eine Überaktivierung des Igf1-Rezeptors den Zellzyklus beschleunigte, die Vorläuferzellanzahl und dadurch die Netzhautgröße vergrößerte, während gleichzeitig der stereotypische Netzhautaufbau erhalten blieb. Bemerkenswerterweise waren Stammzellen nicht für mitogene Stimuli empfänglich, was auf die Vorläuferzellvervielfältigung als Bestimmungsfaktor der Netzhautgröße und -zusammensetzung hindeutet. Um die extrinsische Regulierung der Stammzellnische zu verstehen untersuchte ich das Zusammenspiel von Stamm- und Immunzellen. Ich fand heraus, dass Ccl25b-positive Stammzellen von Ccr9a-positiven Immunzellen phagozytiert werden. Durch Mutation von *ccl25b* wurde die Reaktivierung

der Immunzellen nach Stammzellverletzung verhindert, wodurch die Signalwirkung von Ccl25b–Ccr9a in der Interaktion von Immun- und Stammzellen in Homöostase und nach Verletzung eingeordnet wird.

Zusammenfassend zeigen meine Ergebnisse, dass akkurates postembryonales Wachstum und Gewebeintaktheit sowohl auf zellintrinsische als auch zellextrinsische Mechanismen der Wachstumsregulierung in der Netzhautstammzellnische angewiesen sind.

Contents

Abbreviations

2D	two-dimensional
3D	three-dimensional
AC	amacrine cell
atho7	atonal homolog 7
ATP	adenosine triphosphate
bp	base pairs
BC	bipolar cell
BCIP	5-bromo-4-chloro-3-indolyl phosphate base pair
BrdU	bromodeoxyuridine
BSA	bovine serum albumin
Cas	CRISPR-associated system
ccl25	chemokine (C-C motif) ligand 25
ccr9	chemokine (C-C motif) receptor 9
cDNA	complementary DNA
CE	ciliary epithelium
CFP	cyan fluorescent protein
cmlc2	cardiac myosin light chain 2
CMZ	ciliary marginal zone
cndp1	carnosine dipeptidase 1
CNS	central nervous system
CRISPR	clustered regularly interspaced short palindromic repeats
d	dorsal
D. melanogaster	Drosophila melanogaster
DAPI	4',6-diamidino-2-phenylindole
digUTP	digoxigenin deoxyuridine triphosphate
DMSO	Dimethylsulfoxid
DNA	deoxyribonucleic acid
dNTP	deoxynucleoside triphosphate
dfp	days post fertilisation
E. coli	Escherichia coli
EDTA	ethylendiamine tetraacetic acid
EdU	5-Ethynyl-2'-deoxyuridine
ERT2	selectively tamoxifen-sensitive estrogen receptor
EtBr	ethidium bromide
eGFP	enhanced green fluorescent protein
ERM	embryonic rearing medium

EtOH	ethanol
FGF2	fibroblast growth factor 2
fwd	forward
Gaudí^{RSG}	Gaudí red switch green
GCL	ganglion cell layer
gDNA	genomic DNA
GFP	green fluorescent protein
HC	horizontal cell
her9	hairy-related 9
hESC	human embryonic stem cell
iArCoS	induced arched continuous stripe
igf	insulin-like growth factor
IIS	Insulin-like growth factor and insulin signaling
igfr	insulin-like growth factor receptor
INL	inner nuclear layer
ins	insulin
insr	insulin receptor
IPL	inner plexiform layer
iPSC	induced pluripotent stem cell
IRS	insulin receptor substrate
ISC	intestinal stem cell
HSC	hematopoietic stem cell
Kras	kirsten rat sarcoma viral oncogene homologue
L	ligand
l	lateral
LB	lysogeny broth
lcp1	lymphocyte cytosolic protein 1
m	medial
Mapk	mitogen-activated protein kinase 1
MaSC	mammary gland stem cells
MG	Müller glia
mRNA	messenger RNA
NBT	nitro blue tetrazolium chloride
NGS	normal goat serum
NR	neural retina
NSC	neural stem cell
o/n	overnight
ON	optic nerve
ONL	outer nuclear layer
OPL	outer plexiform layer

OT	optic tectum
PAM	protospacer adjacent motif
PBS	phosphate buffered saline
PCR	polymerase chain reaction
Pcna	proliferating cell nuclear antigen
PFA	paraformaldehyde
PI3K	phosphatidylinositol-4,5-bisphosphate 3-kinase
PGZ	periventricular grey zone
PRC	photoreceptor cell
PTU	phenylthiourea
PTW	phosphate buffered saline plus Tween 20
R	receptor
RaGC	radial glia cell
RFP	red fluorescent protein
RGC	retinal ganglion cell
RNA	ribonucleic acid
rNTP	ribonucleoside triphosphate
RPC	retinal progenitor cell
RPE	retinal pigment epithelium
RSC	retinal stem cell
RTK	receptor tyrosine kinase
RT-PCR	reverse transcription PCR
rx2	retinal homeobox transcription factor 2
SD	standard deviation
sgRNA	single guide RNA
shc	Src homology collagen
shh	sonic hedgehog
sox2	sex determining region Y-box 2
TAE	Tris-acetate-EDTA-buffer
tlx	tailless
TMX	tamoxifen
TUNEL	terminal deoxynucleotidyl transferase dUTP nick end labeling
U	unit
UTR	untranslated region
UV	ultraviolet radiation
v	ventral
wt	wildtype
X-Gal	5-Brom-4-chlor-3-indol-ß-D-galactopyranosid

1 Introduction

The Japanese rice fish medaka (*Oryzias latipes*) is a well-established model organism within the teleost infraclass. A variety of genetic tools are available in medaka, such as efficient transgenesis (Grabher and Wittbrodt, 2007), the Cre/LoxP recombination system (Centanin et al., 2014) and CRISPR/Cas9-mediated targeted mutagenesis (Ansai and Kinoshita, 2014; Stemmer et al., 2015). Additionally, recent years have brought about an invaluable new resource in medaka, the first wild vertebrate inbred panel, which will allow genetic dissection of morphological, behavioural and physiological phenotypes (Spivakov et al., 2014). A distinguishing feature of fish and amphibians to higher vertebrates is their continued life-long growth enabled by postembryonic stem cells, rendering them well-suited model organisms for investigating adult homeostatic stem cells in a variety of tissues. All species with life-long growth face particular challenges: Throughout postembryonic growth, most organs scale in size proportional to the increase in body length while simultaneously maintaining functionality. In medaka, retinal stem cells (RSCs) facilitate postembryonic neurogenesis by ultimately generating new neurons which are integrated into the growing organ. Since function and shape of eyes are intimately linked, activity of stem and progenitor cells is tightly coordinated to establish proper cell type composition and number and to prevent aberrant growth of tissue (Ritchey et al., 2012). In this thesis I investigated two complementary mechanisms of growth control in the RSC niche of the postembryonic medaka retina.

1.1 The vertebrate retina

Vision is one of the major senses involved in a multitude of behaviours like mating, navigation, predator evasion and feeding (Collett and Land, 1975; Darmaillacq et al., 2004; Kraft et al., 2011; Lustig et al., 2012). The visual system is the designated sensory system for detection and processing of visual stimuli and is part of the central nervous system (CNS). The retina is the sensory organ of the system whereas the optic tectum (OT) receives visual input for further processing via retinotectal axons of retinal ganglion

cells (RGCs) projecting to the neuropil in the OT. Retina and OT form a functional unit, and retinal impairment or differential environmental conditions result in subsequent changes in the contralateral OT (Hall and Tropepe, 2018; Raymond et al., 1983).

The retina is a highly conserved organ throughout all vertebrate species with regard to structure and morphology. It is also the most accessible exterior part of the CNS and therefore amenable to mechanical manipulation as well as *in vivo* imaging. The retina comprises two distinct tissues, the neural retina (NR) and the retinal pigment epithelium (RPE).

The NR consists of seven main cell types, six neuronal cell types and one glial cell type, which are arranged in three nuclear layers (Figure 1.1). Rod and cone photoreceptors (PRCs) reside in the outer nuclear layer (ONL). The inner nuclear layer (INL) comprises amacrine cells (ACs), bipolar cells (BCs), horizontal cells (HCs) and Müller glia (MG) cells. Retinal ganglion cells (RGCs) are located in the ganglion cell layer (GCL), with retinotectal axons projecting as optic nerve (ON) to the OT. The nuclear layers are separated by plexiform layers, where synaptic connections between the different retinal cell types are established. The outer plexiform layer (OPL) is located between the ONL and the INL, and the inner plexiform layer (IPL) separates the INL from the GCL. To prevent light entry at other sites than the lens, the NR is enclosed by the RPE.

In teleosts, the retinal stem cell niche is located in the peripheral region of the retina within the ciliary marginal zone (CMZ) (Centanin et al., 2011; Raymond Johns, 1977). Both RPE and NR originate from one common pool of retinal stem cells (RSCs) that express the *retina-specific homeobox gene 2* (*rx2*) (Reinhardt et al., 2015). During embryonic development, the different neuroretinal cell types arise from multipotent retinal progenitor cells (RPCs), which was demonstrated by lineage tracing approaches in rodent, bird, amphibian and teleost models (Fekete et al., 1994; He et al., 2012; Holt et al., 1988; Turner et al., 1990; Wetts and Fraser, 1988). The differentiation of RPCs into mature cell types during retinal neurogenesis follows a strict order, generating RGCs first and BCs as well as MG cells last ((Wong and Rapaport, 2009), reviewed in (Cepko et al., 1996)).

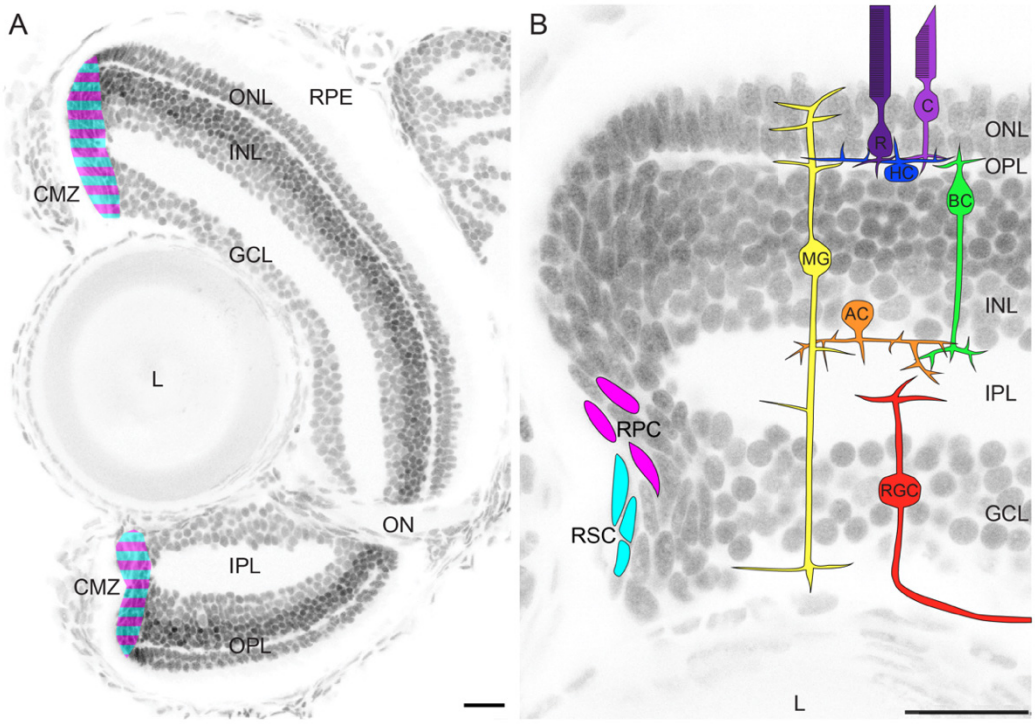

Figure 1.1: Structure of the medaka retina.
(A) Central cryosection of a hatchling medaka retina with DAPI staining. At hatch, the NR is directly adjacent to the lens. The three nuclear layers are divided by the two plexiform layers, where OPL separates ONL and INL, and IPL separates INL and GCL. The NR is surrounded by the RPE on the apical side. In the ventral central retina, RGC axons project from the GCL through all retinal layers to the OT via the ON. The CMZ (magenta) at the retinal periphery contains RSCs and RPCs. (B) Cryosection of a dorsal hatchling medaka retina with schematic drawings of cell type localisation within the NR. The CMZ harbours RSCs (cyan) and RPCs (magenta). Rod (violet) and cone (purple) photoreceptors are located in the ONL. The INL is composed of HCs (blue), BCs (green), ACs (orange) and MG cells (yellow) that span the entire width of the NR. The GCL contains RGCs (red). Scale bars are 20 µm.

1.2 The CMZ: a postembryonic neural stem cell niche

An essential requirement for species with continuous life-long growth is the maintenance of postembryonic stem cells in all tissues. After completion of embryonic development and once the retina is fully differentiated, the CMZ harbours RSCs and RPCs that facilitate and maintain this continued life-long growth in teleosts and amphibians (Hollyfield, 1971; Johns and Easter, 1977; Raymond Johns, 1977; Straznicky and Gaze, 1971). Throughout postembryonic neurogenesis, multipotent RSCs give rise to all seven retinal cell types (Centanin et al., 2014; 2011; Raymond et al., 2006; Wan et al., 2016). RPCs display a restricted proliferative potential, are more

heterogeneous and comprise several populations in different stages of lineage specification (Centanin et al., 2014; Pérez Saturnino et al., 2018; Raymond et al., 2006; Wan et al., 2016). Neurogenesis occurs at the peripheral retina in the CMZ, where newborn neurons are integrated into the NR, while older neurons are located in the central area of the retina (Centanin et al., 2011; Raymond Johns, 1977; Raymond et al., 2006). During homeostatic growth, RSCs divide predominantly in an asymmetric manner with a peripheral–central division axis (Centanin et al., 2014; Wan et al., 2016). Thereby one daughter cell stays in place in the most peripheral domain and remains a slow-dividing RSC while the other daughter cell is located more centrally and becomes a fast-cycling RPC (Wan et al., 2016; Xue and Harris, 2012). To accommodate the increasing retinal radius and therefore the expanding stem cell compartment, RSCs additionally undergo infrequent symmetric divisions throughout postembryonic growth (Centanin et al., 2014). RSCs do not only generate new neuroretinal cells, but also facilitate the growth of RPE and ciliary epithelium (CE). The CE develops from the peripheral-most tip of the NR in juvenile teleosts (Soules and Link, 2005), which was evident in lineage tracing experiments where NR clones originating in postembryonic RSCs were continuous with the CE (communication with colleagues and personal observation). Some effort has been dedicated to elucidating pathways, transcription factors and other signaling molecules whose expression pattern specify different populations of RSCs and RPCs within the peripheral to central CMZ (Lust et al., 2016; Perron et al., 1998; Pérez Saturnino et al., 2018; Raymond et al., 2006; Reinhardt et al., 2015; Xue and Harris, 2012). In the postembryonic CMZ of medaka, multipotent RSCs and RPCs are defined by *rx2* and *sex determining region Y-box 2* (*sox2*) expression, whereas *tailless* (*tlx*) and *hairy-related 9* (*her9*) are expressed in a partially overlapping, more central domain comprising predominantly RPCs with few RSCs (Lischik, 2019; Möller, 2017; Reinhardt et al., 2015). The basic helix-loop-helix transcription factor *atonal homolog 7* (*atoh7*) labels a population of lineage-committed RPCs in a mutually exclusive pattern with an RPC population displaying activated Notch signaling, both of which give rise to a set of complementary neuroretinal cell types (Lust et al., 2016; Pérez Saturnino et al., 2018).

In contrast to fish and amphibians, higher vertebrates exhibit – if at all – reduced proliferative capacity in postembryonic retinal structures equivalent to the anamniote CMZ. In the postnatal to adult chick retina, proliferative cells are located in the CMZ at the retinal periphery, where they give rise to new neurons to facilitate postembryonic ocular growth ((Fischer and Reh, 2000; Morris et al., 1976), reviewed in (Fischer et al., 2013)). These findings were confirmed in another avian species by Kubota and colleagues. In the quail retina, proliferative cells are present at the retinal margin, however numbers decrease over time until adulthood, and the CMZ is diminished in comparison to chicks (Kubota et al., 2002). Moreover, the same study investigated the postembryonic proliferative capacity of cells at the retinal margin of a marsupial and a rodent species: in the juvenile opossum retina, the retinal margin also contains few proliferating cells that differentiate into retinal neurons (Kubota et al., 2002). While in postnatal mammals no proliferation occurs within the retinal margin, they do have a structure analogous to the anamniote CMZ, the pigmented ciliary body. Studies on primary cell culture of cells isolated from the postembryonic pigmented ciliary body of rodents demonstrated their capacity to proliferate, self-renew and differentiate into multiple retinal cell types *in vitro* (Ahmad et al., 2000; Tropepe et al., 2000). *In vivo*, proliferation of cells in the pigmented ciliary body, but not the retinal margin was observed in juvenile mice (Kubota et al., 2002). Strikingly, activation of Sonic hedgehog (Shh) signaling resulted in sustained proliferative cells at the retinal margin of juvenile mice, re-establishing a niche with persistent postembryonic proliferation, injury-induced proliferation response, multipotent neurogenic properties and gene expression reminiscent of the lower vertebrate CMZ (Moshiri and Reh, 2004). Taken together, these observations in anamniote as well as mammalian species strengthens the hypothesis that throughout vertebrate evolution, active RSCs and the CMZ as their niche were progressively lost (reviewed in (Centanin and Wittbrodt, 2014)).

1.3 Evolutionary adaptation of retinal features

The teleost clade is the largest and most successful infraclass within the Actinopterygii. It comprises of more than 26000 different species, accounting for up to 96 % of all existing fish species (reviewed in (Nelson et al., 2016;

Ravi and Venkatesh, 2018; Volff, 2005)). Teleosts occupy a tremendous variety of habitats, ranging from puddles to brackish water, from lentic to lotic fresh water, from epipelagic to bathypelagic zones in seawater. Moreover, teleosts display a vast diversity in body size and mass, covering everything between 7 mm and more than 7 m length. Throughout teleost evolution, many morphological features have adapted for specific environmental conditions of the respective species, enabling teleosts to occupy these diverse ecological niches with great success.

One such adaptation is evident in the visual system, where retinal size, architecture and cell type composition vary significantly between species dependent on photic environment. Already between adult specimens of Cab medaka and zebrafish (*Danio rerio*) the number of rod photoreceptors in the retina differ substantially, even though they occupy rather similar habitats in shallow fresh water, for example rice paddies (Arunachalam et al., 2013; Engeszer et al., 2007; McClure et al., 2006). While light-sensitive rods are responsible for vision at low levels of illumination, colour perception depends on cones. The ONL in adult Cab medaka comprises two rows of nuclei, cones on the apical and rods on the basal side. Adult zebrafish, however, possess one layer of cones and 3–4 layers of rods (Figure 1.2A–B) (Lust and Wittbrodt, 2018). This structural divergence likely reflects differences in photic environment throughout postembryonic stages within their natural habitats, as Cab medaka are surface-dwelling fish throughout their entire lives while zebrafish transition from surface-dwelling larvae to adults inhabiting deeper, often turbid water (reviewed in (Kirchmaier et al., 2015; Lenkowski and Raymond, 2014)). Since the early 20th century, scientists have been fascinated by deep-sea creatures and fishes. Several studies have investigated the structural differences and specific morphological adaptations of the eye and retina in deep-sea teleosts and have put their findings into context with environment and habitat. The mesopelagic lanternfish family (Myctophidae) was found to exhibit a large variation in relative eye size that could not be explained by depth distribution or exposition to bioluminescence (de Busserolles et al., 2013). Pankhurst investigated the retinal structure of shallow marine teleosts with attention to their ecological niche and observed an increase of rod density and rod to BC convergence, which related with high theoretical scotopic

sensitivity in nocturnal species, whereas diurnal species exhibited high theoretical acuity (Pankhurst, 1989). Another study examined the spatial distribution of RGCs in species from different photic zones and habitats, where all investigated species exhibited specific patterns of RGC density distinct from the other species (Collin and Partridge, 1996). One of the most common adaptations to dim light environments is the increase in light-sensitive rod density (Figure 1.1C). Some deep-sea species display retinae with only rods and no cones, where rod outer segments are stacked in two or more banks (Figure 1.2D–E). Directly associated with this is a decrease in width of INL and GCL, whose cell type composition and number is very diverse between species (Darwish et al., 2015; de Busserolles et al., 2014; Wagner et al., 1998).

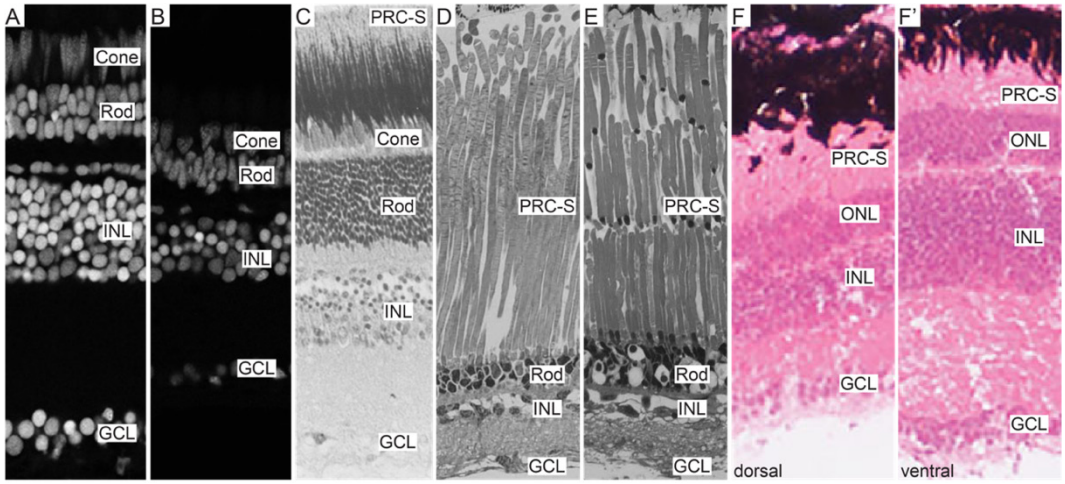

Figure 1.2: Structural differences in the teleost retina.
(A–B) Sections of adult zebrafish (A) and medaka (B) retinae highlighting the differences in rod numbers between zebrafish and medaka retinae. Adapted with permission from (Lust and Wittbrodt, 2018). (C) Section of *Pempheris adspersa* retina features a thick rod layer accounting for half of the NR with fewer cone, INL and GCL cells. Adapted with permission from (Pankhurst, 1989). (D–E) Sections of *Xenodermichthys copei* (D) and *Notacanthus chemnitzii* (E) retinae with single- (D) or multibank (E) photoreceptor segments (PRC-S). Adapted with permission from (Wagner et al., 1998). (F–F') Sections of *Anableps anableps* retina with differing dorsal (F) and ventral (F') structure, demonstrating increased INL thickness in the ventral part. Adapted with permission from (Perez et al., 2017).

One interesting example for retinal adaptation to a particular behaviour and ecological niche is the four-eyed fish (*Anableps anableps*). This species features eyes that partly protrude over the top of their skull and are above the water surface while the lower half of the eye is submerged just below the surface. Subsequently, composition and width of the NR differs between

ventral and dorsal halves (Figure 1.2F–F'), which are equipped for aerial and aquatic vision, respectively. There, the ventral retina features an INL that is twice as thick as the dorsal INL, concordant with increased proliferation in the ventral compared to the dorsal CMZ during larval development (Perez et al., 2017). Interestingly, visual acuity was positively correlated with relative eye size as well as habitat complexity based on published data on 81 species belonging to the Actinopterygii, which was examined with regard to morphological as well as environmental and ecological variables (Caves et al., 2017). Therefore, modifying retinal size and structure might potentially be an important step towards enabling species to cope with different light conditions and occupy new niches.

1.4 The Igf/insulin signaling pathway

Signaling pathways often display a high degree of conservation within vertebrates, sometimes reaching back to invertebrates, for instance Wnt signaling components are present throughout all metazoan clades (reviewed in (Holstein, 2012)). Other conserved pathways include Toll-like receptor signaling (Purcell et al., 2006), Hedgehog signaling (reviewed in (Huangfu and Anderson, 2006)) as well as the Insulin-like growth factor (Igf) and Insulin signaling (IIS) pathway (reviewed in (Das and Dobens, 2015; Pertseva and Shpakov, 2002)). The complex and multifactorial IIS pathway is fundamental for embryonic development, regulation of postembryonic proliferation, apoptosis and cell cycle progression as well as ageing and longevity in nematodes, insects, teleosts to mammals (reviewed in (Barbieri et al., 2003; Caruso and Sheridan, 2011; Junnila et al., 2013; Kaletsky and Murphy, 2010; Nässel et al., 2015; Vincent and Feldman, 2002)). Dysregulations of the IIS pathway are involved in the formation of some major diseases like cancer, metabolic and neurodegenerative disorders (reviewed in (Puche and Castilla-Cortázar, 2012)).

The teleost IIS system is comprised of several ligands and receptors, some of which are present as two or more paralogues due to the teleost-specific genome duplication (reviewed in (Caruso and Sheridan, 2011)). In the genome assembly ASM223467v1 for the medaka strain HdrR, three *igf* receptor paralogues (*igf1ra/b* and *igf2r*) and two ligand paralogues (*igf1* and *igf2*) are annotated. Furthermore, the IIS pathway comprises two *insulin*

receptors (*insra* and *insrb*) and ligands (*ins1* and *ins2*). A teleost-specific *igf3* has been described, which was shown to regulate gonadal development and maturation (Li et al., 2015; 2011; Nóbrega et al., 2015; Wang et al., 2008). Wang and colleagues also identified an *igf3* sequence *in sillico* in medaka, which is not annotated in the ASM223467v1genome assembly (Wang et al., 2008).

The Igf1r and Insr of the IIS pathway belong to the receptor tyrosine kinase (RTK) family, are heterotetrameric transmembrane proteins and depend on ligand binding at their extracellular domain for activation. Subsequent auto-phosphorylation by the tyrosine kinase in the intracellular domain and phosphorylation of cytoplasmic target proteins and adaptor molecules such as Insulin receptor substrate (Irs) and Src homology collagen (Shc) activates the signaling cascade (reviewed in (Caruso and Sheridan, 2011; Laviola et al., 2007; Wood et al., 2005)). Downstream of the receptors, the signal is transduced via the Mitogen-Activated Protein Kinase 1 (Mapk) and phosphatidylinositol-4,5-bisphosphate 3-kinase (PI3K)–Akt pathways to ultimately mediate cellular responses such as proliferation, apoptosis, or growth (Pozios et al., 2001).

In teleosts, several studies have investigated the expression and localisation of Igf pathway components during embryonic and larval development in a variety of teleost species such as zebrafish, goldfish (*Carassius auratus)*, gilt-head bream (*Sparus aurata*), shi drum (*Umbrina cirrosa*) and African cichlids (*Astatotilapia burtoni*) (Ayaso et al., 2002; Boucher and Hitchcock, 1998b; Radaelli et al., 2003a; 2003b; Zygar et al., 2005). Consistently, Igf ligands and receptors were found to be expressed in the retina. In zebrafish, *igf1r* expression in the retina was shown by *in situ* hybridisation in embryonic and hatchling stages (Ayaso et al., 2002). Studies in postembryonic goldfish retinae demonstrated that *igf1* is expressed in the retina and its binding sites are localised in the CMZ and IPL. Northern blot analysis and *in situ* hybridisation furthermore showed that *igf1ra/b* mRNA is present in the goldfish retina as well (Boucher and Hitchcock, 1998b; Otteson et al., 2002). Zygar and colleagues investigated the expression and localisation of *igf1* and *igf1r* in postembryonic retinae of African cichlids. They detected *igf1* mRNA and protein in cone PRCs and observed that Igf1 protein levels oscillate throughout the day with highest abundance at night.

Igf1r mRNA was present in rod and cone PRCs as well as rod progenitors (Zygar et al., 2005).

Moreover, several studies have been conducted to elucidate IIS pathway functions during embryogenesis, most of which have been carried out in zebrafish. Igf1r-mediated signaling was found to be required for proper embryonic development, especially of anterior neuronal structures, and inhibition thereof resulted in reduced body size, growth arrest and developmental retardation (Eivers et al., 2004; Schlueter et al., 2007a). Additionally, *igf1r* knockdown resulted in increased neuronal apoptosis, reduced proliferation and adversely affected cell cycle progression (Schlueter et al., 2007a). Another study reported that Igf1rb was required for proper migration and survival of primordial germ cells, whereas *igf1ra* knockdown did not affect primordial germ cells but induced somatic apoptosis in a variety of tissues (Schlueter et al., 2007b). Overexpression of *igf1* and *igf2* lead to expansion of anterior neural tissues combined with reduced posterior structures and defects in midline and notochord formation, respectively (Eivers et al., 2004; Zou et al., 2009).

1.5 Igf signaling in the postembryonic retina

In recent years, a lot of work has been done using human embryonic (hESCs) or induced pluripotent stem cells (iPSCs). Studies reported that Igf1r-mediated signaling was required for the pluripotency and self-renewal capacities of hESCs, and inhibition thereof resulted in reduced survival, self-renewal and increased differentiation of hESC cultures (Bendall et al., 2007; Wang et al., 2007). Moreover, in a co-culture of hESCs with visceral endoderm-like cells leading to differentiation into cardiomyocytes, insulin supplementation and subsequent Igf1r-mediated signaling activity was sufficient to promote differentiation into the neuroectodermal over the mesendodermal lineage (Freund et al., 2007). Cell cultures with hESCs and iPSCs have been used to derive organ-like structures (Spence et al., 2011). This is also utilised to generate retinal organoids, where Igf signaling was shown to promote formation of 3D laminated retinae containing NR and RPE as well as accessory structures like lens and corneal epithelium (Mellough et al., 2015). These *in vitro* data suggest that Igf1r-mediated signaling might play a role in stem cell niches *in vivo*, potentially also in

neural lineages. Some evidence for this assumption was collected in higher vertebrate species. In the postnatal avian retina for example, Igf1 and insulin exposure resulted in increased proliferation in the CMZ, however newly hatched birds still exhibit an inherent neurogenic capacity (Fischer and Reh, 2000; Kubota et al., 2002). Strikingly, in adult quail retinae, where proliferation does not occur anymore in physiological conditions, proliferating cells were observed in the CMZ upon stimulation with insulin (Kubota et al., 2002).

Furthermore, teleost models have been employed to assess different aspects like localisation and physiological role of Igf signaling in the retina with its continuously active postembryonic neural stem cell niche. In various teleost species, expression of IIS pathway ligands and receptors was detected in the postembryonic retina by different methods such as *in situ* hybridisation, Northern blot analysis, immunohistochemistry and RT-PCR (Ayaso et al., 2002; Boucher and Hitchcock, 1998b; Otteson et al., 2002; Zygar et al., 2005). In some teleost species, postembryonic neurogenesis is sustained not only by the CMZ, but MG cells generate progenitor cells that exclusively give rise to rod PRCs in homeostasis (Bernardos et al., 2007; Otteson et al., 2001; Raymond et al., 2006), and the IIS pathway has been implicated in regulating these processes. In organ slice cultures of juvenile African cichlid retinae as well as *in vivo*, proliferation of rod progenitors was increased upon stimulation with insulin or Igf1 while Igf1r inhibition decreased their proliferation (Mack and Fernald, 1993; Zygar et al., 2005). Later, these results were corroborated in goldfish retinae *in vivo*, where elevated *igf1* mRNA levels in the retina resulted in increased proliferation of CMZ cells and also revealed increased rod precursor proliferation (Otteson et al., 2002), whereas inhibition of Igf1r decreased rod progenitor proliferation levels (Zygar et al., 2005). In retinae of adult African cichlid fish, expression of *igf1/2* as well as Igf1 protein, whose levels showed daily variation with highest abundance at night, was observed in cone PRCs, and *igf1r* expression occurred in rod progenitors as well as PRCs (Mack et al., 1995; Zygar et al., 2005). Adult specimens of the Mozambique tilapia (*Oreochromis mossambicus*) displayed a similar expression pattern, with *igf1* mRNA localised in PRCs and some INL neurons (Reinecke et al., 1997). These findings are in agreement with receptor-binding experiments

performed in juvenile goldfish, where Igf1 binding sites were detected in the IPL throughout the differentiated retina (Boucher and Hitchcock, 1998b). Concordant with the hypothesis that Igf1r-mediated signaling regulates proliferation of rod progenitor cells derived from many of the above mentioned studies, adult zebrafish were subjected to photic deprivation, whereupon proliferation of rod progenitors increased in an Igf1r-dependent manner (Lahne et al., 2019). Additionally, an *ex vivo* approach with goldfish retinae revealed increased proliferation in the CMZ upon insulin or Igf incubation (Boucher and Hitchcock, 1998a), and Igf1 was found to have binding sites in the CMZ (Boucher and Hitchcock, 1998b). All these data suggest that the IIS pathway is integral for retaining neural stem and/or progenitor cells in a proliferative state, possibly in a manner where local paracrine and autocrine signaling functions might be divergent and uncoupled from systemic endocrine signals, although definitive, high-resolution evidence for *igf* ligand expression in the teleost CMZ is still missing.

1.6 The teleost immune system and the role of chemokines therein

The immune system is the mechanism by which organisms protect themselves against intrinsic and extrinsic threats to their health. Intrinsic hazards encompass deficiencies of the immune system like autoimmune diseases and cancer, whereas pathogens and injuries pose extrinsic threats to an organism. From a functional point of view, the immune system can further be classified into innate and adaptive immunity. Adaptive or acquired immunity is established upon exposure to a pathogen and elicits a response specifically designed to eliminate said pathogen (reviewed in (Alberts et al., 2017; Boehm, 2011)). In contrast, innate immunity relies on less specific approaches including leukocyte and inflammation responses (reviewed in (Alberts et al., 2017; Riera Romo et al., 2016)). Adaptive as well as innate immunity is present throughout the vertebrate clade, even though the systems exhibit some differences between mammals and lower vertebrates (reviewed in (Boehm, 2011; Zapata and Amemiya, 2000)). For instance, teleosts have many of the mammalian lymphoid tissues such as spleen and thymus but do not possess lymph nodes or bone marrow, however

the head kidney was implicated as bone marrow equivalent as it exerts hematopoietic functions (Kobayashi et al., 2016; Zapata, 1979).

Cytokines are essential components of the innate immune system in anamniotes as well as mammalians (reviewed in (Riera Romo et al., 2016)). They are small, secreted molecules important for cell signaling and comprise different classes, one of which are chemotactic cytokines or chemokines. Teleosts feature more chemokine ligands and receptors than mammals, however orthologues could not be identified for all human ligands and receptors (DeVries et al., 2006). Chemokine ligands (L) are subdivided into four distinct classes (CC, CXC, CX3C, XC) dependent on the position of the cysteine residues, and receptors (R) are categorised depending on which type of chemokine they bind (Bacon et al., 2002). Functionally, two groups of chemokines have been identified: the first acts under pathological conditions and is expressed upon inflammation to attract leukocytes, mainly neutrophils and macrophages; the second is constitutively expressed under homeostatic conditions in specific organs and cell types, regulates homeostatic migration and exerts chemotactic effects for specialised leukocytes essential for developing acquired immunity (reviewed in (Zlotnik and Yoshie, 2012)). However, this classification is not mutually exclusive, as some chemokines have dual functions in homeostasis as well as inflammation response (reviewed in (Zlotnik and Yoshie, 2012)). Chemokine receptors belong to the G protein-coupled receptor family, which contain seven transmembrane domains, and are expressed by leukocytes responsive to the chemoattractant ligand ((Zaballos et al., 1999), reviewed in (Sokol and Luster, 2015; Zlotnik and Yoshie, 2012)).

Phylogenetic analysis categorised Ccl chemokines into seven groups, the Ccl19/21/25 group of homeostatic chemokines being one with high evolutionary conservation to mammalian chemokines (reviewed in (Peatman and Liu, 2007)). In mammals, *ccl25* was shown to be expressed in thymus, small intestine and liver and displayed chemoattractant properties for selected leukocytes (Vicari et al., 1997), and its sole functional receptor *ccr9* was expressed in T cells in thymus, lymph nodes and spleen (Zaballos et al., 1999). Subsequently, this non-promiscuous ligand-receptor pair was shown to be involved in lymphocyte homing to the small intestine and T cell maturation ((Wurbel et al., 2007; 2001), reviewed in (Svensson and Agace,

2006)). The medaka and zebrafish genomes contain two paralogues for both *ccr9* (*ccr9a/b*) and *ccl25* (*ccl25a/b*) (Aghaallaei et al., 2010). Expression of *ccr9a/b* in medaka was detected during embryonic development and as injury response in migratory cells in larvae (Aghaallaei et al., 2010). Medaka and zebrafish embryos displayed *ccl25a* expression in the thymus, while *ccl25b* expression was visible in surrounding tissue, and the thymic expression pattern of *ccr9a* and *ccr9b* defined two spatially distinct subpopulations of thymocytes (Aghaallaei et al., 2010; Bajoghli et al., 2009; 2015; Hess and Boehm, 2012). Furthermore, the importance of the Ccl25a–Ccr9 axis in thymus homing was demonstrated by knockdown experiments in medaka and zebrafish embryos, where thymopoiesis was decreased and in synergy with *cxcl12a* knockdown completely abolished (Bajoghli et al., 2009; Hess and Boehm, 2012). These insights propose a similar role of the Ccl25–Ccr9 axis in leukocyte chemoattraction from lower vertebrates to mammals.

1.7 Retinal immune cells in homeostasis and injury

Immune cells in the retina and other neural tissues are essential for proper development and maintenance of the CNS (reviewed in (Asensio and Campbell, 1999; McMenamin et al., 2019)). Already in the early 1980s, microglia were shown to colonise the NR during mouse embryonic development to clear apoptotic neurons, and subsequently establish an evenly distributed network in the plexiform layers (Hume et al., 1983). CNS-resident microglia exist in two states (Figure 1.3): in homeostasis, microglia are ramified with a non-migratory small cell body and elaborate, highly motile and exploratory processes with which they probe their environment ((Nimmerjahn et al., 2005), reviewed in (Sarma et al., 2013)). Upon injury, proximate microglia become reactive, adopt a migratory amoeboid state characterised by larger irregular cell bodies and fewer processes, which is accompanied as well by transcriptional changes ((Ling, 1982; Mitchell et al., 2019), reviewed in (Sarma et al., 2013)). During retinal colonisation in postnatal rodents, microglia first exhibited an amoeboid morphology, before adopting a ramified morphology later in development and once they had reached their final position in the plexiform layers ((Boya et al., 1987; Hume et al., 1983), reviewed in (Rathnasamy et al., 2019)). In an optic nerve crush

injury paradigm in adult mice, microglia density and cell body size increased, while distance to neighbours and roundness of cell bodies decreased (Davis et al., 2017).

In the postembryonic teleost retina of zebrafish, ramified microglia with small cell bodies were shown to be located in the INL, GCL and flanking the plexiform layers (Mitchell et al., 2018), which is in agreement with microglia localisation after initial colonisation during retinal development (Herbomel et al., 2001). In larval and adult zebrafish, photic, chemical or mechanical injury paradigms induced the transition of resident microglia from ramified to amoeboid morphology, subsequent migration to lesion sites and phagocytosis of cell debris (Craig et al., 2008; Mitchell et al., 2018; White et al., 2017).

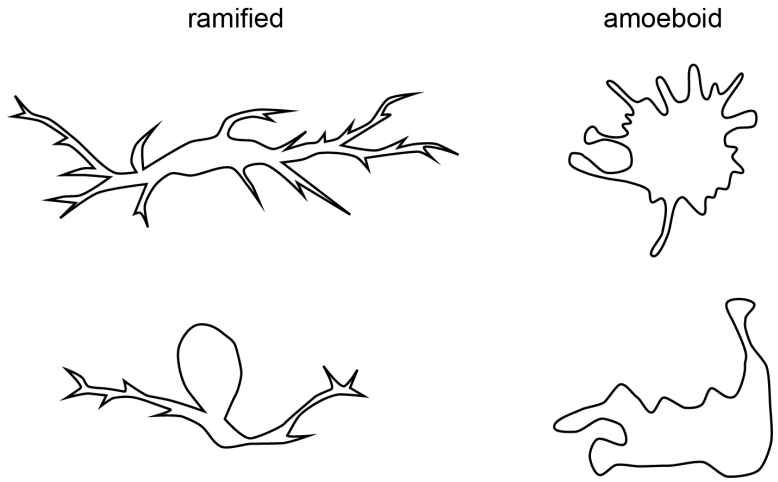

Figure 1.3: Macrophage morphology.
In homeostasis, ramified macrophages are non-migratory with small cell bodies and many thin processes. After injury, amoeboid macrophages are migratory with larger irregular cell bodies and few thick processes. Lower cells are redrawn from retinal immune cells in medaka (from Figure 2.21 and Figure 2.22).

Also in medaka, immune cells in hatchling retinae rapidly migrated to the wound site upon laser-induced PRC injury (Lust, 2017). Interestingly, acute inflammation was found to be required and sufficient for successful CNS regeneration in zebrafish (Kyritsis et al., 2012), and microglial inhibition or ablation before injury resulted in delayed replenishment of lost retinal neurons (Conedera et al., 2019; White et al., 2017). The collective data from these studies indicate that the ocular immune system is crucial for an adequate response to retinal insult and regeneration initiation, possibly by regulating inflammation.

1.8 Stem cell regulation by immune cells and chemokines

In recent years, evidence for an interaction between stem and immune cells has increased, with the main focus on regenerative and clinically relevant contexts, but also in tissue homeostasis (reviewed in (Naik et al., 2018)). For example, in the postnatal mouse hippocampus, microglia were shown to clear apoptotic newborn neurons, thus contributing to preserving homeostasis within the postembryonic neurogenic niche (Sierra et al., 2010). Impaired phagocytosis of apoptotic neurons results in inflammatory responses and ultimately neuronal degeneration (reviewed in (Diaz-Aparicio et al., 2016)). Also in postnatal mice, a specific population of bone marrow mononuclear phagocytes was found to support hematopoietic stem cell (HSC) retention, whose depletion resulted in reduced expression of the chemokine *cxcl12* by niche cells and increased egress of HSCs (Chow et al., 2011). Deletion of the Cxcl12 receptor *cxcr4* in the bone marrow decreased HSC numbers, implicating Cxcl12–Cxcr4 signaling in homeostatic maintenance of the HSC niche (Sugiyama et al., 2006). Similarly, depletion of resident macrophages in intestinal stem cell (ISC) crypts resulted in Paneth cell differentiation and subsequent ISC reduction as well as impaired crypt homeostasis resulting in divergent lineage decisions (Sehgal et al., 2018). Furthermore, Chakrabarti and colleagues discovered that murine mammary gland stem cells (MaSC) expressing the Notch ligand Dll1 activate Notch-positive resident macrophages, resulting in Wnt ligand expression which maintains numbers and function of MaSCs (Chakrabarti et al., 2018).

Very few studies exist that examine a potential role of chemokine signaling in stem cell maintenance and homeostasis. Apart from the role of Cxcl12–Cxcr4 signaling in murine HSCs, Cxcr5 was implicated in regulating neurogenesis in the adult zebrafish brain. There, radial glia cells (RaGCs) mediate proliferation and neurogenesis and express the chemokine receptor *cxcr5* (Kizil et al., 2012). However, neither resulted *cxcr5* overexpression in increased RaGC proliferation in homeostasis nor did dominant negative Cxcr5 influence the proliferative capacity of RaGCs, and only in an injury

paradigm, cxcr5 expression was found to be upregulated and required for successful regeneration (Kizil et al., 2012).

Altogether, *in vivo* studies on this topic are still scarce, especially in homeostatic stem cell niche function. Furthermore, how immune cells home to tissue-specific stem cell niches and which molecular factors and pathways mediate the interaction between stem and immune cells is not understood yet (reviewed in (Naik et al., 2018)), with few exceptions. In light of the above-mentioned reports, it seems also likely that different niches and environments use distinctive ways of communication between stem and immune cells.

Aim

The aim of this study was to elucidate different aspects of growth control in a postembryonic neural stem cell niche, the CMZ of the medaka retina. Organisms with continuous postembryonic growth face two major challenges: first, organs have to scale in proportion to overall organismal growth. Second, continuous proliferation of stem and progenitor cells necessary for sustained growth needs to be tightly controlled to prevent formation of aberrant tissue. How both of these challenges are overcome and which factors and pathways are involved in these processes is poorly understood. Previous work, relying heavily on large scale mutagenesis screens, has identified several pathways and mechanisms that inhibit or slow down postembryonic retinal growth. However, to date increased growth and underlying molecular mechanisms have not been observed in any teleost model system. Moreover, it is unclear whether the retinal stem cell niche in teleosts is even permissive of such signals. The retinal stem cell niche might comprise a surveillance system which restricts abnormal proliferation of retinal stem cells, thus protecting retinal morphology and structure against undesired modification.

First, I wanted to address whether a prominent regulator of organismal growth, the IIS pathway, is involved in maintenance and homeostasis of the stem cell niche in the postembryonic medaka retina. Therefore, I investigated the expression of pathway components and performed loss- as well as gain-of-function experiments.

Second, I wanted to characterise the effects of gain-of-function transgenesis on stem and progenitor cell populations in the CMZ. Thus, I examined different parts of the visual system to explore resultant changes in quantity, proliferative capacity and cell cycle duration of stem and progenitor cells.

Third, I wanted to examine the interaction of retinal stem and immune cells and the function of the conserved Ccl25–Ccr9 axis therein. To this end, I utilised transgenic reporter fish to describe expression domains in the postembryonic medaka retina. Moreover, I generated a stable line carrying a *ccl25b* mutation and analysed retinal immune cell behaviour in homeostasis and upon CMZ injury in wildtype and homozygous mutant larvae.

2 Results

2.1 Igf1r signaling is the rate-limiting step in determining retinal size in medaka

2.1.1 Igf signaling pathway components are expressed and the pathway is active in the CMZ

Previously, teleost models have been employed to investigate expression patterns of IIS pathway components during embryogenesis as well as in postembryonic stages. Expression of ligands and receptors were observed in the retina. Igf signaling was furthermore shown to be vital for proper development of anterior neural tissues and retinal neurogenesis, with Igf1r inhibition resulting in morphological defects (Eivers et al., 2004; Otteson et al., 2002; Schlueter et al., 2007a). However, most of the expression analyses were performed in whole-mount, thus lacking high spatial resolution of expression patterns. Therefore, before being able to address an involvement of the Igf signaling pathway in regulating postembryonic retinal stem and progenitor cells in medaka, a detailed description of the expression domains within the postembryonic medaka retina and specifically the CMZ was necessary.

To determine the expression pattern of select Igf pathway components, I performed a small whole-mount *in situ* hybridisation screen at hatchling stage. I observed expression of *igf1ra*, *igf2* and *insrb* (Figure 2.1A–C') as well as *igf2ra/b*, *ins1* and *foxo1a/b* (data not shown) in the medaka retina and specifically in the CMZ. Additionally, *igf1ra* mRNA was present in the ONL and INL (Figure 2.1A–A'), *igf2* mRNA in the ONL, INL and GCL (Figure 2.1B–B') and *insrb* was expressed in the INL (Figure 2.1C–C'). Furthermore, Eva Hasel and Clara Baader previously observed expression of Igf downstream effectors *kras* and *akt2* in CMZ, INL and GCL (Baader, 2016; Hasel, 2017).

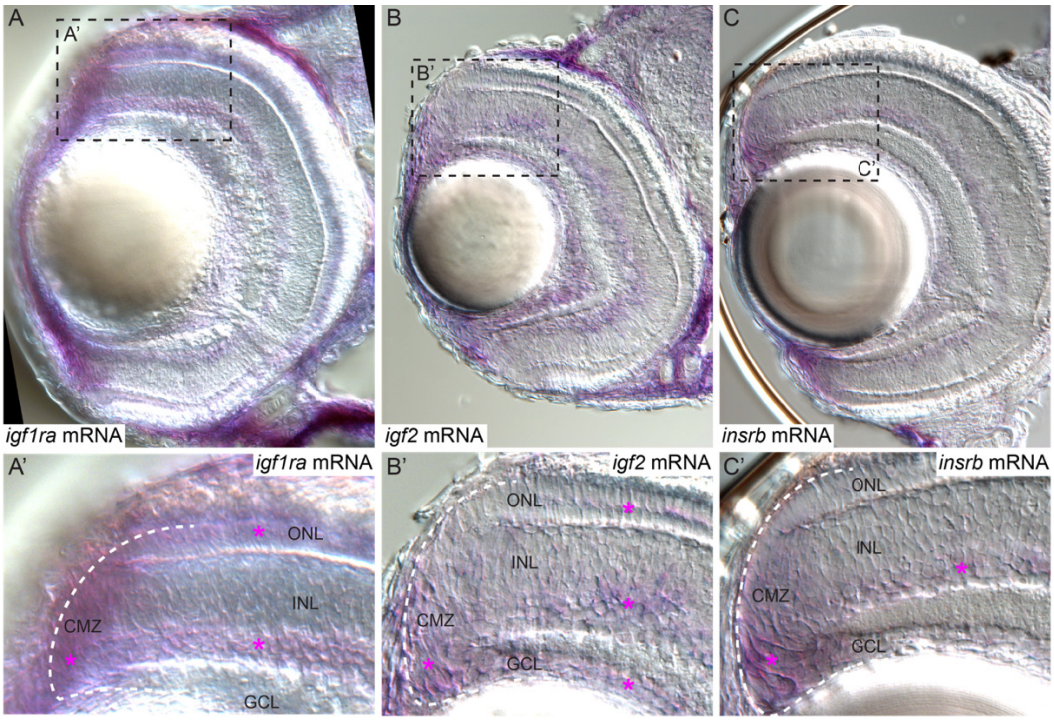

Figure 2.1: Igf pathway components are expressed in the retina.
(A–C') Cryosections of whole-mount *in situ* hybridisations. Expression of *igf1ra* (A–A') is visible in CMZ, ONL and INL (asterisks). *Igf2* (B–B') is expressed in CMZ, ONL, INL and GCL. CMZ and INL show expression of *insrb* (C–C').

Activity of receptor tyrosine kinases like Igf1r is mediated by ligand-dependent dimerisation and subsequent trans-phosphorylation. To assess whether Igf1r is not only expressed but also active in the CMZ, I performed immunostainings against phosphorylated Igf1r on retinal cryosections. Single cells in the progenitor domain of the CMZ as well as MG cells in the differentiated part of the retina were positive for phosphorylated Igf1r (Figure 2.2A–A').

Taken together, these results show that ligands, receptors and downstream effectors of the Igf signaling cascade are expressed and that Igf1r is active in progenitors in the CMZ of the medaka retina, consistent with findings in other teleost species.

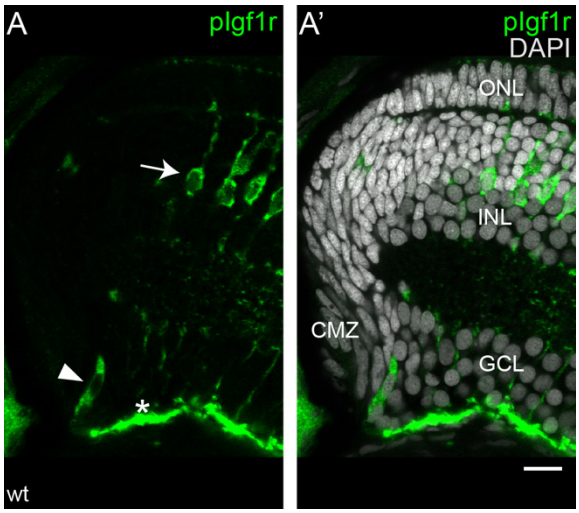

Figure 2.2: Igf1r is active in single cells in the CMZ and in MG cells.
(A-A') Cryosection of wt hatchling with pIgf1r (green) staining shows that Igf1r is active in single cells in the CMZ (arrowhead, n = 65 cells in 58 sections from 10 retinae) and in MG cells (arrow, asterisk) in the INL. Scale bar is 10 µm.

2.1.2 Inhibition of Igf1r decreases proliferation in the CMZ

Igf1r-mediated signaling was shown to be upregulated upon injury and necessary for proper regeneration of different tissues such as heart, fin and retina in zebrafish (Chablais and Jazwinska, 2010; Choi et al., 2013; Huang et al., 2013; Wan et al., 2014). Moreover, upon inhibition of Igf1r signaling cardiac development was impaired due to decreased cardiomyocyte proliferation (Choi et al., 2013; Huang et al., 2013). These observations together with my expression analysis allow to hypothesise that Igf signaling could play a role in regulating proliferation in the CMZ.

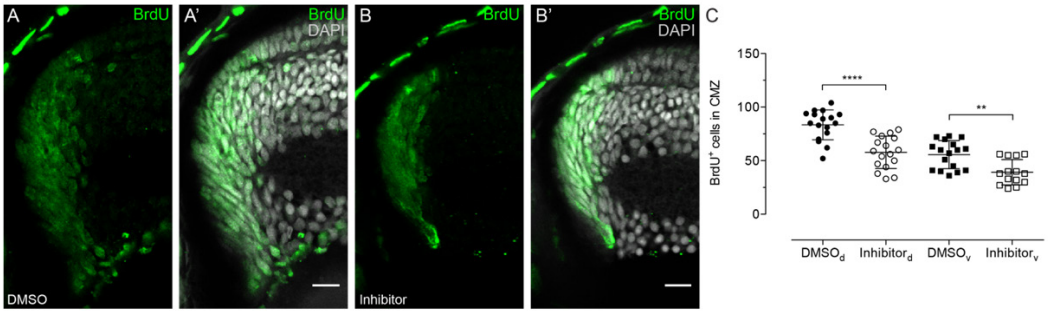

Figure 2.3: Inhibition of Igf1r signaling decreases the number of proliferating cells in the CMZ.
(A–B') Wt hatchlings were incubated for 24 h in BrdU and 10 µM Igf1r inhibitor NVP-AEW541 or DMSO. Cryosections of DMSO- (A–A') and inhibitor-treated (B–B') retinae with BrdU staining (green) display decreased BrdU incorporation upon Igf1r inhibition. Scale bars are 10 µm. (C) Quantification of the number of BrdU-positive cells in one Z plane per central section shows decrease in inhibitor-treated retinae (n ≥ 14 sections from 6 retinae) compared to DMSO (n = 17 sections from 6 retinae) (mean ± SD, ****$P_d < 0.0001$, **$P_v = 0.0011$).

To determine the impact of Igf1r signaling on homeostatic proliferation of retinal stem and progenitor cells, I made use of the widely-used Igf1r inhibitor NVP-AEW541 (Chablais and Jazwinska, 2010; Choi et al., 2013; Huang et al., 2013). At hatch, fish were incubated in 10 µM NVP-AEW541 or DMSO together with BrdU for 24 h, and analysed afterwards by immunostaining against BrdU (Figure 2.3A–B'). Quantification of the number of BrdU-positive cells in inhibitor- and DMSO-treated fish confirmed that proliferation in the CMZ was decreased by 30 % upon Igf1r signaling inhibition (Figure 2.3C).
This validates that Igf1r-mediated signaling is crucial for homeostatic proliferation in the CMZ.

2.1.3 Constitutive activation of Igf1r in retinal stem and progenitor cells results in eye size increase

In a stem cell niche like the CMZ, which is responsible for homeostatic postembryonic growth, tight regulation of proliferation in essential to maintain tissue integrity and function. So far, several projects in the lab have aimed at disturbing the controlled proliferation of CMZ stem and progenitor cells, however excessive proliferation could never be induced. The question which signals are sufficient to shift the balance in the retinal stem cell niche towards increased proliferation therefore remains unanswered. The fact that Igfr signaling components are expressed in and crucial for homeostatic proliferation of the CMZ let me to hypothesise that increasing Igfr signaling could be a way to shift retinal stem and progenitor cell niche in the medaka CMZ towards increased proliferation. Therefore, I generated a construct in which a constitutively active variant of Igf1ra (Cd8a:igf1ra) is expressed under the control of the *rx2* promoter (Figure 2.4A). The *cd8a:igf1ra* variant was generated by an in-frame fusion of the codon-optimised extracellular and transmembrane domain of *cd8a* and the intracellular domain of *igf1ra* by Stephan Kirchmaier, as previously described (Carboni et al., 2005). As indirect fluorescent readout, *rx2::lifeact-eGFP* was co-injected with *rx2::cd8a:igf1ra* to generate transgenic *rx2::cd8a:igf1ra rx2::lifeact-eGFP* fish (hereafter referred to as *rx2::cd8a:igf1ra* fish). Transgenic *rx2::cd8a:igf1ra* hatchlings displayed a prominent increase in eye size compared to wildtype siblings (Figure 2.4B–C), but had an otherwise normal-looking head and body length. The eye size increase first became

apparent in the F1 generation after crossing two potential F0 founders. Randomly chosen hatchlings with GFP expression were genotyped for *cd8a:igf1r*, which was present in all tested fish and thereafter *rx2::cd8a:igf1ra* was presumed to have co-integrated with *rx2::lifeact-eGFP*. GFP-positive fish nonetheless exhibited a phenotypic range from very slightly enlarged to substantially expanded eyes.

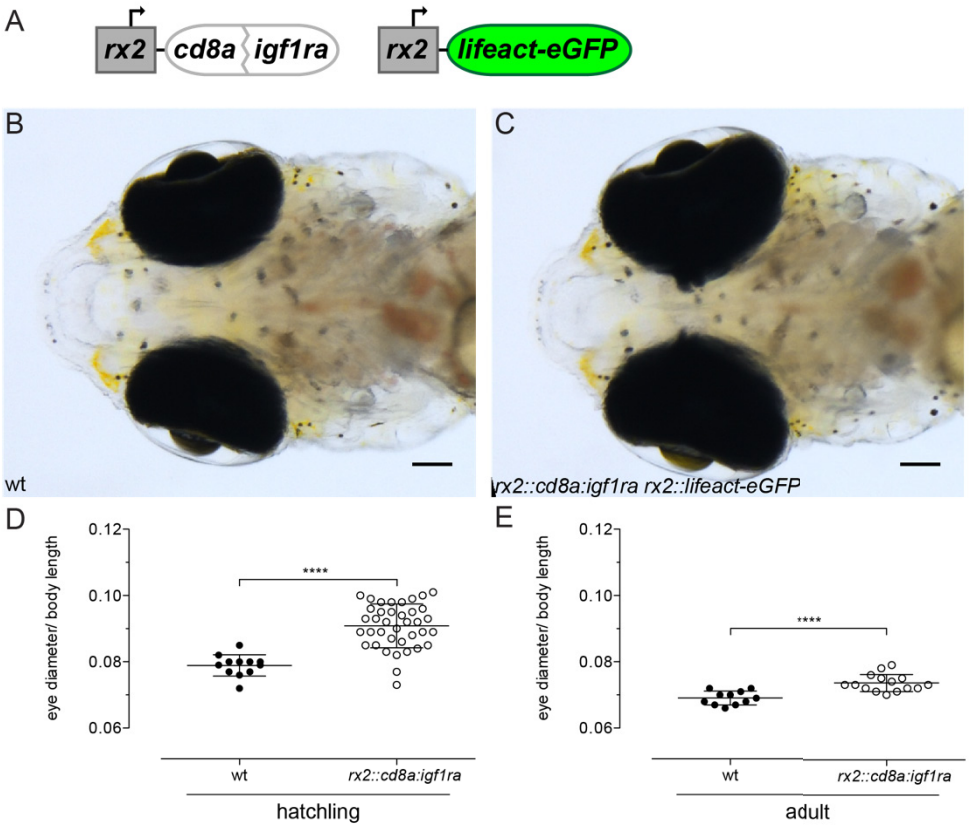

Figure 2.4: Constant activation of Igf1r in the Rx2 domain results in increased eye size.
(A) Schematic representation of the constructs used to generate transgenic *rx2::cd8a:igf1ra* fish. Extracellular and transmembrane domain of *cd8a* are fused to the intracellular domain of *igf1ra* to generate a constitutively active receptor variant (*cd8a:igf1ra*). *Rx2::lifeact-eGFP* was co-injected as indirect fluorescent readout. (B–C) Eye size of *rx2::cd8a:igf1ra* hatchlings (C) is larger compared to wt siblings (B). Scale bars are 100µm. (D–E) Quantification of relative eye size (eye diameter normalised to body length) of wt (D: n = 12; E: n = 11) and *rx2::cd8a:igf1ra* (D: n = 38; E: n = 15) hatchlings (D) and adults (E) (mean ± SD, ****P < 0.0001).

Quantification of relative eye size, meaning eye diameter normalised to total body length, confirmed a significant size increase of *rx2::cd8a:igf1ra* hatchling eyes (Figure 2.4D). For these measurement, whole batches were used and there was no selection for phenotype, separation into wildtype and

rx2::cd8a:igf1ra hatchlings was solely based on GFP expression. To raise new generations and for all experiments, however, hatchlings were screened and selected for considerable increase in eye size. The eye size difference persisted throughout postembryonic growth until adulthood, although the difference in relative eye size was less pronounced in 3-month old adults (Figure 2.4E). With the progression through postembryonic growth, average relative eye size decreased in both wildtype and *rx2::cd8a:igf1ra* fish, from 0.079 to 0.069 and 0.091 to 0.074, respectively (Figure 2.4D-E). To raise following generations of *rx2::cd8a:igf1ra* fish, one *rx2::cd8a:igf1ra* male was selected for outcrossing to wildtypic females and offspring was screened for high phenotypic penetrance.

2.1.4 Retinal enlargement stems from neuroretinal expansion through increase in cell number

Size increase of a tissue can arise due to different mechanisms of tissue expansion, for example increase in cell size or number, or stretching and increase in fluid or pressure. To elucidate the origin of the increase in eye size, I investigated this phenotype in transverse cryosections of wildtype and *rx2::cd8a:igf1ra* hatchlings. The increase in eye size of *rx2::cd8a:igf1ra* hatchlings originated from an expansion of the NR (Figure 2.5A–B). Interestingly, the overall retinal architecture of *rx2::cd8a:igf1ra* hatchlings was intact, meaning the stereotypical structure of the NR with the CMZ at the periphery and three nuclear and two plexiform layers in the differentiated part was undisturbed. Furthermore, the Rx2 expression pattern in the peripheral domain in the CMZ as well as in MG cells and PRCs was identical between wildtype and *rx2::cd8a:igf1ra* hatchling retinae (Figure 2.5A–B). To characterise this neuroretinal expansion in more detail, the thickness of the NR was measured in cryosections of *rx2::cd8a:igf1ra* and wildtype retinae. I measured the thickness of the retinal column in the peripheral but fully laminated region of the retina, along a line perpendicular to the IPL (Figure 2.5C–D). In both dorsal as well as ventral retina, retinal column thickness was increased by 20 µm on average (Figure 2.5E). To determine whether the expansion is due to enlarged cell size, I counted the number of nuclei in a 400 μm^2 region in the INL as an approximation for cell size. The number of nuclei was reasonably constant, ranging in between 31 and 40 with an average of 36 nuclei in both wildtype and *rx2::cd8a:igf1ra* retinae (Figure 2.5F).

To elucidate whether the increased thickness of the retinal column stems from one single layer or whether several or all layers are enlarged in *rx2::cd8a:igf1ra* retinae, I additionally analysed the thickness of all neuroretinal layers individually.

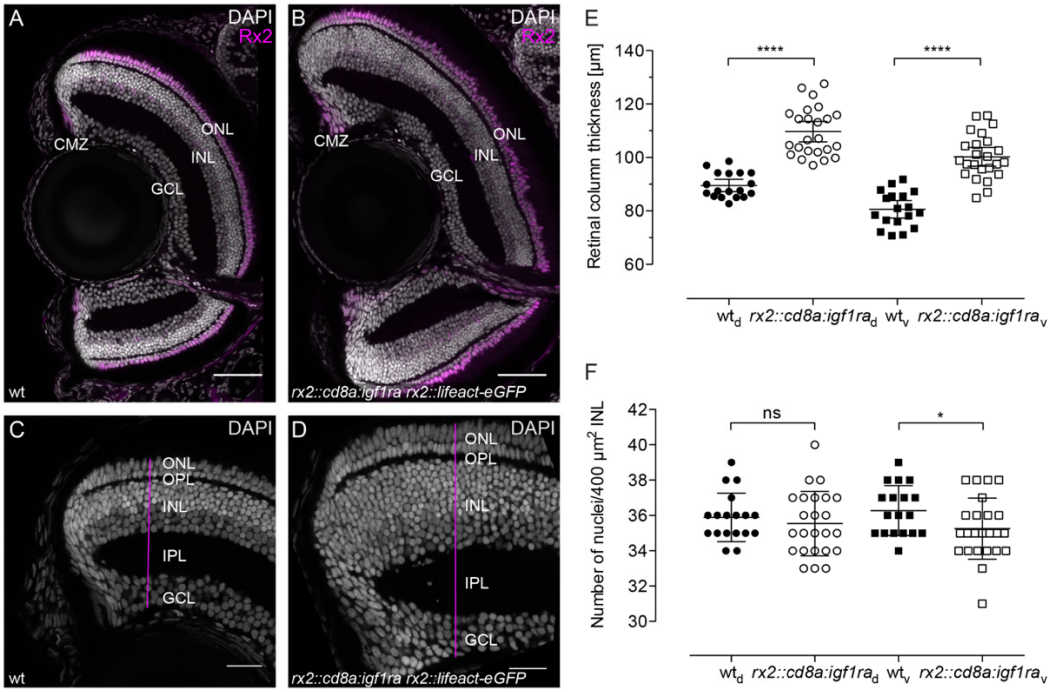

Figure 2.5: Retinal enlargement stems from neuroretinal expansion through increase in cell number.
(A–B) Cryosections of wt (A) and *rx2::cd8a:igf1ra* (B) retinae with staining against Rx2 (magenta) display neuroretinal expansion. Scale bars are 50 µm. (C–D) Thickness measurements were done along a line (magenta) perpendicular to the IPL. Thickness of the whole retinal column and all individual layers were measured in the laminated part close to the CMZ in wt (n = 18 sections from 12 retinae) and *rx2::cd8a:igf1ra* (n = 24 sections from 14 retinae) retinae. Scale bars are 20 µm. (E) Quantification of retinal column thickness shows increase in *rx2::cd8a:igf1ra* (n = 24 sections from 14 retinae) compared to wt (n = 18 sections from 12 retinae) retinae (mean ± SD, $^{****}P_{d/v} < 0.0001$). (F) Quantification of nucleus number per 400 µm² INL shows similar amounts in *rx2::cd8a:igf1ra* (n = 24 sections from 14 retinae) and wt (n = 18 sections from 12 retinae) retinae (mean ± SD, $^{ns}P_d = 0.5031$, $^{*}P_v = 0.0456$).

Quantification revealed that all nuclear layers and the OPL increased their width, with the most prominent expansion taking place in the INL (Figure 2.6A–E), accounting for 13–15 µm of the 20 µm increase in *rx2::cd8a:igf1ra* retinae. The IPL, however, did not increase its thickness, but decreased its width in the ventral but not the dorsal retina (Figure 2.6B).
Taken together, these data show that expression of *cd8a:igf1ra* in the Rx2 domain in the retina results in increased retinal size, and the enlargement

stems from a neuroretinal expansion through an increase in cell number rather than cell size.

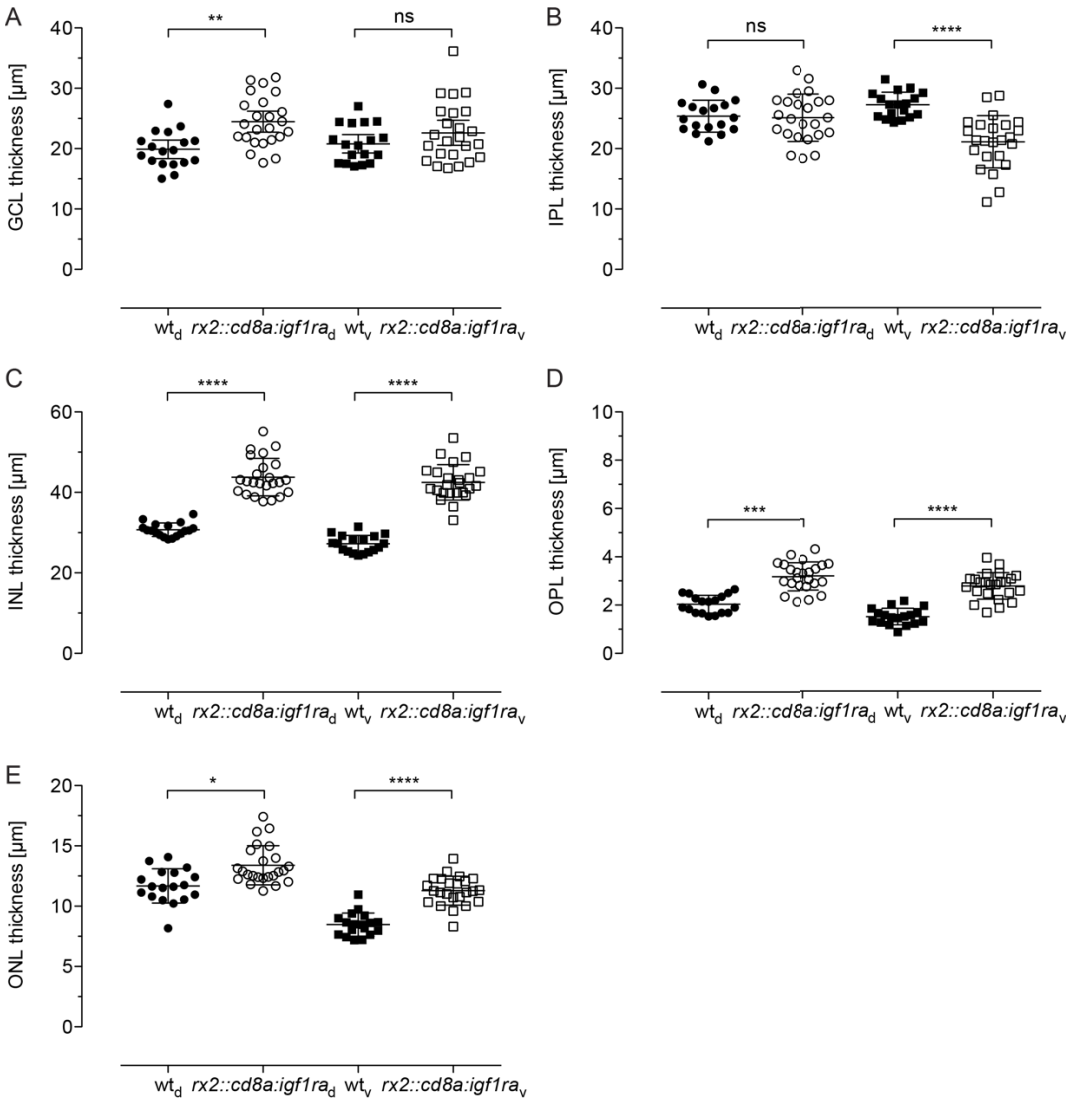

Figure 2.6: Neuroretinal thickness is increased throughout all nuclear layers. (A-E) Quantification of dorsal and ventral retinal layer thickness in *rx2::cd8a:igf1ra* (n = 24 sections from 14 retinae) compared to wt (n = 18 sections from 12 retinae) retinae (mean ± SD). Expansion of GCL in (A) (**$P_d = 0.0046$, $^{ns}P_v = 0.1744$), INL in (C) (****$P_{d/v} < 0.0001$), OPL in (D) (***$P_d = 0.0002$, ****$P_v < 0.0001$) and ONL in (E) (*$P_d = 0.0427$, ****$P_v < 0.0001$), but not IPL in (B) ($^{ns}P_d = 0.7863$, ****$P_v < 0.0001$) is evident.

2.1.5 *Cd8a:igf1ra* expression results in increased downstream signaling activation in the CMZ

A good measure for Igf1r signaling activity is the phosphorylation status of its downstream effector Akt. Studies in zebrafish have shown that abundance of phosphorylated Akt (pAkt) is reduced upon Igf1r inhibition by

morpholinos, dominant negative *igf1r* mRNA or small-molecule inhibitors (Chablais and Jazwinska, 2010; Schlueter et al., 2007a; 2006).

To address whether the Cd8:igf1ra fusion receptor induces downstream signal transduction via PI3K–Akt in the CMZ of the medaka retina I performed immunostainings against pAkt on cryosections. In retinae of wildtype hatchlings, faint pAkt was present in the peripheral domain in the CMZ (Figure 2.7A–A'), whereas in *rx2::cd8a:igf1ra* retinae pAkt staining covered a larger area and appeared brighter, overlapping with the *cd8a:igf1ra* expression domain (Figure 2.7B–B'''). Strong pAkt signal was also evident in PRCs, which express *cd8a:igf1ra* as well.

This establishes that ectopic expression of *cd8a:igf1ra* is indeed able to activate the PI3K–Akt signaling cascade downstream of Igf1r in the CMZ of medaka.

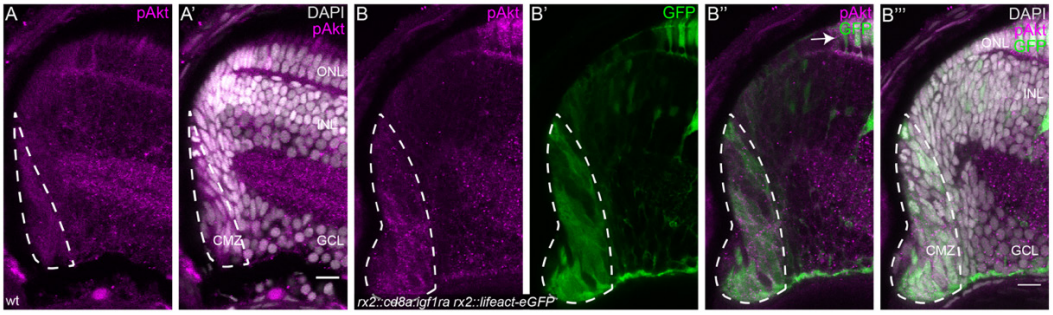

Figure 2.7: *Cd8a:igf1ra* expression results in increased downstream signaling activation in the CMZ.

(A-B''') Cryosections of wt (A-A') and *rx2::cd8a:igf1ra* (B-B''') retinae. The pAkt-positive domain (magenta, dashed lines) is enlarged in *rx2::cd8a:igf1ra* (B-B''') compared to wt (A-A') retinae, co-localising with GFP signal (green) also in PRCs (arrow) (B-B'''). Scale bars are 10 µm.

2.1.6 Over-activated Igf1r signaling decreases cell cycle length

Igf1r signaling is known to influence cell cycle progression. This was shown in different models and contexts, both *in vitro* as well as *in vivo*. In cultured murine spermatogonial stem cells, IGF1R inhibition lead to cell cycle arrest and reduced proliferation, whereas stimulation with IGF1 promoted G2/M cell cycle progression (Wang et al., 2015). In zebrafish embryos, *igf1r* morpholino injection lead to defects at the G1/S transition resulting in growth retardation and ultimately developmental arrest (Schlueter et al., 2007a).

Therefore, I next determined cell cycle and S phase length of the retinal progenitor population in wildtype and *rx2::cd8a:igf1ra* hatchlings.

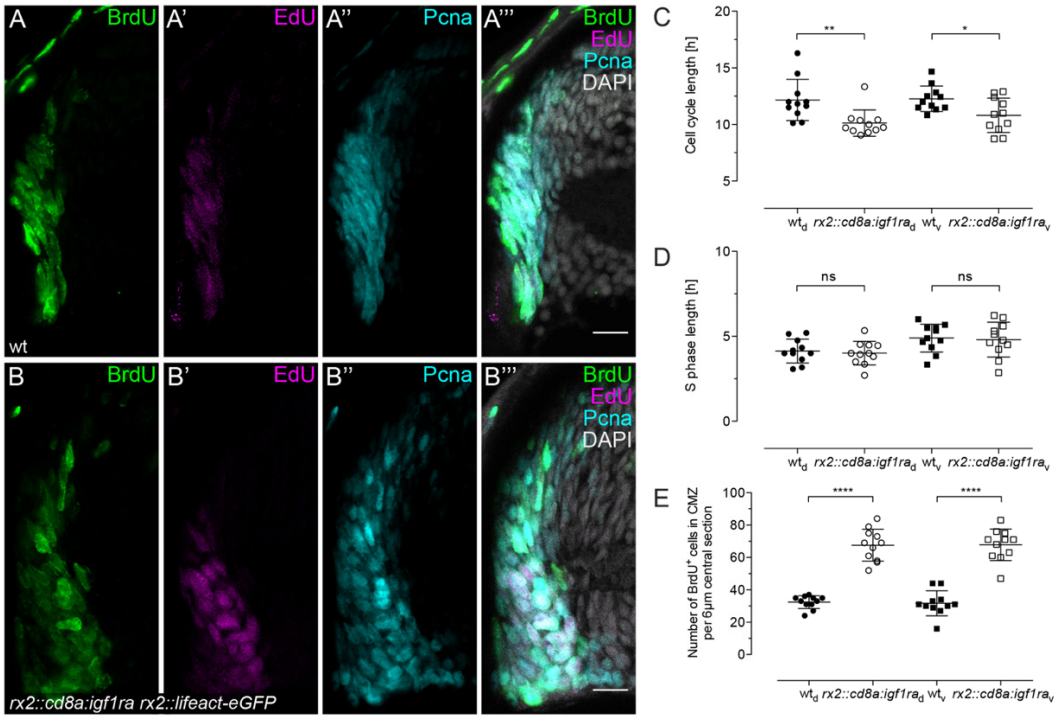

Figure 2.8: Constant activation of Igf1r signaling decreases cell cycle length of RPCs.

(A–B''') Cryosections of wt (A–A''') and *rx2::cd8a:igf1ra* (B–B''') retinae incubated for 2 h in BrdU and 30 min in EdU to determine cell cycle length. Staining against BrdU (green), EdU (magenta) and Pcna (cyan) show partial overlap in the CMZ. Scale bars are 10 µm. (C) Quantification of cell cycle length shows a reduction of 1–2 h in *rx2::cd8a:igf1ra* (n = 11 sections from 4 retinae) compared to wt (n = 11 sections from 4 retinae) retinae (mean ± SD, $^{**}P_d = 0.0053$, $^{*}P_v = 0.0188$). (D) Quantification of S phase length in *rx2::cd8a:igf1ra* (n = 11 sections from 4 retinae) compared to wt (n = 11 sections from 4 retinae) retinae (mean ± SD, $^{ns}P_d = 0.6764$, $^{ns}P_v = 0.8223$). S phase length is not altered in *rx2::cd8a:igf1ra* retinae. (E) Quantification of BrdU-positive cell number in the CMZ per 6 µm central section shows that numbers have more than doubled in *rx2::cd8a:igf1ra* (n = 11 sections from 4 retinae) compared to wt (n = 11 sections from 4 retinae) retinae (mean ± SD, $^{****}P_{d/v} < 0.0001$).

Previously, cell cycle and S phase length was investigated in the embryonic mouse retina using BrdU and EdU pulses and I performed the same experimental regime (Das et al., 2009; Klimova and Kozmik, 2014). Hatchlings were incubated in BrdU for 2 h, washed and incubated in EdU for 30 min before analysis. Immunostainings against BrdU, Pcna and EdU (Figure 2.8A–B''') allowed to quantify different fractions of single and double-positive cells, from which cell cycle and S phase length were calculated. In *rx2::cd8a:igf1ra* retinae, the cell cycle length was decreased from 12 h to 10.5

h on average (Figure 2.8C), whereas S phase length was constant with an average duration of 4.5 h (Figure 2.8D). Moreover, in *rx2::cd8a:igf1ra* compared to wildtype retinae, the number of BrdU-positive cells in the CMZ was more than doubled (Figure 2.8E).

Taken together, these data show that in *rx2::cd8a:igf1ra* retinae, more cells in the CMZ go through the cell cycle with increased speed, thereby amplifying retinal cell numbers resulting in increased retinal size.

2.1.7 Cndp1 is expressed in retinal stem cells in the peripheral CMZ and in the choroid plexi

Since Rx2 is expressed in both retinal stem and progenitor cells, it is impossible to untangle which cell population in the CMZ is responsible for the amplification of cell numbers in *rx2::cd8a:igf1ra* fish. Up until now, several genes and their specific expression domain in the CMZ of the medaka retina have been identified and characterised (Reinhardt et al., 2015), however a reporter for stem cells only was not available so far.

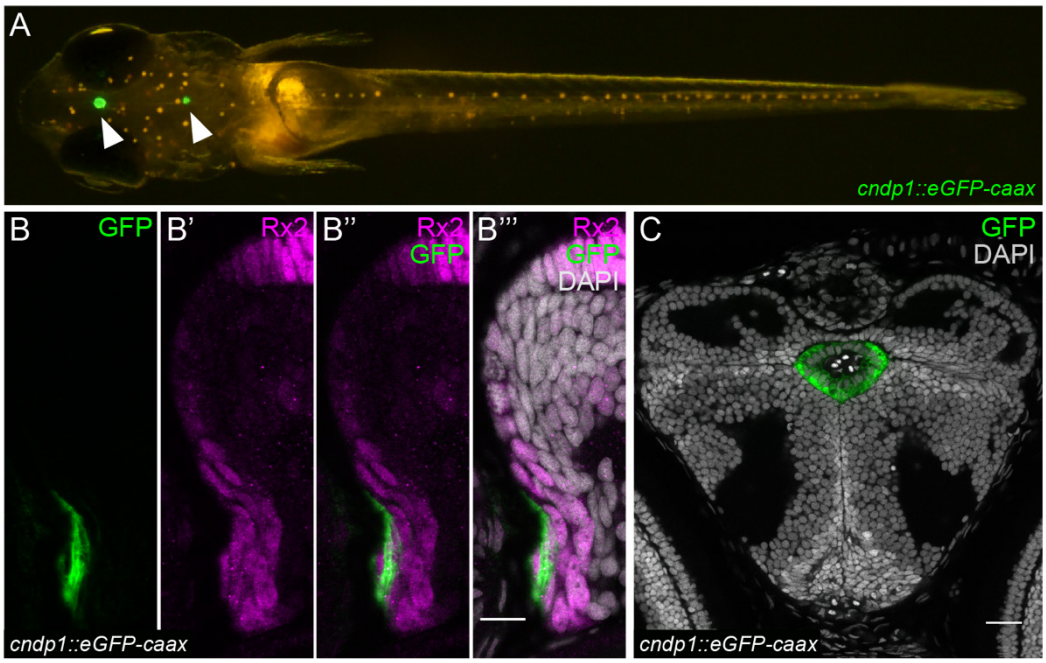

Figure 2.9: *Cndp1* is expressed in the CMZ and the choroid plexi.
(A) *Cndp1::eGFP-caax* hatchling shows GFP expression in the choroid plexi in the brain (arrowheads). (B-B''') Cryosection of a *cndp1::eGFP-caax* hatchling retina with staining against GFP (green) in a peripheral subset of the Rx2 (magenta) domain in the CMZ. Scale bar is 10 µm. (C) Cryosection of a *cndp1::eGFP-caax* hatchling brain. The diencephalic choroid plexus is positive for GFP (green). Scale bar is 20 µm.

The first neuroretinal stem cell marker, *ccl25b*, was recently characterised in the lab (Eggeler, 2017; Said, 2016). *Ccl25b* is widely expressed throughout the whole medaka hatchling, which is disadvantageous for genetic manipulation. Previous experiments in the lab presented *cndp1* as promising candidate with a restricted retinal expression domain (Haas, Centanin, B. Wittbrodt & J. Wittbrodt, unpublished data).Therefore, I characterised the 5 kb promoter region upstream of *cndp1* by generating two reporter lines. Macroscopically, expression of *cndp1::eGFP-caax* in medaka hatchlings was visible only in the retina and the choroid plexi in the brain (Figure 2.9A). I validated this expression pattern microscopically by performing immunostainings on cryosections of *cndp1::eGFP-caax* hatchlings. In the retina, *cndp1::eGFP-caax* was expressed exclusively in a small, peripheral subset of Rx2-positive cells in the peripheral CMZ (Figure 2.9B–B'''). Both diencephalic and myelencephalic choroid plexus were also GFP-positive (Figure 2.9C), and GFP signal was not detected in any other tissue. The *cndp1::H2A-mCherry* reporter had an identical expression pattern to the *cndp1::eGFP-caax* reporter, which I validated by crossing both reporters and performing immunostainings on cryosections (data not shown).

In 2-month old adult fish, *cndp1::eGFP-caax* expression was still restricted to retina and choroid plexi. The CE, which is connected to the CMZ in juvenile and adult fish, was Rx2- and GFP-positive as well (Figure 2.10A–A'''). Within the CMZ and corresponding to the hatchling expression pattern, GFP signal was visible in a Rx2 subdomain conjoined with the proximal part of the CE (Figure 2.10B–B''').

To assess the lineage relation and proliferative potential of *cndp1*-expressing cells in the CMZ, I employed lineage tracing. As the Gaudí^{RSG} line is a well-established tool in the lab (Centanin et al., 2014), I generated a construct where an inducible Cre^{ERT2} is expressed under the control of the *cndp1* promoter (Figure 2.11A). Upon induction with Tamoxifen, the Cre is able to translocate to the nucleus, where it mediates recombination of the mCherry-flanking loxP sites, ultimately resulting in expression of H2B-eGFP which is inherited by all daughter cells (Centanin et al., 2014; Livet et al., 2007). The *cndp1::Cre^{ERT2}* plasmid was injected into 1-cell stage Gaudí^{RSG}-positive medaka embryos. Successfully injected embryos were identified by cardiac expression of the insertional marker *cmlc2::CFP* and

induced with Tamoxifen at hatch. After 2-3 weeks, fish were analysed for retinal GFP expression by whole-mount immunostaining (Figure 2.11B).

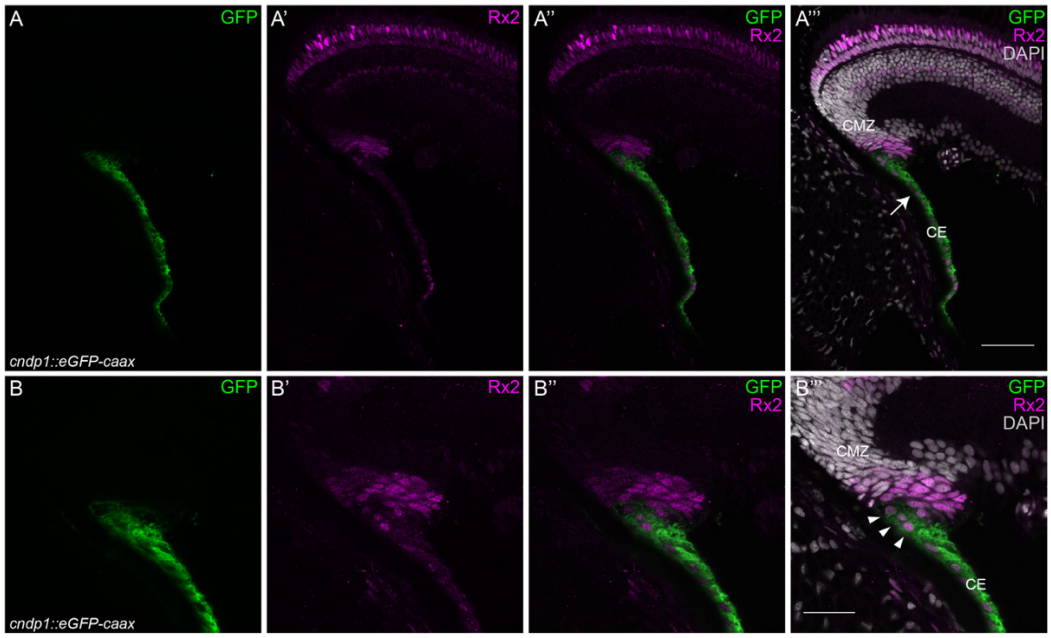

Figure 2.10: The *cndp1::eGFP-caax* reporter drives expression in the peripheral retina throughout life.
(A-A''') Cryosection of *cndp1::eGFP-caax* retina at adult stage. The CE is GFP-positive (green) (arrow). Scale bar is 50 µm. (B-B''') Cryosection of *cndp1::GFP-caax* retina at adult stage at higher magnification. In the CMZ, *cndp1*-driven GFP expression is restricted to a subset of Rx2-positive cells (magenta) (arrowheads). Scale bar is 25 µm.

Retinae displayed GFP-positive clones that originated in the CMZ and were continuous to the differentiated retina (Figure 2.11C–C'), while also extending into the CE. The clones were induced arched continuous stripes (iArCoSs, (Centanin et al., 2014)) and labelled cells in all three nuclear layers (Figure 2.11D–D'). Interestingly, I also observed one clone in the RPE (Figure 2.11E–E').Taken together, *cndp1* is expressed throughout postembryonic growth in a restricted domain in the retina and in the choroid plexi, which makes it a good candidate for promoter-driven genetic manipulation. To functionally validate the potential of *cndp1*-expressing cells, I performed lineage tracing experiments, which confirmed that these cells are indeed multipotent retinal stem cells.

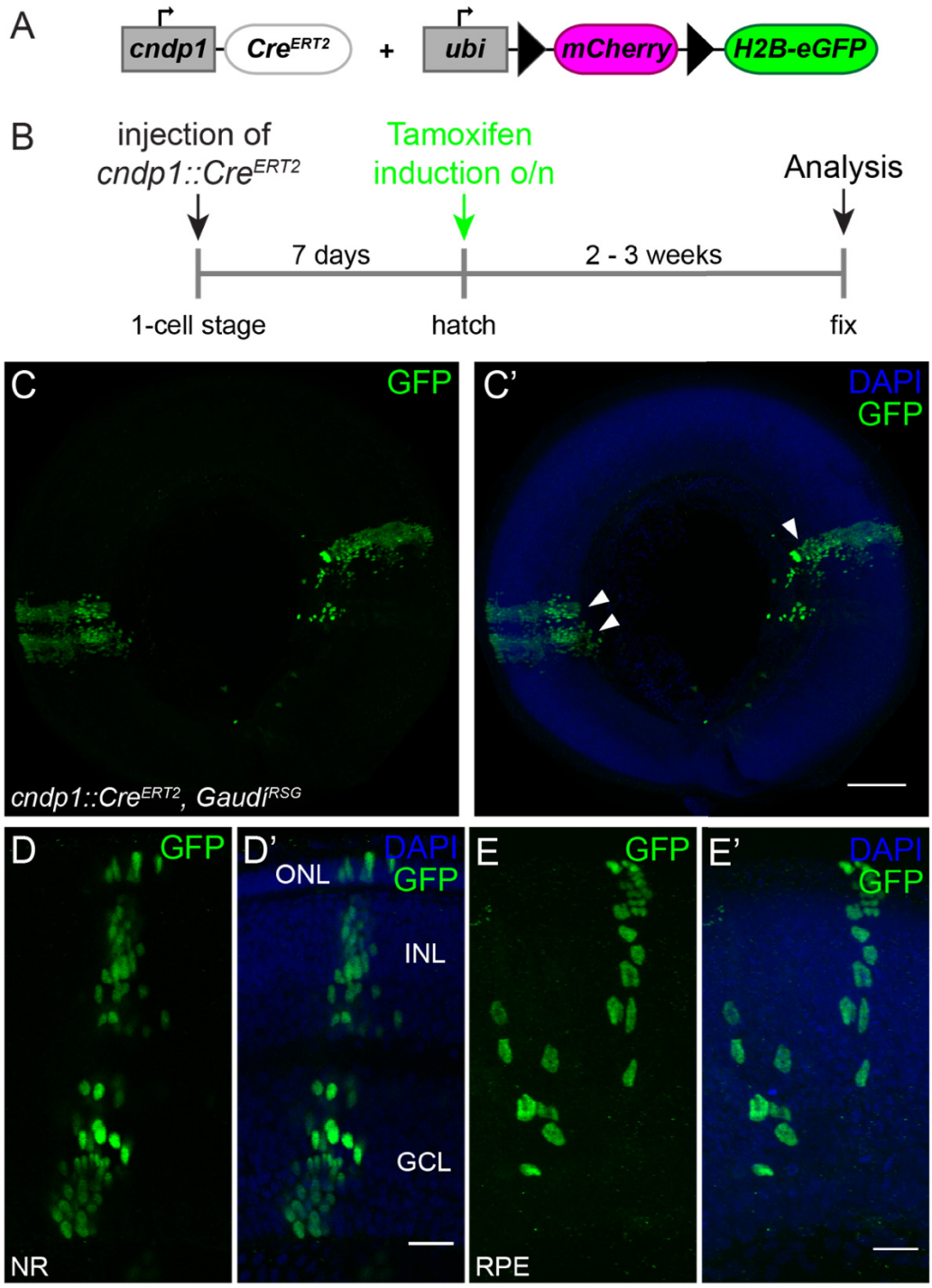

Figure 2.11: *Cndp1*-expressing cells are multipotent retinal stem cells.
(A) Schematic representation of the constructs used for lineage tracing. Upon tamoxifen induction, *mCherry* will be floxed out and *H2B-eGFP* will be expressed in Gaudí^{RSG} fish. (B) Experimental outline: *cndp1::Cre^{ERT2}* is injected in 1-cell stage Gaudí^{RSG} embryos. At hatch, fish are incubated in Tamoxifen overnight and grown for 2 - 3 weeks before analysis. (C-E') Whole-mount immunostainings of *cndp1::Cre^{ERT2}*, Gaudí^{RSG} retinae against GFP (green) with neuroretinal clones labelling the whole retinal column (D-D') and extending into the CE, originating from multipotent neuroretinal stem cells (arrowheads) (n = 7 clones in 3 retinae), and a RPE clone (E–E') (n = 1 clone in 3 retinae). Scale bars are 100 µm (C-C') and 20 µm (D-E').

2.1.8 The retinal progenitor but not stem cell population is amplified by Igf1r signaling over-activation

After the establishment of *cndp1* as stem-cell specific marker, I next addressed which cell population in the CMZ was responsible for the amplification of cell numbers in *rx2::cd8a:igf1ra* hatchlings. To tackle this question, I made use of two different marker genes with specific expression domains in different retinal stem and progenitor cell populations. I used the *cndp1::H2A-mCherry* reporter line to identify retinal stem cells, and the Rx2 antibody to label both retinal stem and progenitor cells (Reinhardt et al., 2015).

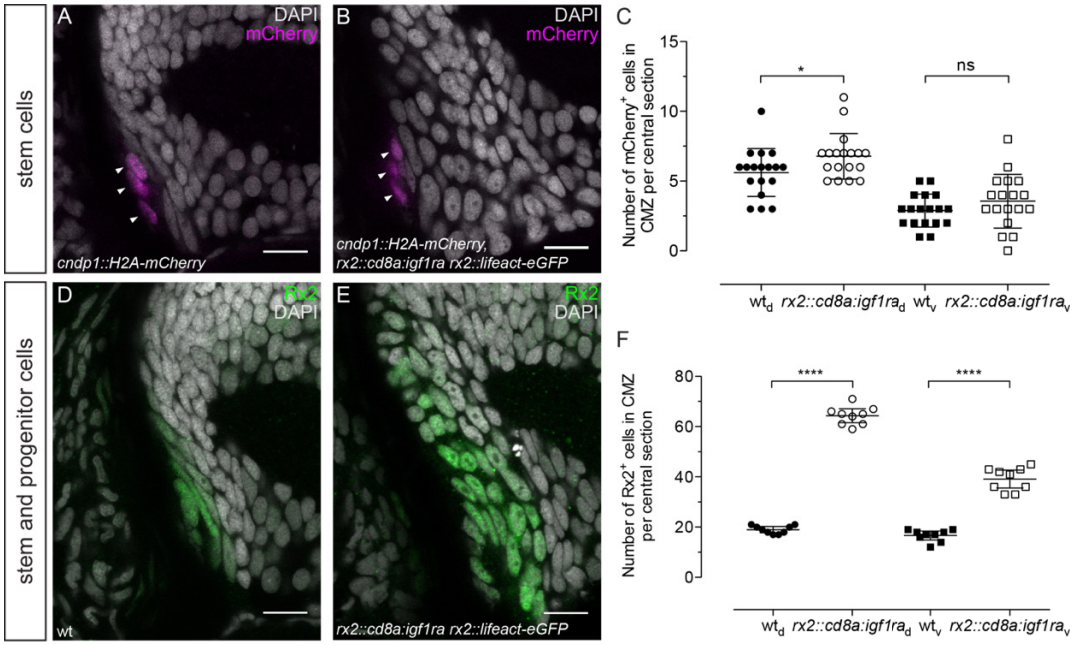

Figure 2.12: Constant activation of Igf1r signaling amplifies retinal progenitor cell numbers.

(A-B) Cryosections of wt (A) and *rx2::cd8a:igf1ra* (B) *cndp1::H2A-mCherry* reporter retinae. mCherry (magenta) is visible in peripheral-most cells in the CMZ (arrowheads). (C) Quantification of H2A-mCherry-positive cell number in the CMZ of central sections does not indicate an expansion of cndp1-expressing stem cells in *rx2::cd8a:igf1ra* (n = 18 sections from 6 retinae) compared to wt (n = 18 sections from 6 retinae) retinae (mean ± SD, $^{*}P_{d} = 0.0442$, $^{ns}P_{v} = 0.2177$). (D-E) Cryosections of wt (D) and *rx2::cd8a:igf1ra* (E) retinae. Rx2 staining (green) marks peripheral cells in the CMZ. (F) Quantification of Rx2-positive cell number in the CMZ of central sections demonstrates that Rx2-positive stem and progenitor cells have more than doubled in *rx2::cd8a:igf1ra* (n = 9 sections from 6 retinae) compared to wt (n = 9 sections from 6 retinae) retinae (mean ± SD, $^{****}P_{d/v} < 0.0001$).

To assess the number of *cndp1*-expressing stem cells, I performed immunostainings on cryosections of wildtype and *rx2::cd8a:igf1ra* hatchlings positive for the *cndp1::H2A-mCherry* reporter (Figure 2.12A–B). In both wildtype and *rx2::cd8a:igf1ra* retinae the number of mCherry-positive stem

cells per section was low, ranging in between 0 and 11. Stem cell numbers were rather stable, with a very slight increase in *rx2::cd8a:igf1ra* retinae (Figure 2.12C). In contrast to that, immunostainings on cryosections displayed an expansion of the Rx2 domain in *rx2::cd8a:igf1ra* versus wildtype hatchlings (Figure 2.12D–E). Quantification confirmed that the Rx2-positive stem and progenitor cell population in the CMZ was more than doubled in *rx2::cd8a:igf1ra* compared to wildtype retinae, from an average of 18 Rx2-positive cells in wildtype to 64 cells in the dorsal and 39 in the ventral CMZ of *rx2::cd8a:igf1ra* retinae (Figure 2.12F).
These results demonstrate that the progenitor but not the stem cell population in the CMZ is amplified by Igf1r signaling over-activation.

2.1.9 Expression of *cd8a:igf1ra* in RSCs does not result in increased eye size

In contrast to progenitor cells, the stem cell population in *rx2::cd8a:igf1ra* hatchlings is not enlarged. Possible reasons for this could be that the lack of stem cell expansion is specific to *rx2::cd8a:igf1ra* hatchlings or that retinal stem cells are not susceptible to increased proliferation upon *igf1r* expression. To investigate this further, I generated a transgenic line where *cd8a:igf1ra* expression is under the control of the *cndp*1 promoter, hence only stem cells will express the constitutively active *igf1ra* variant. Together with the *cndp1::cd8a:igf1ra* construct, I co-injected *cndp1::H2B-eGFP* as indirect fluorescent readout, and to obtain a line that is well-comparable to the *rx2::cd8a:igf1ra* line. I analysed the morphology and GFP expression pattern by immunostaining on cryosections of wildtype *cndp1::H2B-eGFP* and *cndp1::cd8a:igf1ra cndp1::H2B-eGFP* hatchlings. The choroid plexi were enlarged in *cndp1::cd8a:igf1ra* compared to wildtype hatchlings (Figure 2.13A–B), indicating that the construct is functional. The size of the GFP expression domain in the CMZ was however unaltered (Figure 2.13C). To substantiate the observation that expression of *cd8a:igf1ra* in *cndp1*-expressing retinal stem cells does not lead to increased eye size, I raised two independent lines from different founders and quantified relative eye size at hatch. Neither *cndp1::cd8a:igf1ra* line displayed an alteration in relative eye size compared to its wildtype siblings (Figure 2.13D–D').
These results show that the *cndp1*-expressing retinal stem cell population is not able to expand upon Igf1r signaling over-activation. This further

substantiates the previous findings that only the progenitor but not stem cell population is amplified in *rx2::cd8a:igf1ra* retinae.

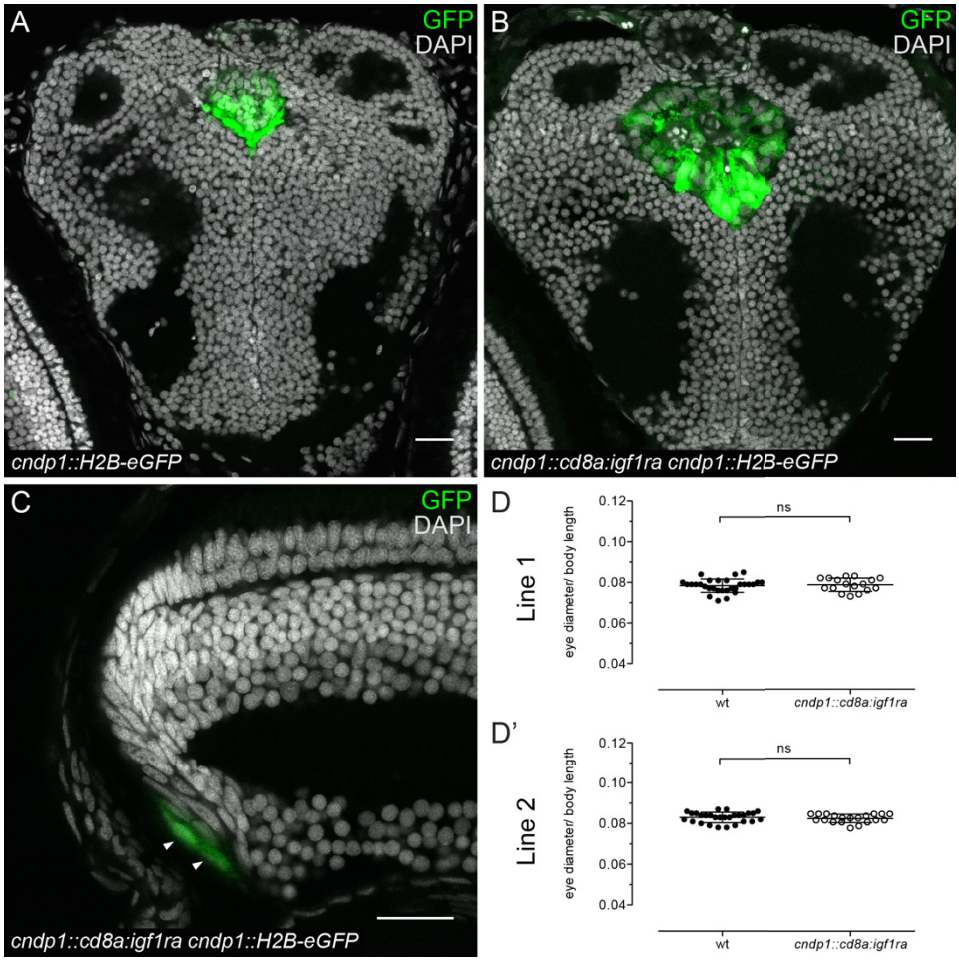

Figure 2.13: Expression of *cd8a:igf1ra* in RSCs does not result in increased eye size.

(A-C) Cryosections of wt (A) and *cndp1::cd8a:igf1ra* (B-C) *cndp1::H2B-eGFP* reporter hatchlings. The choroid plexi are positive for nuclear GFP (green) and enlarged in *cndp1::cd8a:igf1ra* (B) compared to wt (A) brains. *Cndp1*-driven GFP expression (green, arrowheads) in the CMZ of *cndp1::cd8a:igf1ra* hatchlings (C) is not expanded. Scale bars are 20 µm. (D-D') Quantification of relative eye size (eye diameter normalised to body length) of wt (D: n = 29; D': n = 28) and *cndp1::cd8a:igf1ra* (D: n = 17; D': n = 20) hatchlings derived from two different founders (mean ± SD, $^{ns}P_{D} = 0.7457$, $^{ns}P_{D'} = 0.7590$).

2.1.10 Expression of *GFP-kras^{12V}* in retinal stem and progenitor cells does not result in increased eye size

In retinal progenitor cells, Igf1r signaling is able to increase the amount and speed of proliferation. In order to assess whether this feature is inherent to Igf1r signaling specifically or whether the same effect can be observed by substituting *cd8a:igf1ra* for another mitogen, I generated transgenic *rx2::eGFP-kras^{12V}* fish. Oncogenic Kras variants are potent mitogens that are

used to induce tumorigenesis in zebrafish cancer models for rhabdomyosarcoma, brain tumours and hepatocellular and pancreatic carcinoma (Ju et al., 2015; Nguyen et al., 2012; Park et al., 2008; Storer et al., 2013). In *rx2::eGFP-kras^{12V}* fish, an oncogenic, constitutively active version of *kras* fused to GFP (*eGFP-kras^{12V}*, (Mayrhofer et al., 2017)) was expressed under the control of the *rx2* promoter. Two independent lines were raised from different founders and assayed for expression pattern and relative eye size. I performed immunostainings on cryosections of *rx2::eGFP-kras^{12V}* hatchlings, where *GFP-kras^{12V}* expression was visible in the CMZ, MG cells and PRCs (Figure 2.14A–A'). However, retinal morphology was unaltered.

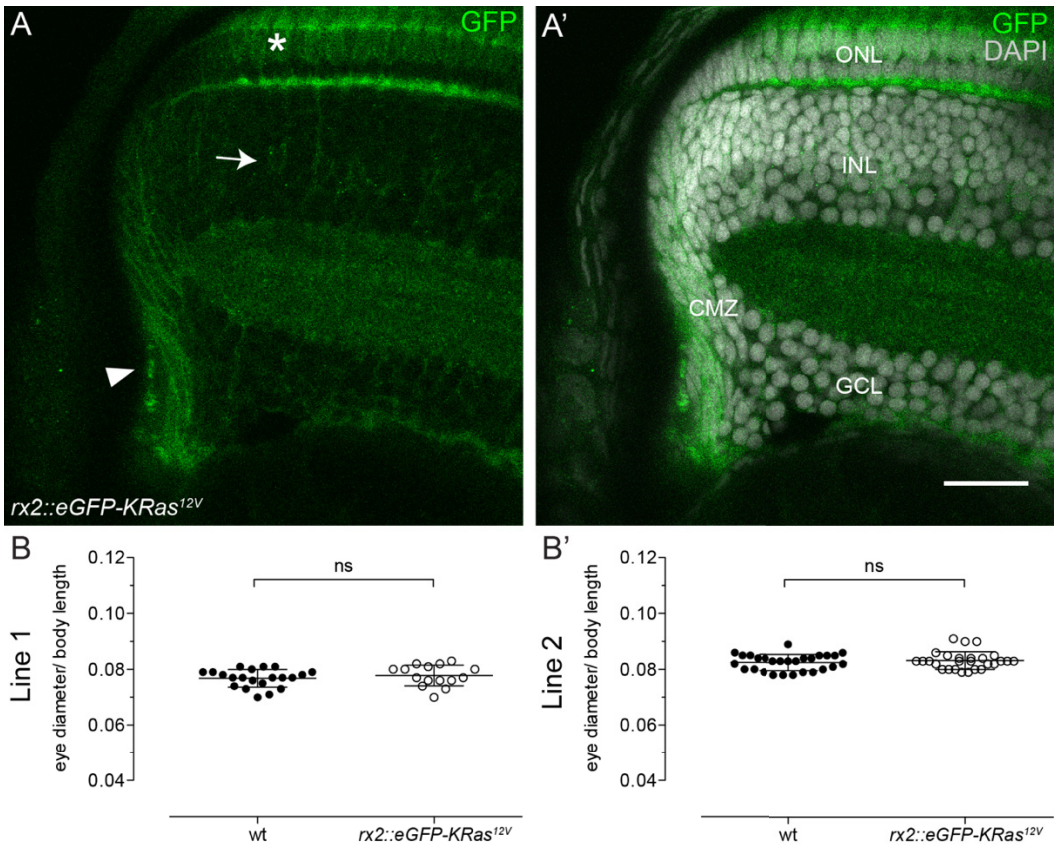

Figure 2.14: Expression of *GFP-kras^{12V}* as mitogen in the Rx2 domain does not result in increased eye size.

(A–A') Cryosection of *rx2::eGFP-kras^{12V}* hatchling retina. Expression of the GFP-KRas^{12V} fusion protein (green) is visible in the CMZ (arrowhead), MG cells (arrow) and PRCs (asterisk). Scale bar is 20 µm. (B–B') Quantification of relative eye size (eye diameter normalised to body length) of wt (B: n = 21; B': n = 28) and *rx2::eGFP-KRas^{12V}* (B: n = 15; B': n = 27) hatchlings derived from two different founders (mean ± SD, $^{ns}P_B$ = 0.3976, $^{ns}P_{B'}$ = 0.3814).

Quantification of relative eye size in hatchlings of the two *rx2::eGFP-kras*^{12V} lines and wildtype siblings confirmed that eye size did not increase in either line (Figure 2.14B–B').

This indicates that eye size cannot easily be modulated by any mitogen, at least not by the GFP-Kras^{12V} variant used here. Furthermore, these results confer some specificity to the ability of Igf1r signaling in controlling the expansion of the retinal progenitor population.

2.1.11 Neuropil area in the optic tectum is enlarged but tectal proliferation is not affected

The visual system is a specific part of the central nervous system responsible for sensing and processing of visual stimuli. Eye and optic tectum form a functional unit, and impairment of the eyes or differential environmental conditions result in subsequent changes in the contralateral optic tectum (Hall and Tropepe, 2018; Raymond et al., 1983). For instance, eye enucleation reduces tectal proliferation in goldfish, whereas after optic nerve crush proliferation is first reduced and then increased upon reinnervation (Raymond et al., 1983). While the eye and specifically the retina is the sensory organ of the system, the optic tectum is the corresponding processing unit which receives visual input via retinotectal axons of the RGCs. The optic tectum comprises two distinct structures, the neuropil which is innervated by the retinotectal projections, and the periventricular grey zone (PGZ) where tectal neurons reside and are generated at the medial and lateral proliferation zones (Alunni et al., 2010; Hall and Tropepe, 2018; Nguyen et al., 1999; Raymond and Easter, 1983).

To evaluate whether the increased retinal size of *rx2::cd8a:igf1ra* hatchlings results in morphological or proliferative modifications in the optic tectum, neuropil area innervated by RGCs as well as number of proliferative cells in the medial and lateral PGZ niches were examined. By injecting DiI into the eyes of fixed wildtype and *rx2::cd8a:igf1ra* hatchlings, RGC axons were labelled and their position and area coverage in the optic tectum analysed (Figure 2.15A–B). The arborisation area of retinotectal axons was quantified in 2D on maximum projections of Z-stacks covering the whole neuropil. In *rx2::cd8a:igf1ra* tecti, the innervated area was increased by 16 % compared to wildtype siblings (Figure 2.15C). To assess the proliferative activity in the PGZ, wildtype and *rx2::cd8a:igf1ra* hatchlings were incubated in BrdU for

2 h and fixed 30 min later. BrdU-positive cells were located in the medial and lateral proliferative zones of the PGZ (Figure 2.15D–D'). The number of BrdU-positive cells in both niches was not significantly altered in *rx2::cd8a:igf1ra* versus wildtype hatchlings (Figure 2.15E).

Taken together, these results show that even though the arborisation area of retinotectal projections is enlarged in *rx2::cd8a:igf1ra* hatchlings, proliferation in the medial and lateral PGZ niches is unaffected.

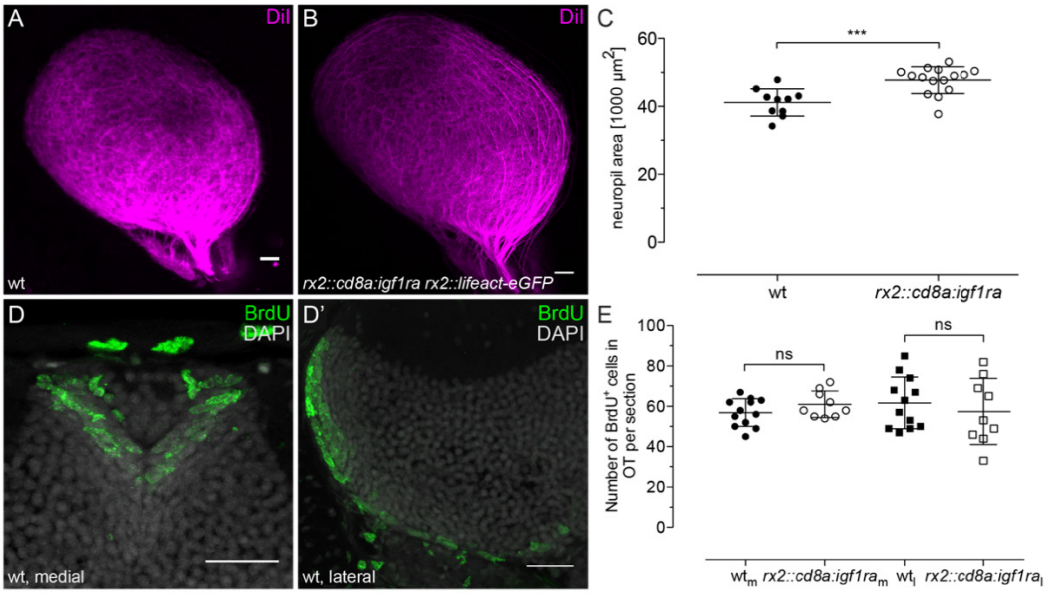

Figure 2.15: Neuropil area in the optic tectum is enlarged but proliferation is not increased.

(A–B) Fixed wt (A) and *rx2::cd8a:igf1ra* (B) hatchlings were injected with DiI (magenta) into the eye and optic tectum was imaged 2 days later. Scale bar is 20 µm. (C) Quantification of DiI-positive neuropil area in 2D in the optic tectum of wt (n = 10) and *rx2::cd8a:igf1ra* (n = 15) hatchlings. Neuropil area is increased in *rx2::cd8a:igf1ra* fish (mean ± SD, ***P = 0.0005). (D–D') Cryosections of medial (D) and lateral (D') proliferative zones in the optic tectum. Hatchlings were incubated in BrdU for 2 h prior to fixation. BrdU-positive (green) cells are located at the medial and lateral side of the periventricular grey zone. Scale bars are 20 µm. (E) Quantification of BrdU-positive cells per section in medial and lateral proliferative zones of the optic tectum in wt (n = 12 sections from 4 fish) and *rx2::cd8a:igf1ra* (n = 9 sections from 3 fish) hatchlings ($^{ns}P_m = 0.1878$, $^{ns}P_l = 0.5141$).

2.2 Dynamic interplay of retinal stem cells with immune cells

Experiments and hypotheses presented in this part were designed in collaboration with Katharina Lust, with experiments generating the following results being performed by me.

2.2.1 The *ccl25b–ccr9a* ligand–receptor pair is expressed in stem cells and immune cells in the retina

Stem cells have characteristic features such as constant proliferation and active stemness signaling networks. Cancer cells also display many stem cell characteristics; even though stem cells in the teleost retina undergo constant cell divisions, hyperplastic growth or morphological alterations are rarely observed. We therefore hypothesised that the retinal stem cell niche could be under surveillance of a control system which removes aberrant as well as dying cells. We therefore focused our attention on the immune system and investigated the expression of chemokines and receptors as well as the localisation of immune cells in the CMZ.

The expression domains of the medaka *ccl25* chemokines and their cognate *ccr9* receptors were previously investigated by a master student in the lab (Said, 2016). The ligand *ccl25b* as well as the receptor *ccr9a* were found to be expressed in different parts of the hatchling retina, with *ccl25b* showing a highly specific expression domain in the CMZ. Furthermore, another master student demonstrated by Cre/loxP-mediated lineage tracing that *ccl25b*-expressing cells in the CMZ are multipotent neuroretinal stem cells (Eggeler, 2017).

To examine *ccl25b* and *ccr9a* ligand–receptor expression domains with regard to each other, I established the transgenic double reporter line *ccr9a::eGFP*, *ccl25b::H2B-RFP* and performed immunostainings against GFP and RFP on cryosections of hatchling retinae. *Ccl25b*-driven RFP expression was restricted to few cells in the most peripheral part of the CMZ resembling the *cndp1* expression domain, while *ccr9a*-driven GFP expression was visible in MG cells and in cells in the CMZ close to the *ccl25b* domain (Figure 2.16A–A'''').

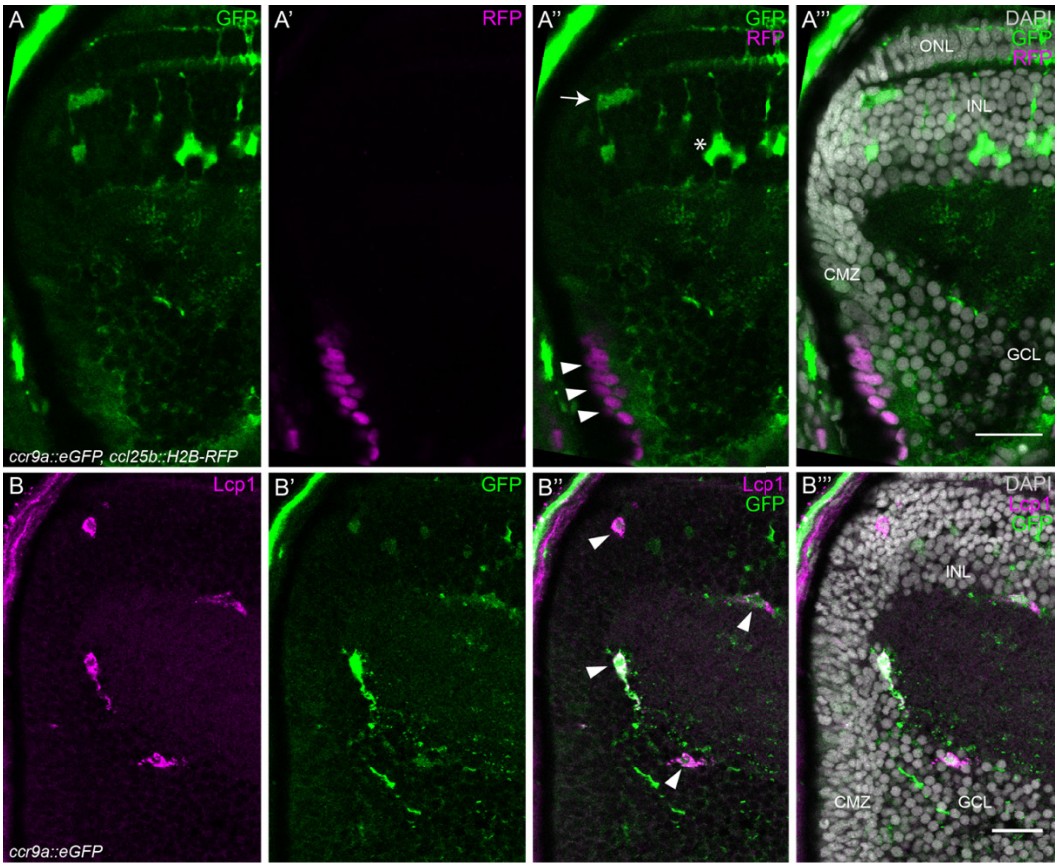

Figure 2.16: The *ccl25b*–*ccr9a* ligand-receptor pair is expressed in stem cells and immune cells in the retina, respectively.
(A–A''') Cryosection of a *ccr9a::eGFP*, *ccl25b::H2B-RFP* hatchling retina. *Ccl25b*-driven H2B-RFP expression is located in the peripheral CMZ (magenta, arrowheads). *Ccr9a*-driven GFP expression (green) is visible in single immune-like cells near the CMZ (arrow) as well as in MG cells in the INL (asterisk). (B–B''') Cryosection of a *ccr9a::eGFP* hatchling retina. Lcp1 staining (magenta) overlaps with *ccr9a*-driven GFP expression (green) (arrowheads) (n = 307/316 Lcp1-positive cells are GFP-positive in 53 sections from 8 retinae). Scale bars are 20 µm.

The GFP-positive cells close to the CMZ displayed a non-neuronal, immune cell-like morphology. To confirm that these cells are indeed immune cells, I performed immunostainings on *ccr9a::eGFP* hatchling retinae against lymphocyte cytosolic protein 1 (Lcp1), which is expressed in cells of the leukocyte lineage, specifically in macrophages and monocytes (Figure 2.16B–B''') (Herbomel et al., 1999; 2001; Jones et al., 1998). Of all Lcp1-positive cells in the retina, 97% were also GFP-positive. Double positive cells were predominantly located in or close to the CMZ, validating that this population of *ccr9a*-expressing cells are in fact immune cells.

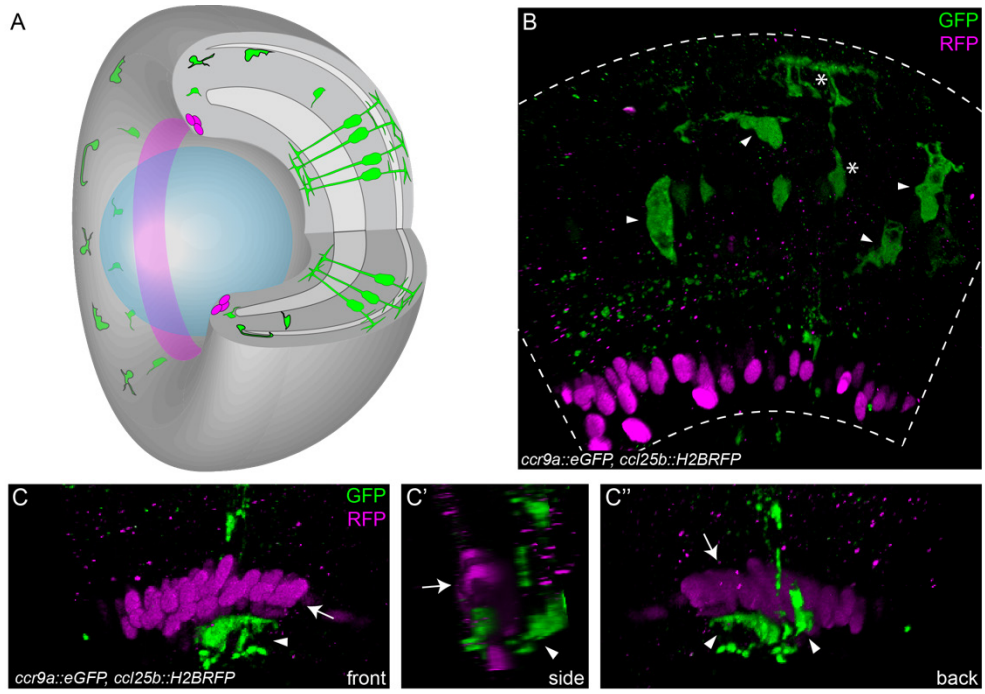

Figure 2.17: Ccr9a-positive immune cells form a network close to the retinal stem cell niche.
(A–B) Schematic drawing (A) and 3D projection (B) of a whole-mount *ccl25b::H2B-RFP* (magenta), *ccr9a::eGFP* (green) hatchling retina, where *ccr9a*-positive immune cells (arrowheads) are located in the central CMZ. MG cells express *ccr9a::eGFP* as well (asterisks). (C–C'') 3D reconstruction of a whole-mount *ccr9a::eGFP*, *ccl25b::H2B-RFP* hatchling retina in front, side and back view, where a *ccr9a*-positive immune cell (arrowheads) is located close to *ccl25b*-positive RSCs (arrow).

To further determine the spatial relationship between *ccl25b*-positive retinal stem cells and *ccr9a*-positive immune cells I performed whole-mount immunostainings on *ccr9a::eGFP*, *ccl25b::H2B-RFP* hatchling retinae. I generated 3D datasets from these whole-mount retinae and investigated the localization of GFP- and RFP-positive cells in these. To summarize and visualize the different expression domains, I created a 3D schematic drawing of a hatchling retina containing *ccl25b*-expressing neuroretinal stem cells as well as *ccr9a*-expressing MG and immune cells (Figure 2.17A). A 3D projection of a whole-mount *ccr9a::eGFP*, *ccl25b::H2B-RFP* retina confirmed the expression pattern that was observed in cryosections, with the immune cells in the central part of the CMZ and *ccl25b* expression in few cells in the peripheral CMZ (Figure 2.17B). Moreover, in the 3D projection the immune cell morphology of *ccr9a*-positive cells with irregularly shaped cell bodies and processes extending in various directions was evident. In rare cases immune cells in direct contact with or very close proximity to the retinal stem cells were detected (Figure 2.17C–C'').

Taken together, these data show that *ccr9a*-positive cells in the retina are Lcp1-expressing immune cells, which are localized close to *ccl25b*-positive neuroretinal stem cells. Furthermore, the *ccr9a*-positive immune cells form a network around the retinal stem cell niche.

2.2.2 *Ccr9a*-positive immune cells contain phagosomes with RSC-derived material

An important function of immune cells, especially macrophages, is their capacity to phagocytose cell debris from apoptotic or otherwise damaged cells (McMenamin et al., 2019; Villani et al., 2019). The proximity of *ccr9a*-positive immune cells and *ccl25b*-positive retinal stem cells indicates that phagocytosis of dying *ccl25b*-positive stem cells during retinal homeostasis could take place. To test this hypothesis and detect stem cell-derived material in immune cells, I used a label retention strategy taking advantage of the long stability of H2B-tagged fluorophores in phagosome compartments (Villani et al., 2019). Whole-mount immunostaining against GFP and RFP in *ccr9a::eGFP*, *ccl25b::H2B-RFP* hatchling retinae enabled labeling RFP-expressing neuroretinal stem cells along with material derived from them. Indeed, some GFP-positive immune cells contained RFP-positive stem cell-derived material (Figure 2.18A–A'''). Quantifying number and localization of immune cells containing RFP-positive phagosomes showed that on average 21 GFP-positive cells per retina carried stem cell-derived phagosomes (Figure 2.18B). Furthermore, the distribution of cells with RFP-positive phagosomes was not equal around the retinal circumference but enriched in the anterior and posterior sides, with only few occurrences at the dorsal- and ventral-most positions (Figure 2.18B–C).

To assess the dynamics of immune cell and stem cell interactions as well as phagocytosis, *in vivo* imaging is needed. I had the opportunity to visit Leica Microsystems Germany for a demonstration of the two-photon Leica DIVE imaging setup, which allows multi-colour two-photon imaging. In collaboration with Karl-Heinz Körtje one *in vivo* time-lapse movie of a *ccr9a::eGFP*, *ccl25b::H2B-RFP* hatchling was acquired. In the movie, one *ccr9a*-expressing immune cell actively transported an RFP-positive phagosome through the retina, within 40 min the phagosome together with part of the cell body had moved approximately 10 µm away from the original location (Figure 2.19A–A''').

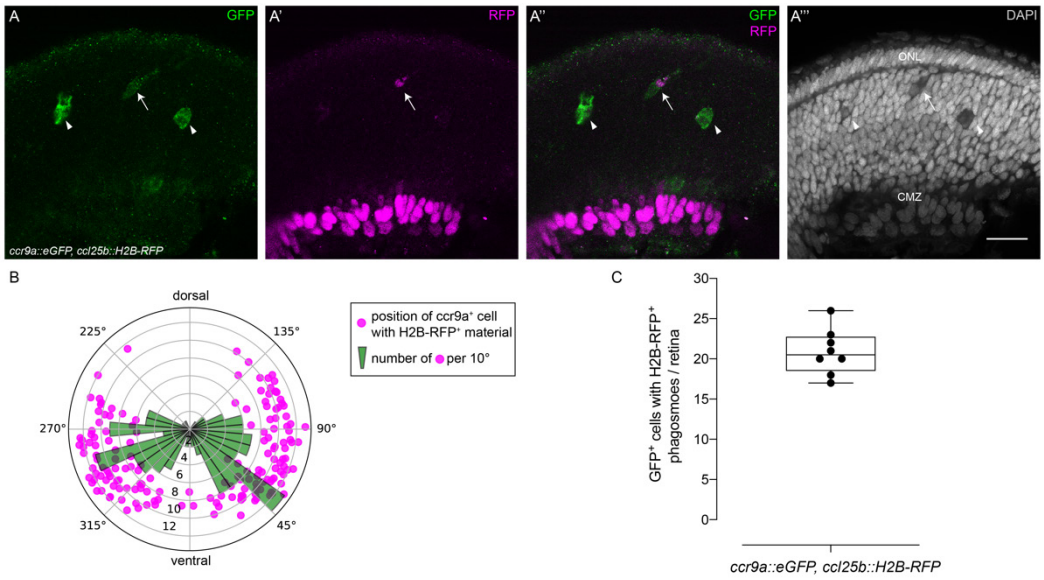

Figure 2.18: *Ccr9a*-positive immune cells contain phagosomes with RSC-derived material.
(A–A''') Whole-mount immunostaining of a *ccr9a::eGFP, ccl25b::H2B-RFP* hatchling retina. Some immune cells labelled by *ccr9a*-driven GFP expression (green) contain phagosomes with *ccl25b*-derived H2B-RFP-positive material (arrow) while others do not (arrowheads). Scale bar is 20 µm. (B) Quantification of number and localization of *ccr9a*-positive immune cells containing H2B-RFP-positive phagosomes (n = 167 H2B-RFP-positive phagosomes in 8 retinae). Dots (magenta) represent the localization of phagosomes, bars (green) depict the number of phagosomes per 10° bin. Most phagosomes are located in the anterior and posterior part of the retina. (C) Quantification of number of *ccr9a*-positive immune cells with H2B-RFP-positive phagosomes per retina (n = 8 retinae; box plot: median, 25th and 75th percentile, whiskers show maximum and minimum data points).

Taken together, these results demonstrate that immune cells in the retina phagocytose material derived from retinal stem cells and actively transport these phagosomes through the retina to remove cell debris.

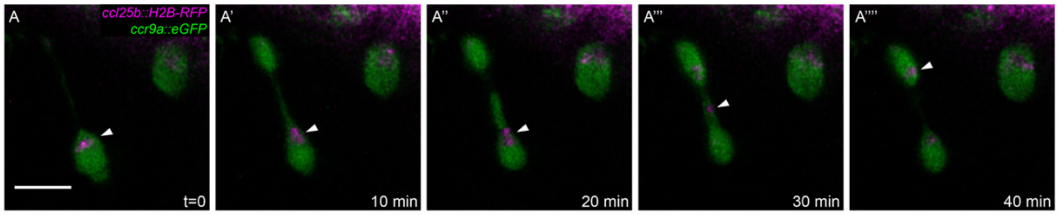

Figure 2.19: *Ccr9a*-positive immune cells transport RSC-derived phagosomes through the retina.
(A–A'''') *In vivo* imaging of a *ccr9a::eGFP* (green), *ccl25b::H2B-RFP* (magenta) hatchling retina, where a *ccr9a*-expressing immune cell transports an H2B-RFP-positive phagosome through the retina (arrowhead). Scale bar is 10 µm.

2.2.3 The *ccl25b* mutant allele has a 333 bp deletion resulting in truncated *ccl25b* transcript

As described above, the chemokine *ccl25b* and its cognate receptor *ccr9a* are expressed in stem and immune cells in the retina, respectively. To address whether this defined expression domain of *ccl25b* is functionally relevant for retinal stem cells and their interaction with the immune system, I generated a *ccl25b* mutant fish line. The medaka *ccl25b* gene comprises six exons, of which exons 3–5 contain the coding sequence. Two sgRNAs targeting exon 4 and 5 of *ccl25b* were injected. Genotyping of F1 mutants revealed a 333 bp deletion in the *ccl25b* locus, thereby completely eliminating exon 4 including the CC motif along with two-thirds of exon 5 (Figure 2.20A).

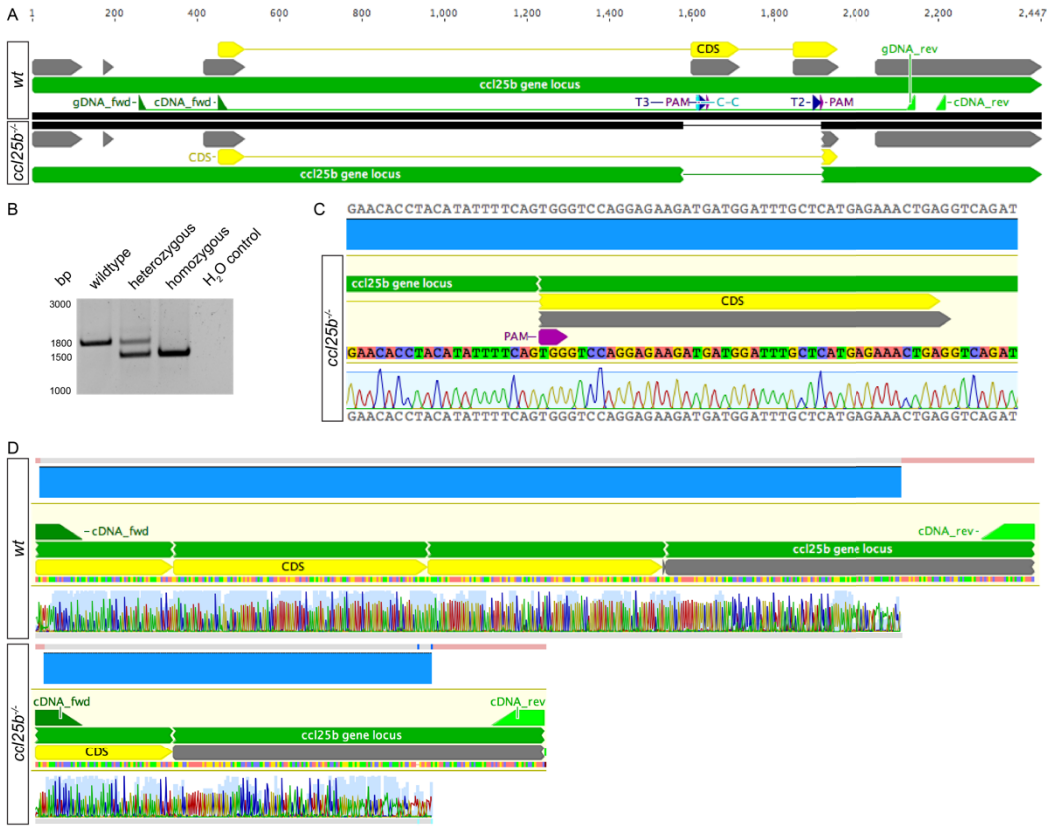

Figure 2.20: The *ccl25b* mutant has a 333 bp deletion resulting in truncated *ccl25b* transcript.
(A) Genomic locus of *ccl25b* in wt and *ccl25b*$^{-/-}$ fish. In *ccl25b*$^{-/-}$ mutants, a 333 bp deletion is introduced, eliminating exon 4 with the CC motif and part of exon 5. (B–C) PCR amplification of genomic DNA of wt, *ccl25b*$^{+/-}$ and *ccl25b*$^{-/-}$ fish shows a deletion of around 300 bp in the *ccl25b* mutant allele, which was confirmed by sequencing (C). (D) Transcript analysis of wt and *ccl25b*$^{-/-}$ cDNA shows that *ccl25b*$^{-/-}$ transcript is truncated and contains only the coding exon 3 while the remainder of exon 5 is spliced out.

PCR amplification of genomic DNA of wildtype *ccl25b*$^{+/+}$, heterozygous *ccl25b*$^{+/-}$ and homozygous *ccl25b*$^{-/-}$ fish showed a deletion of approximately 300 bp in the *ccl25b* mutant allele, which was additionally confirmed by sequencing (Figure 2.20B–C). Transcript analysis of wildtype and *ccl25b*$^{-/-}$ hatchlings showed that the remainder of exon 5 was spliced out, resulting in a severely truncated transcript containing 64 of 291 translated base pairs (Figure 2.20D).

Taken together, the *ccl25b* mutant allele described here features a genomic 333 bp deletion and produces a truncated transcript which contains only 22 % of the wildtype coding sequence.

2.2.4 Homeostatic and injury response behaviour of *ccr9a*-positive immune cells is altered in *ccl25b* mutant

Immune cells are known to exhibit patrolling movements during tissue homeostasis (Lust, 2017; Nimmerjahn et al., 2005). Moreover, they are recruited to injury sites to clear away cell debris and thus contribute to regeneration or repair of the wounded tissue (Kyritsis et al., 2012; Lust, 2017; Martins et al., 2019).

To visualize *ccr9a*-positive immune cells in *ccl25b*$^{-/-}$ hatchlings, the *ccr9a::GFP* reporter was crossed into *ccl25b* mutants to generate a *ccl25b*$^{-/-}$ *ccr9a::GFP* line. I performed two-photon *in vivo* time-lapse imaging of wildtype and *ccl25b*$^{-/-}$ hatchling retinae positive for the *ccr9a::GFP* reporter to assess homeostatic as well as injury response behaviour of *ccr9a*-positive immune cells. First, I analysed homeostatic behaviour of immune cells in the CMZ in time-lapse movies of 10 h length. Interestingly, wildtypic GFP-positive immune cells in the CMZ remained largely static, but extended processes in various directions, also connecting to neighbouring immune cells (Figure 2.21A–A''). In a colour-coded temporal projection this observation was confirmed, cell bodies remained fixed at their position with dynamic process movements (Figure 2.21B). In contrast to that, immune cells in retinae of *ccl25b*$^{-/-}$ hatchlings were more motile during the 10 h time-lapse acquisition period (Figure 2.21C–C''). This is also reflected in the colour-coded temporal projection of *ccl25b*$^{-/-}$ immune cells, where the increased movement was clearly visible (Figure 2.21D).

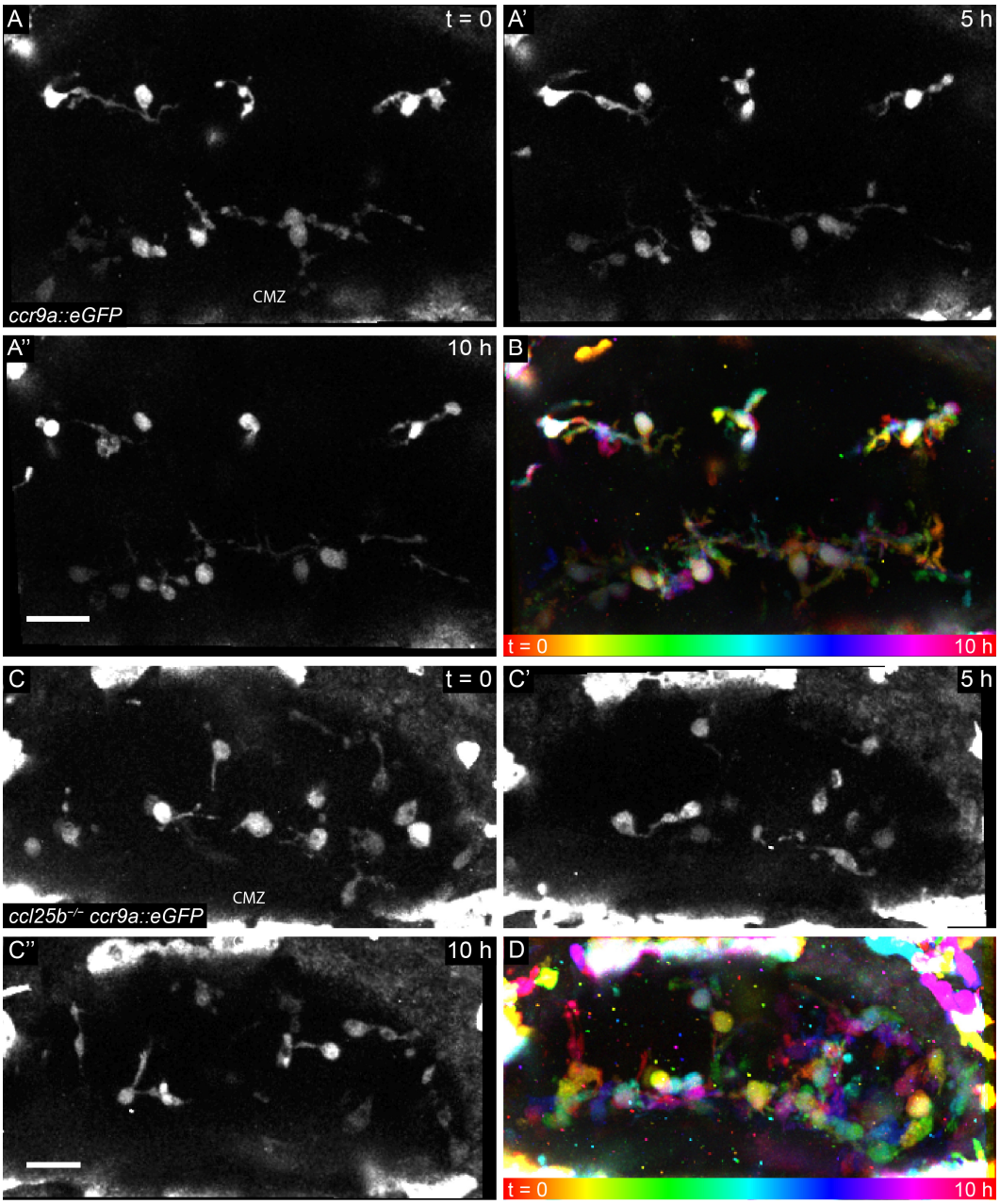

Figure 2.21: Homeostatic behaviour of *ccr9a*-positive immune cells is altered in *ccl25b* mutants.
(A–A'') *In vivo* imaging of a wt *ccr9a::eGFP* hatchling retina for 10 h. *Ccr9a*-positive immune cells remain largely static in their position (n = 6 fish). Scale bar is 20 µm. (B) Colour-coded temporal projection confirms stable position of cell bodies, whereas the processes are dynamic. (C–C'') *In vivo* imaging of a *ccl25b*$^{-/-}$ *ccr9a::eGFP* hatchling retina for 10 h. *Ccr9a*-positive immune cells are migratory (n = 4 fish). Scale bar is 20 µm. (D) Temporal colour-coded projection shows increased movement of *ccl25b*$^{-/-}$ *ccr9a::eGFP* immune cells.

Second, an injury paradigm was introduced into the experiment. Using two-photon mediated laser ablation, a wound of at least 20 µm diameter was inflicted to the approximate stem cell region in hatchling retinae. The reaction of immune cells to the injury was recorded for 4 h and analysed by manual tracking of cell body position combined with temporal colour-coding.

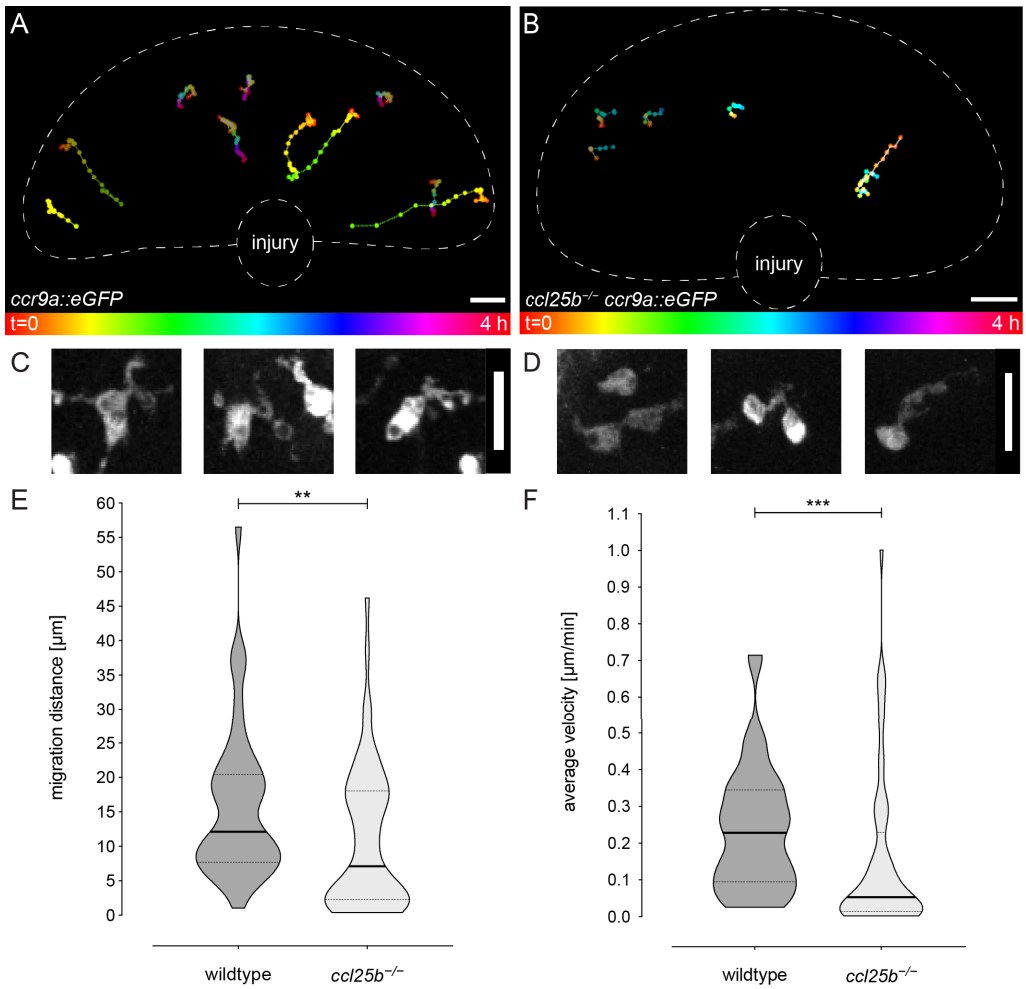

Figure 2.22: Injury response behaviour of immune cells in *ccl25b* mutant retinae is inconsistent but differs from wildtype.
(A–B) Representative tracks of immune cell migration in hatchling retinae in combination with temporal colour-coding of immune cell tracks. After laser-ablation injury to the stem cell region in the CMZ the response was recorded for 4 h with a temporal resolution of 2 min with *in vivo* time-lapse movies. Scale bars are 20 µm. (A) Wt immune cells rapidly migrate to the wound (n = 44 cells from 5 fish). (B) Immune cells in *ccl25b*$^{-/-}$ *ccr9a::eGFP* hatchlings are less motile, move more slowly and migrate shorter distances (n = 47 cells from 7 fish). (C–D) Morphology differs between wt (C) and less motile *ccl25b*$^{-/-}$ (D) GFP-positive immune cells. Scale bars are 20 µm. (E) Quantification of immune cell migration distance from (A–B) (**P = 0.0058; violin plots: lines show median, 25th and 75th percentile). The migration distance is smaller in *ccl25b*$^{-/-}$ than wt immune cells. (F) Quantification of average migration velocity of immune cells from (A–B) (***P = 0.0001; violin plots: lines show median, 25th and 75th percentile). The average migration velocity is reduced in *ccl25b*$^{-/-}$ compared to wt immune cells.

In wildtype retinae all *ccr9a*-expressing immune cells in the vicinity of the wound site migrated rapidly and precisely to the injured area (Figure 2.22A). The reaction of GFP-positive immune cells in *ccl25b*$^{-/-}$ retinae was divergent: in 1 out of 8 fish, immune cells exhibited wildtype-like migration. The

majority of hatchlings, however, displayed immune cells with decreased or halted motility (Figure 2.22B), whose morphology also differed from wildtypic immune cells in that their cell bodies were more rounded, whereas migratory immune cells rather presented elongated, irregularly shaped cell bodies (Figure 2.22C–D). Moreover, immune cells in *ccl25b*$^{-/-}$ fish migrated shorter distances with slower migration velocity compared to wildtypic ones (Figure 2.22E–F).

These data demonstrate that Ccl25b is not necessary for immune cell homing in the retina, as immune cells are present in *ccl25b*$^{-/-}$ mutants. The homeostatic behaviour, however, is slightly altered with immune cells displaying a higher motility without injury cue. Upon injury, most *ccl25b*$^{-/-}$ immune cells are static and fail to migrate to the wound site. The divergent injury response of immune cells in *ccl25b*$^{-/-}$ mutants additionally indicates that the phenotype might not be fully penetrant, as in some fish immune cells migrate seemingly normal.

3 Discussion

In this thesis, I investigated two aspects of growth control in a neural stem cell niche. I found that on the one hand the RSC niche is permissive of specific mitogenic signaling and on the other hand there is a protective system of immune cells in place which can safeguard the stem cell niche against undesired alterations. Using a combination of expression analysis and gain- or loss-of-function approaches, I investigated the function of Igfr-mediated signaling in the postembryonic RSC niche of medaka. Ligands and receptors of the IIS pathway are expressed in the hatchling retina and specifically in the CMZ. Furthermore, the pathway is active in sparse progenitors in the CMZ. While inhibition of Igfr signaling leads to decreased proliferation of retinal stem and progenitor cells, over-activation results in properly shaped but enlarged eye size originating from cell number increase. I determined that the cause of this lies in the expansion of progenitor cells which go through the cell cycle faster. Surprisingly, retinal stem cells are not affected by this over-activation. Importantly, the mitogenic reaction in the RSC niche seems to be specific to Igf signaling over-activation as other mitogens are unable to elicit a proliferative response.
Furthermore, by employing expression analysis, targeted mutagenesis and *in vivo* imaging, I examined the function of the conserved Ccl25–Ccr9 axis in postembryonic RSC niche of medaka. *Ccl25b* and *ccr9a* are expressed in retinal stem and immune cells, respectively. *Ccr9a*-positive immune cells form a network around the RSC niche and contain phagosomes with RSC-derived material. Upon injury to retinal stem cells, immune cells migrate to the wound site, however immune cells in *ccl25b*$^{-/-}$ mutants do not become reactive in response to the injury cue.

3.1 Circadian rhythm of proliferation is connected to Igf signaling

To assess Igf1r-mediated signaling activity, I examined the pattern of phosphorylated and therefore activated Igf1r in the hatchling retina by immunohistochemistry. In the retina of adult African cichlids, the amount of Igf1r protein is constant throughout the whole day, however Igf1 protein

levels fluctuate in a daily rhythm with highest abundance at night and comparably low levels during the day (Zygar et al., 2005). For that reason, I sacrificed hatchlings for analysis either at 12:00 after feeding them, at 18:00 or at 0:00. Indeed, only in the fish fixed at midnight, sparse progenitor cells in the CMZ were pIgf1r-positive, indicating that the pathway is active predominantly during the night in the CMZ. Rod progenitor proliferation in the ONL of African cichlids also peaks at the night, and the rhythmic expression of clock genes in the retina regulates rhythmic expression of *pcna* (Chiu et al., 1995; Song et al., 2017). Moreover, Igf1 acts as zeitgeber for the cellular circadian clock by regulating expression of the clock gene *bmal1* in mouse cell lines (Breit et al., 2018). Furthermore, cryptochromes, which are part of the circadian clock, regulate the circadian rhythm of Igf1, and Cryptochrome-deficient mice display reduced *igf1* mRNA and protein levels as well as decreased organ and body size (Chaudhari et al., 2017).

I found that proliferation of cells in the CMZ decreased significantly in response to incubating fish for 24 h in Igf1r inhibitor and BrdU. This is in line with reports from embryonic and adult zebrafish, where cardiomyocyte proliferation decreases upon Igf1r inhibition (Choi et al., 2013; Huang et al., 2013). Interestingly, I performed a preliminary inhibition experiment, where I incubated fish for 26 h in the Igf1r inhibitor, but added BrdU only for the last two hours (14:00 to 16:00) (data not shown). There, no difference in number of proliferating cells was visible, which might be due to the circadian rhythm of Igf1 and greater influence of the IIS pathway on proliferation in the retina during the night. Taken together, all this evidence indicates a function of Igf1–Igf1r signaling in regulating cell proliferation in a circadian manner. The contribution of the circadian rhythm to proliferation in the teleost CMZ has not been investigated yet, but in order to address this, proliferation rates in the postembryonic medaka CMZ could be analysed by BrdU incorporation with regard to circadian cycle.

As proliferation is a process with high energy demand, it would make sense to execute cost-intensive metabolic tasks predominantly during a phase of low energy consumption by behavioural processes (reviewed in (Pittendrigh, 1993)), which for diurnal animals is during the night. Therefore, repeating the BrdU/EdU incorporation experiment for cell cycle assessment during the night could illuminate whether cell cycle length is also subjected to

circadian rhythmicity. In line with this assumption, I observed that juvenile *rx2::cd8a:igf1ra* fish tended to grow slower than wildtype siblings, but reached the same size as wildtypes with some delay, which might reflect their higher energy investment in retinal cell proliferation at the expense of behaviours resulting in sufficient nutrient intake and overall organismal growth.

Additionally, UV-induced DNA damage could be minimised by favouring retinal proliferation at night. The zebrafish HSC niche in the kidney is protected from DNA damage by an umbrella of pigment cells located above the niche, and in albino mutants, UV-induced DNA damage is increased (Kapp et al., 2018). The teleost retina is shielded by the RPE around its apical surface, however retinal cells are naturally exposed to light by entry through the lens. In light of the above-mentioned findings, preferential proliferation of light-exposed RSCs and RPCs during low light phases could be implemented as protective mechanism against DNA damage. This could be addressed by analysing cyclobutane pyrimidine dimers, which are the most common form of UV-induced DNA damage, in medaka hatchlings transgenic for *rx2::cd8a:igf1ra* compared to wildtype fish. Furthermore, it would be interesting to investigate whether nocturnal teleosts or species in low light environments also exhibit circadian proliferation, or whether proliferative rhythmicity is an adaptive mechanism in diurnal, light-exposed species. To this end, proliferation in the RSC niche could be assayed in specimens from the bathypelagic zone as well as nocturnal or crepuscular species by immunohistochemistry or *in situ* hybridisation for proliferation markers.

3.2 Igf1r activity in MG cells does not act as mitogenic signal

Intriguingly, all MG cells were pIgf1r-positive in day- as well as night-fixed hatchlings. In *in situ* hybridisations, I saw expression if *igf1ra* in the INL, which might include MG cells. On the other hand, *igf1rb* expression was not analysed in this thesis. However, Wan and colleagues show expression of *igf1ra* and *igf1rb* mRNA in both MG cells as well as neurons of the NR in adult zebrafish (Wan et al., 2014). Apart from that report, most expression data are restricted to whole-mount *in situ* hybridisations in embryonic and

larval teleosts. There, conflicting data exists and *igf1ra* and *igf1rb* are reported to have largely overlapping expression domains, including the head region with the eyes, in either distinct or ubiquitous patterns (Li et al., 2014; Maures et al., 2002). When knocking down either receptor in zebrafish embryos, development is delayed, embryos are smaller than siblings and expression of marker genes such as *rx1* is reduced (Schlueter et al., 2006). Another paper by the same first author states that Igf1rb, but not Igf1ra is important for primordial germ cell migration and survival (Schlueter et al., 2007b). Thus, it seems that both paralogues have largely similar functions during embryonic development, but additionally some aspects of their signaling tasks have diverged. Therefore, to address whether pIgf1r staining in medaka MG cells recognizes Igf1ra, Igf1rb or both, expression of both paralogues could be investigated by fluorescent *in situ* hybridisation. To decipher roles inherent to either paralogue as well as additive roles, single and double mutants could be useful tools to study retinogenesis during embryonic development. For functional investigation in a postembryonic organism, and specifically in homeostatic growth of the retina, conditional knockout alleles would be ideally suited.

In the zebrafish retina, *igf1* expression is induced upon injury in proliferating MG cells and *igf1ra* knockdown decreases proliferation, indicating that Igf signaling is necessary for injury-induced MG cell-derived progenitor formation (Wan et al., 2014). In the medaka retina, however, Igf signaling does not seem to act as proliferative signaling pathway in MG cells. First, Igf1r-mediated signaling is constantly active in all MG cells. Second, Igf1r-mediated signaling over-activation in MG cells in *rx2::cd8a:igf1ra* fish has no apparent effect. Zebrafish and medaka MG cells are known to display substantial differences upon injury and with regard to gene expression profiles, and some signaling pathways have divergent roles in medaka and zebrafish. For instance, in medaka MG cells, *atoh7* expression is not upregulated upon injury, in contrast to zebrafish (Lust et al., 2016). Moreover, the level of Sox2 is decreased after injury in medaka MG cells, while it is maintained in zebrafish (Lust and Wittbrodt, 2018). Without injury cue, the inhibition of Notch signaling in zebrafish induces MG cell proliferation (Conner et al., 2014), whereas in medaka Notch inhibition prevents MG cell proliferation and upregulation results in increased

proliferation of MG cell-derived progenitors (Lust et al., 2016). Therefore, the role of Igf signaling in medaka MG cells could differ from the injury response function that it holds in zebrafish. In medaka, active Igf1r-mediated signaling in MG cells might act as cell survival rather than mitogenic signal. Its role therein is also described in zebrafish embryonic development, where knockdown of *igf1r* by morpholinos or a dominant negative receptor variant results in increased neuronal apoptosis (Schlueter et al., 2007a). Furthermore, Igf signaling is involved in a range of functions in the CNS, from neurogenesis and synaptogenesis to migration and integration of neurons, and importantly seems to exert divergent or opposing functions dependent on experimental approach, tissue or cell type and developmental stage (reviewed in (Nieto-Estévez et al., 2016)). To delineate the role of Igf signaling in medaka MG cells, analysis of MG cell shape and morphology after Igf1r inhibition could indicate its necessity for MG cell survival. Additionally, assaying proliferation of MG cells and expression levels of Igf pathway components in homeostatic as well as injury contexts in wildtype and *rx2::cd8a:igf1ra* fish could clarify whether Igf1r-mediated signaling holds any mitogenic function in the injury response of medaka.

3.3 Local vs. systemic Igf signaling

It is well-established that the IIS pathway is a key regulator of organismal growth during embryonic development and postembryonic growth across vertebrate species. In canines, single nucleotide polymorphisms in *igf1* and *igf1r*, predicted to influence ligand–receptor binding, are present in most small dog breeds and nearly absent from large breeds (Hoopes et al., 2012; Sutter et al., 2007), emphasising the importance of Igf signaling in determining body size. Growth hormone (Gh) induces *igf* expression in liver as well as other tissues, and Igf1 deficiency results in a variety of clinically relevant conditions such as intrauterine growth restriction or GH insensitivity in humans (reviewed in (Puche and Castilla-Cortázar, 2012)). Also in teleosts, the importance of the Gh–Igf axis has been described (reviewed in (Dai et al., 2015)). *Gh* overexpression in zebrafish results in elevated *igf1* mRNA levels and increased body length and weight (Ishtiaq Ahmed et al., 2011). Igf1 stimulation similarly enhances overall growth of juvenile coho salmon (*Oncorhynchus kisutch*), dependent on nutritional

status and endogenous growth rate (McCormick et al., 1992). On the other hand, localised Igf signaling has been observed in different contexts: several fetal mouse organs like brain, heart and intestine produce Igf1 in explant cultures (D'Ercole et al., 1980). Moreover, ample evidence for a localised signaling function of Igf in postembryonic rod neurogenesis of the teleost retina exists (Mack and Fernald, 1993; Otteson et al., 2002; Zygar et al., 2005). Therefore, the expression data presented here, with IIS pathway ligands and receptors locally expressed in the medaka CMZ, suggest that postembryonic neurogenesis might underlie a local signaling loop, probably integrating feedback from a systemic nutritional status to ensure coordinated growth of all organs. This hypothesis could be tested by conditional mutation or targeted knockdown of IIS ligands in the retina and quantification of subsequent effects on proliferation and organ size. The source of the local signal – probably IIS ligands – could be one of the accessory tissues of the retina like lens, ciliary epithelium or the annular ligament, which is located distally directly adjacent to the CMZ. Expression of *igf2* in this tissue is evident in the *in situ* hybridisation and could be further consolidated by performing a higher resolution expression analysis or transcriptomics for additional IIS pathway ligands. Additionally, retinal proliferation in fast growing juvenile and slowly growing adult stages in combination with dietary restriction should be compared to address the influence of nutritional status and inherent growth rate on organ-specific proliferation capacity. Moreover, it might be interesting to assess whether Igf1r over-activation displays the same potency in other postembryonic stem cell niches as in the retina. There, the size increase of the choroid plexi in *cndp1::cd8a:igf1ra* fish is a first indicator that other tissues are receptive for Igf signaling over-activation and consequential organ growth.

3.4 Susceptibility of retinal stem and progenitor cells to different mitogens

Stem and progenitor cells differ in their proliferation and differentiation capacity. Strikingly, by over-activating Igf1r-mediated signaling, the Rx2-postive progenitor, but not stem cell population was expanded. Furthermore, specific Igf1r over-activation in *cndp1*-expressing RSCs only did not have an effect on retinal size, indicating that RSCs might not be

susceptible to enhanced Igf1r signaling. In contrast, RPC number was more than doubled in response to constant activation of Igf1r signaling, rendering the Rx2-positive progenitor population receptive for this mitogenic stimulus. The difference in reaction might be due to the absence or unresponsiveness of the downstream signal transduction machinery necessary to induce the observed increase in cell cycle speed and number of proliferating cells. Another option could be stem cell-intrinsic resistance to mitogenic over-stimulation. For instance, tumour suppressor genes could either be constitutively expressed or induced upon mitogenic cue to diminish the effects of undesired mitogenic signaling in stem cell populations. A role for p53 in neural stem cell regulation has been described, with p53 knockout mice displaying increased proliferation and higher probability for overgrowth in the brain (reviewed in (Solozobova and Blattner, 2011)). Therefore, challenging p53 medaka mutants by expression of *cd8a:igf1ra* in RSCs and assessing resultant effects might illuminate whether p53 is involved in regulating RSC proliferation in medaka. Furthermore, transgenic *cndp1::cd8a:igf1ra cndp1::H2B-eGFP* and *cndp1::H2B-eGFP* hatchlings could be subjected to FACS sorting for RSCs and subsequent generation of transcriptome, proteome and phosphoproteome datasets. Comparing data from physiological stem cell niches as well as stem cell niches exposed to mitogenic stimulation could give insight into which factors are differentially regulated and might be worth investigating further.

Evidence for Igf signaling-dependent proliferation in the postembryonic avian and teleost retina identify proliferative cells in the CMZ or at the retinal margin but fail to distinguish between RSCs and RPCs (Boucher and Hitchcock, 1998a; Fischer and Reh, 2000; Kubota et al., 2002; Otteson et al., 2002). MG cells in the adult retina of some teleost species like zebrafish or goldfish are considered to be retinal stem cells as they give rise to rod PRCs in homeostasis and to all retinal cell types after injury (reviewed in (Otteson and Hitchcock, 2003)). There, knockdown of *igf1ra* inhibits generating MG cell-derived progenitors, and stimulation with Insulin or Igf1 and Fibroblast growth factor 2 (Fgf2) leads to MG cell proliferation, even without injury cue (Wan et al., 2014). Moreover, in larval development of *Drosophila melanogaster*, Insulin/Igf-like peptides induce reactivation and proliferation of neural stem cells (Chell and Brand, 2010), indicating that

the IIS pathway is important at least for these specific stem cell populations. Peripheral infusion of Igf1 results in increased proliferation in the adult rat hippocampus, however the proliferating population is described as progenitors (Åberg et al., 2000). Furthermore, Ziegler and colleagues summarised the role of the IIS pathway in neural stem and progenitors, drawing the conclusion that Igf1r-mediated signaling is essential for progenitor cells, whereas Insr-mediated signaling might be more important for stem cell homeostasis (reviewed in (Ziegler et al., 2015)), which is in agreement with the unresponsiveness of RSCs to Igf1r-mediated over-activation described in this thesis. As IIS activity is dependent on the interplay of different ligand, receptors and accessory proteins, species- and tissue-specific functions of this signaling cascade seem likely, making it necessary to address its function within a defined context. Single cell transcriptomics and single molecule fluorescent *in situ* hybridisation for downstream effectors of Igf signaling on *cndp1::H2A-mCherry* reporter hatchlings could clarify precise expression domains of IIS pathway components within the postembryonic medaka CMZ to further elucidate whether differences in expression between RSCs and RPCs are causal for the insensitivity of RSCs to Igf1r-mediated signaling.

I showed that upon Igf1r over-activation, cell cycle speed as well as number of proliferating RPCs is increased. However, it is unclear whether the observed acceleration of the cell cycle is sufficient to explain the substantial progenitor expansion. To address this, it would be interesting to integrate the data on number of stem and progenitor cells, cell cycle length and retinal expansion into a computational model of postembryonic retinal growth (Tsingos et al., 2019). Modelling different parameters of RPC proliferation competence, for example number of allowed cell divisions, time-sensitive restriction of proliferative potential or mechanical expulsion from the physical environment of the CMZ, could provide insight into regulatory mechanisms of proliferation within the progenitor population and the exact function of Igf1r signaling therein.

Interestingly, expressing the constitutively active $kras^{12V}$ variant in stem and progenitor cells did not alter eye size, even though Ras is a downstream effector of Igf1r-mediated signaling. There are several possible explanations for this observation. First, it might be that at hatchling stage, the timepoint

of eye size analysis, the effect of *kras*^{12V} expression was not noticeable yet, although in adult transgenic *rx2::GFP-kras*^{12V} fish no alterations in eye size or gross morphology were observed either. However, zebrafish cancer models using Kras as oncogenic mitogen mostly reported tumour onset in late juvenile stages combined with varying penetrance (Ju et al., 2015; Nguyen et al., 2012; Park et al., 2008). Possibly, the number of fish raised to adulthood was too small to observe any effects on eye morphology. Second, Kras^{12V} might not be competent to induce proliferation in the medaka retina, or expression in the transgenic lines is not potent enough. Retinal expression of tumour suppressor genes like *retinoblastoma 1* could contribute to inhibiting Kras^{12V}-mediated oncogenicity by ensuring proper cell cycle exit of progenitor cells (Gyda et al., 2012). Most zebrafish cancer models drive oncogene expression with a transactivator system to amplify expression independent of inherent promoter activity. Therefore, it might be interesting to generate a transgenic line where *GFP-kras*^{12V} is expressed under the control of the *rx2* promoter combined with the lexPR transactivator system to amplify expression levels. Third, the potency of Igf1r signaling to increase eye size might depend on other signal transduction mechanisms than the one conveyed by the Ras–Mapk signaling cascade. Inhibition of either Mapk or PI3K results in attenuated Igf1-dependent cell proliferation, but simultaneous inhibition leads to complete arrest of proliferation in a zebrafish cell line (Pozios et al., 2001). Likewise, Igf stimulation enhances phosphorylation of both Mapk and Akt, suggesting a synergistic role of both signaling cascades in regulating Igf1-dependent proliferation (Pozios et al., 2001). In hatchling retinae, I observed increased activation of the PI3K–Akt cascade upon *cd8a:igf1ra* expression, indicating that at least part of the Igf1r-mediated signaling in the CMZ is transduced via these effectors. Immunohistochemistry for phosphorylated Mapk might provide insight into the Igf1r-mediated activation of Mapk signaling in the teleost retina. The importance of Mapk and PI3K signal transduction in regulating proliferation in the medaka CMZ could be addressed by using specific inhibitors for either signaling cascade on wildtypic as well as transgenic *rx2::cd8a:igf1ra* hatchlings in combination with BrdU to address their contribution to postembryonic proliferation.

3.5 Evolutionary and ecological significance of retinal size and architecture

Retinal size, morphology and structure displays great diversity throughout the teleost clade. This is – at least in part – due to the wide range of habitats that are occupied by teleost fish. Whereas surface-dwelling fish like medaka have two layers of PRCs, one light-sensitive rod and one cone layer responsible for colour vision, zebrafish possess already three to four layers of rods and one layer of cones for enhanced light perception, even though they live in only slightly deeper waters (Lust and Wittbrodt, 2018). Contrasting with this, retinae of many deep-sea fish possess predominantly rods at the expense of other retinal neurons (Darwish et al., 2015; de Busserolles et al., 2014; Wagner et al., 1998). Furthermore, visual acuity is positively correlated with eye size (Caves et al., 2017). Taken together, the adaptation to environmental niches suggests that retinal size as well as structure is crucial for visually guided behaviours in diverse habitats. I showed that over-activation of Igf1r-mediated signaling in a small cell population in the CMZ is sufficient to drastically alter retinal size and structure, uncoupled from overall organismal growth. Moreover, the susceptibility of RPCs to increased Igf signaling indicates that a spontaneous event or evolutionary selection resulting in altered Igf signaling within the CMZ might be able to permanently modify retinal size and composition, thereby facilitating the occupation of new ecological niches and subsequent speciation. As this hypothesis cannot be addressed easily, a first step could be to analyse expression of IIS pathway components in a variety of species from different habitats and correlate this to relative eye size, NR thickness and retinal composition.

One interesting example of a specific retinal adaptation is the four-eyed fish *Anableps anableps*, which displays structural differences between ventral and dorsal sides of the retina. In the ventral part, the INL is twice as thick as in the dorsal part, while the other layers do not differ in thickness. Moreover, during larval development, more proliferative cells are present in the ventral compared to the dorsal CMZ (Perez et al., 2017). Therefore, proliferative regulation and cell type composition in the differentiated retina must differ in ventral and dorsal halves. As I found a pronounced increase in INL

thickness upon Igf1r-mediated signaling over-activation, it would be interesting to examine whether Igf signaling plays a role in manifesting the structural differences in the *Anableps anableps* retina. Thus, as a first step, expression of IIS pathway components could be assessed, particularly with regard to expression differences between dorsal and ventral sides. Moreover, inhibitor experiments with subsequent analysis of proliferative fraction might consolidate a functional role of this pathway in CMZ proliferation. In the teleost CMZ, several populations of lineage-specified progenitors reside, and modification of their transcriptional signatures shift cell type ratios (Pérez Saturnino et al., 2018). Assuming that the IIS pathway is expressed and involved in proliferation in the *Anableps anableps* retina, the population of cells in which the pathway is active should be described in detail. Based on the preferential accumulation of INL cells in the ventral retina, one possible scenario is that a progenitor population lineage-committed to generate INL cells is expanded and proliferates more. Likewise, it would be interesting to evaluate the effects of Igf1r-mediated signaling over-activation by expressing *cd8a:igf1ra* in different progenitor populations, for example in Atoh7-, Tlx- or Notch-positive cells. The mitogenic susceptibility of different lineage-committed RPC populations would be addressed while simultaneously assessing structural differences and resultant retinal cell type composition and architecture. Therefore, I hypothesise that Igf signaling might act as an evolutionary module, through which retinal size, morphology and cell type composition is altered by modifying signaling activity in distinct populations of progenitor cells in the CMZ. In order to gather some first functional evidence, *rx2::cd8a:igf1ra* and wt medaka fish could be tested for alterations in visually-guided behaviours. Preliminary results for light-dependent swim depth preference are inconclusive, however other behavioural tests or stringent control of environmental parameters might provide more convincing data.

3.6 The role of Ccl25b–Ccr9a signaling in the retinal stem cell niche of medaka

Innate immunity relies on cell–cell signaling mechanisms to elicit the appropriate response upon injury or infection. Chemokine signaling is one such mechanism and essential for immune cell homing and activation upon

injury or inflammation. The chemokine ligand–receptor pair Ccl25–Ccr9 is involved in lymphocyte homing in different tissue contexts such as thymus and intestine in mammals and covers homeostatic functions (reviewed in (Svensson and Agace, 2006)). In teleosts, *ccr9a/b* is expressed in homeostasis as well as in response to injury in migrating cells, and thymopoiesis depends on the interaction with its ligand *ccl25a* (Aghaallaei et al., 2010; Bajoghli et al., 2009). Preliminary description of *ccl25a/b* and *ccr9a/b* expression domains in the retina revealed distinct expression of *ccl25b* in RSCs (Eggeler, 2017; Said, 2016). I found that *ccr9a* labels a population of mononuclear phagocytic immune cells in close proximity to the stem cell niche in the CMZ. Furthermore, I showed that these *ccr9a*-positive immune cells phagocytose *ccl25b*-positive RSC-derived material and transport it through the retina during postembryonic tissue homeostasis. This suggests that Ccl25b–Ccr9a signaling is involved in homeostatic stem cell surveillance in the CMZ of medaka. To identify the functional role of this signaling axis in the stem–immune cell interaction, the ability of immune cells to phagocytose RSCs in *ccl25b* mutants could be assessed by crossing the *ccr9a::eGFP* and *ccl25b::H2B-RFP* reporters into the *ccl25b* mutant background, which is currently underway. Moreover, a thorough investigation of cell death in the CMZ could provide information on the number, frequency and distribution of dying RSCs. It is also unclear yet how much phagocytic activity of each immune cell is required, whether the phagosomes that were observed contain material from one or more RSCs, or whether more than one immune cell takes up debris from the same RSC. To this end, *in vivo* imaging with a fluorescent caspase sensor could be a first step towards assessing apoptosis in the RSC niche, and TUNEL staining could consolidate and extend these observations in a larger number of fixed samples at different developmental stages. Additionally, it would be interesting to inhibit apoptosis to address whether RSC apoptosis is necessary for the maintenance of proper retinal morphology and integrity. Ultimately, *in vivo* imaging of RSCs undergoing apoptosis and phagocytosis would give valuable insight into the temporal order of events as well as the trigger, with immune cells either actively inducing or passively being attracted by RSC apoptosis.

Chemokines are implicated in activation and functional polarisation of macrophages in different circumstances and environments (reviewed in (Mantovani et al., 2004)), however no role for Ccl25–Ccr9 signaling is known in this context. Upon injury to the stem cell domain of the medaka retina, *ccr9a*-positive immune cells swiftly migrated to the wound site. Interestingly, in the majority of *ccl25b* mutant fish, this migration did not occur. Non-migratory behaviour of immune cells was accompanied by sustained ramified morphology of the immune cells, whereas wildtypic immune cells adopted a more amoeboid shape upon injury cues.

This suggests that in *ccl25b* mutants, the activation of immune cells is impaired, indicating that Ccl25b–Ccr9a signaling might be involved in RSC injury-induced activation of resident immune cells in the medaka retina. Interestingly, the *ccl25b::eGFP* reporter was generated by fusing the GFP to part of the first coding exon of *ccl25b*, and the GFP in this reporter is localised at the cell membrane. As the chemoattractant properties of chemokines depend on their secretion, I hypothesise that in cellular homeostasis, Ccl25b is membrane-localised, and only upon cellular disintegration or leakage Ccl25b will be secreted and therefore be able to attract immune cells. This could explain the observation made here that in *ccl25b* mutants, immune cells fail to become reactive to RSC injuries. Immunohistochemistry for Ccl25b in wildtype and *ccl25b* mutant fish could be utilised to address this hypothesis, identify Ccl25b localisation in homeostatic and injury contexts, and clarify its secretory status in the medaka retina. Concurrently, this challenges the view that Ccl25b is a homeostatic chemokine, although there is a possibility that other chemokines are expressed in RSCs which mediate the injury response. To disentangle this, single cell transcriptomics of RSCs and retinal immune cells could provide insight into which chemokine ligands and receptors are expressed in homeostasis as well as upon injury. Moreover, transcriptomic profiling of resident immune cells could allow to determine their exact identity, which right now is described rather vaguely as mononuclear phagocytic cells.

The majority of *ccl25b* mutant fish exhibited non-migratory, ramified immune cells upon injury or immune cells migration with impaired directionality, while immune cells in 1 out of 8 fish adopted an amoeboid

morphology and migrated to the wound site with wildtype-like behaviour. This indicates that the phenotype upon *ccl25b* mutation is not fully penetrant, however the underlying cause is unclear. On transcript level, the functional domains with the characteristic CC motif in coding exons 4 and 5 of the mutated *ccl25b* were not detected anymore, instead resulting in a shortened transcript with the only remaining coding exon 3 spliced to non-coding exon 6. One possibility is genetic compensation triggered by nonsense-mediated decay of the truncated *ccl25b* transcript (El-Brolosy et al., 2019). Comparative *in situ* hybridisations for *ccl25a* on *ccl25b* mutants displaying migratory and non-motile phenotypes could address a compensatory upregulation of *ccl25a*. Likewise, single cell transcriptomics of *ccl25b*-expressing RSCs might give insight into regulatory differences resulting in either migratory or non-motile immune cells in *ccl25b* mutants.

3.7 Growth control by balanced proliferation and apoptosis in the retinal stem cell niche

Postembryonic growth poses a challenge on organisms, where active stem cell pools have to be stable to sustain tissue homeostasis while simultaneously restricting stem cell numbers in order to maintain proper size and integrity of tissue. Though it is clear that stem cell number is regulated by proliferation and thereby birth of new stem cells, little work has been done on stem cell death as restrictive mechanism. Intriguingly, so far no artificially induced increase in RSC numbers has been observed, despite several attempts at RSC expansion in the lab by manipulating growth factor signaling and introducing oncogenes in the stem cell niche in the medaka retina (Hasel, 2017). I showed that RPCs, but not RSCs are amenable to increased Igf signaling and respond by expansion of the progenitor population. Furthermore, I found that there is a network of retinal immune cells in place which safeguards the niche by phagocytosing RSC-derived material. During embryogenesis of *D. melanogaster*, most neural stem cells in the ventral nerve cord undergo apoptosis, and inhibition thereof results in hyperplastic CNS structures (Peterson et al., 2002; White et al., 1994). Autophagy is implicated in the upholding of stemness and functionality of adult neural stem cells in vitro (reviewed in (Hong et al., 2016)). Emerging evidence indicates an important function of anti-apoptotic

proteins such as B-cell lymphoma 2 (Bcl2) in stem cell maintenance and survival (reviewed in (Soteriou and Fuchs, 2018)). Interestingly, elevated apoptosis induced by *igf1r* knockdown is also rescued by injecting *bcl2-like* mRNA during zebrafish embryogenesis (Schlueter et al., 2007a; 2007b). Moreover, in the mouse intestine, elevated Bcl2 levels protect aberrant ISCs and facilitates tumorigenesis, whereas Bcl2 deficiency reduces adenoma formation by increasing apoptosis in early outgrowths (van der Heijden et al., 2016). Taken together, these data suggest that on the one hand inhibition of apoptosis in stem cells is essential to sustain their population, while on the other hand stem cell death is a necessity to ensure the quality of stem cells. Unfortunately, *in vivo* studies on cell death as mechanism for stem cell maintenance and quality control in a postembryonic niche are underrepresented so far. Therefore, the collective results presented in this thesis present first evidence that the postembryonic stem cell niche in the medaka retina maintains balance not only by RSC and RPC proliferation and restriction thereof, but also by apoptosis of RSCs and subsequent clearance by resident immune cells.

4 Conclusion

The results of this thesis suggest that proper postembryonic growth of the medaka retina relies on mechanisms regulating the birth and death of cells in the stem cell niche. While over-active Igf signaling induces increased cell cycle speed and expansion of RPCs, RSCs are not responsive to this mitogenic stimulus. Consequently, neuroretinal size and thickness are enlarged, whereas overall retinal morphology and architecture is intact. Oncogenic Kras, however, is not able to phenocopy the increased eye size.
Furthermore, retinal immune cells safeguard the stem cell niche and phagocytose RSC-derived material. Disruption of the Ccl25b–Ccr9a signaling axis inhibits the injury-induced reactivation of immune cells into migratory amoeboid cells.
Based on the results presented in this thesis, I hypothesise that the mechanisms for growth regulation in the retinal stem cell niche are at least two-fold. First, proliferation and susceptibility to mitogenic cues of RSCs is stringently controlled to maintain tissue homeostasis. Hence, modulation of retinal size, morphology and cell type composition arises in the progenitor domain and might have been a means throughout evolution and speciation to create the vast retinal diversity evident in the teleost clade. Second, a surveillance network of resident immune cells is in place in the retinal stem cell niche to sustain tissue integrity. There, chemokine signaling via the Ccl25b–Ccr9a axis mediates the interaction of immune cells with stem cells to remove unfit RSCs.

5 Materials & Methods

5.1 Materials

5.1.1 Medaka fish lines

The following medaka stocks and transgenic lines used and/or created for this thesis are summarised in Table 5.1.

All transgenic lines were created by microinjection with Meganuclease (I-SceI) in one-cell stage medaka embryos, except the *ccl25b* mutant, which was generated by the CRISPR/Cas9 system.

Table 5.1: Stocks and transgenic lines used in this thesis.

Name of fish line	**Internal stock number**	**Source**
wildtype Cab	7239, 7524, 7796, 8072, 8368, 8617	(Wittbrodt et al., 2002)
Heino mutants	7542	(Loosli et al., 2000)
rx2::cd8a:igf1ra rx2::lifeact-eGFP	7876, 8114, 8528	this thesis
cndp1::eGFP-caax	7839	this thesis
cndp1::H2A-mCherry	7925	this thesis
cndp1::Cre^{ERT2}, Gaudí^{RSG}	8636	this thesis
cndp1::cd8a:igf1ra cndp1::H2B-eGFP	8218, 8376	this thesis
cndp1::H2B-eGFP	8226	this thesis
rx2::eGFP-kras^{12V}	8293, 8531	this thesis
ccl25b::H2B-RFP	7979, 8506	lab stock
ccr9a::eGFP	7982, 8049, 8148, 8656	lab stock
ccl25b$^{-/-}$ mutant	8273, 8508	this thesis
ccl25b$^{-/-}$ ccr9a::eGFP	8529, 8655	this thesis

5.1.2 Plasmids

Plasmids used to generate new transgenic fish lines are listed in Table 5.2. The constitutively active *igf1ra* construct (*cd8a:igf1ra*) was generated by an in-frame fusion of the codon-optimized extracellular and transmembrane domain of the medaka *cd8a* (synthesized by Geneart) and the intracellular domain of the medaka *igf1ra* by Stephan Kirchmaier, as previously described (Carboni et al., 2005). The *cndp1::Cre^{ERT2}* construct was generated by cloning the 5 kb *cndp1* upstream regulatory region in a pBS/I-SceI-vector containing a tamoxifen-inducible Cre recombinase (Cre^{ERT2}). The plasmid contains *cmlc2::eCFP* as insertional reporter.

Table 5.2: Plasmids used to generate new transgenic lines.

Plasmid name	Plasmid stock number	Source
rx2::cd8a:igf1ra	4846	this thesis
cndp1::H2B-eGFP	5324	this thesis
cndp1::cd8a:igf1ra	5325	this thesis
cndp1::Cre^{ERT2} *cmlc2::eCFP*	5464	this thesis
cndp1::eGFP-caax	2070	lab stock/Petra Haas
cndp1::H2A-mCherry	2110	lab stock/Petra Haas
rx2::lifeact-eGFP	3306	lab stock/Katharina Lust
rx2::eGFP-kras^{12V}	5223	lab stock/Katharina Lust

Plasmids used to generate probes for *in situ* hybridisation are listed in Table 5.3.

Table 5.3: Plasmids used to generate probes for *in situ* hybridisation.

Target gene	Plasmid stock number	Source
igf1ra	4849	this thesis
igf2	4853	this thesis
insrb	4852	this thesis

5.1.3 sgRNAs

Plasmids used to generate sgRNAs for *ccl25b* mutation are listed in Table 5.4.

Table 5.4: Plasmids used to generate sgRNAs.

Name	Plasmid stock number	Source	Target	Sequence
DR274_ ccl25bT2	5272	Katharina Lust	*ccl25b* exon 5	GCGCCAATCC AGAGGACCCG[TGG]
DR274_ ccl25bT3	5273	Katharina Lust	*ccl25b* exon 4	CTTGGCTACG TGAGAGAACT[CGG]

5.1.4 Primers

Primers were ordered from Eurofins MWG Operon and are listed in Table 5.5.

Table 5.5: Primers designed and used in this thesis.

Number	Name	Sequence 5'–3'
JW5305	INSRb ish f	CCACCGATCCTCCTCTGTT G
JW5307	INSRb ish r	GGAACGTACATGTCATTT GCACT
JW5308	IGF1R1 ish f	CGGATGGAGCTCAGGGAA AT
JW5309	IGF1R1 ish r	AGCTCCTTGTGCATGGTG AT
JW5475	IGF2 ish F	TGGAGGAGTGTTGTTTCC GG
JW5476	IGF2 ish R	ACAAACTTGTCCGTGGCG A
JW6114	CD8a BamHI F	ATTAGGATCCATGGACCA GAGATGGATGAAGATC
JW6529	ccl25b Seq primer rev	TCGGCGATAAACACAACCC A

Number	Name	Sequence 5'–3'
JW6530	ccl25b Seq primer fwd	GGGGAGCAGACTCAGCAAAT
JW6725	ccl25b cDNA F_BglII	ATTAAGATCTATGAAGTTTCACACCCTCGTCT
JW7748	caIGF1R1 F NcoI	ATTACCATGGATGGACCAGAGATGGATGAAGA
JW7749	caIGF1R1 R BsaI	ATTAGGTCTCGGGAGGCAGGCCGACGACTGG
JW7750	H2B-EGFP F BspHI	ATTATCATGAATCGCGACGGTACCGCCA
JW7751	H2B-EGFP R BsaI	ATTAGGTCTCGGGAGTCGAGAGGGGCCGCTTTAC
JW8444	cndp1 promoter F KpnI	ATTGGGTACCCGCCAGTGTGATGGATATCT
JW8445	cndp1 promoter R ClaI	TAACATCGATGGTCCAGCCTGCTTTTTTGT
JW8643	ccl25b UTR primer R	GTTTCAGGATACAGTTTTGTCTGT

5.1.5 Chemicals and reagents

Chemicals and reagents used in this thesis are listed in Table 5.6.

Table 5.6: Chemicals and reagents used in this thesis.

Chemical/Reagent	Company
2-Propanol	Sigma-Aldrich
Acetone	Sigma-Aldrich
Adenosine triphosphate (ATP)	Thermo Fisher Scientific
Agar	Roth
Agarose	Sigma-Aldrich
Agarose Low Melt	Roth
Bacto-Trypton	Gibco
BCIP (5-bromo-4-chloro-3-indolyl phosphate)	Roche
Blocking reagent	Roche

Chemical/Reagent	**Company**
Borax anhydrous	Fluka
Bovine Serum Albumin (BSA)	Sigma-Aldrich
BrdU (5-Bromo-2-deoxyuridine)	Sigma-Aldrich
Calcium chloride ($CaCl_2$)	AppliChem
Calcium chloride dihydrate ($CaCl_2 \cdot 2\ H_2O$)	AppliChem
Chloroform	Sigma-Aldrich
DAPI (4',6-Diamidino-2-Phenyindole, Dilactate)	Sigma-Aldrich
Deoxyadenosine triphosphate (dATP)	Thermo Fisher Scientific
Deoxynucleotide triphosphates (dNTPs)	Sigma-Aldrich
DiI stain ($DiIC_{18}(3)$)	Thermo Fisher Scientific
digUTPs	Roche
Disodium hydrogen phosphate (Na_2HPO_4)	Sigma-Aldrich
Disodium hydrogen phosphate dihydrate ($Na_2HPO_4 \cdot 2\ H_2O$)	Sigma-Aldrich
Dimethyl sulfoxide (DMSO)	Roth
Dithiothreitol (DTT)	Thermo Fisher Scientific
EdU	Thermo Fisher Scientific
Ethanol 70 % (denatured) (EtHO)	Roth
Ethanol 96 % (denatured) (EtHO)	Roth
Ethanol 99 % (EtHO)	Sigma-Aldrich
Ethidium Bromide (EtBr)	Sigma-Aldrich
Ethylenediaminetetraacetic acid (EDTA)	Roth
Formamide	Sigma-Aldrich
Glacial acetic acid 96 %	Merck
Glucose	Sigma-Aldrich
Glycerin (Glycerol)	Merck
Glycine	Sigma-Aldrich
Heparin	Gibco

Chemical/Reagent	Company
HEPES (4-(2-hydroxyethyl)-1-piperazineethanesulfonic acid)	Roth
Hydrogen Chloride (HCl)	Merck
Hydrogen peroxide (H_2O_2)	Sigma-Aldrich
Magnesium chloride ($MgCl_2$)	AppliChem
Magnesium sulphate heptahydrate ($MgSO_4 \cdot 7 H_2O$)	Merck
Methanol (MeOH)	Roth
Methylene blue trihydrate	Sigma-Aldrich
N-Phenylthiourea (PTU)	Sigma-Aldrich
Nail polish	Essence
NBT (4-nitro blue tetrazolium chloride)	Roche
Normal Goat Serum (NGS)	Gibco
NVP-AEW541	Selleckchem
Paraformaldehyde (PFA)	Sigma-Aldrich
Phenol/Chloroform/Isoamylalcohol (PCI)	Roth
Polyethylene glycol - 4000 (PEG-4000)	Thermo Fisher Scientific
Potassium acetate (KAc)	AppliChem
Potassium chloride (KCl)	AppliChem
Potassium dihydrogen phosphate (KH_2PO_4)	Merck
Potassium hydrogen phosphate (K_2HPO_4)	Merck
Potassium hydroxide (KOH)	Merck
Proteinase K	Roche
Red sea salt	Red Sea
RNase-free water	Sigma-Aldrich
rNTPs (ATP, CTP, GTP, UTP)	Roche
Roti	Roth
Sheep Serum (SS)	Sigma-Aldrich
Sodium acetate (NaAc)	Grüssing
Sodium chloride (NaCl)	Sigma-Aldrich

Chemical/Reagent	Company
Sodium citrate	Sigma-Aldrich
Sodium dodecyl sulphate sodium salt (SDS)	Serva
Sodium hydrogen carbonate ($NaHCO_3$)	Merck
Sodium hydroxide (NaOH)	Sigma-Aldrich
Sodium tetraborate ($Na_2B_4O_7$)	Sigma-Aldrich
Sucrose	Roth
Tamoxifen	Sigma-Aldrich
Tricaine (MS-222)	Sigma-Aldrich
Tris base	Roth
Tris-hydrochloride (Tris-HCl)	Sigma-Aldrich
Triton X-100	Sigma-Aldrich
Trizol	Invitrogen
Tween20	Sigma-Aldrich
X-Gal	Thermo Fisher Scientific
Yeast Extract	Roth

5.1.6 Molecular materials

Molecular materials used in this thesis are listed in Table 5.7.

Table 5.7: Molecular materials used in this thesis.

Material	Company
Anti-Digoxigenin-AP Fab fragments	Roche
GeneRuler DNA Ladder Mix	Thermo Fisher Scientific
DNA Purple loading dye	Thermo Fisher Scientific
Deoxynucleotide Triphosphates Set (dNTPs)	Thermo Fisher Scientific
MachT1 chemically competent *E. coli*	Thermo Fisher Scientific
RNA from torula yeast Type VI	Sigma-Aldrich
RNA Loading Dye 2x Rapid	Thermo Fisher Scientific

5.1.7 Enzymes

Enzymes used in this thesis are listed in Table 5.8.

Table 5.8: Enzymes and corresponding buffers used in this thesis.

Enzyme	Company
I-SceI Meganuclease and 10x I-SceI buffer	NEB
Restriction enzymes and buffers	NEB/Thermo Fisher Scientific
T4 DNA Ligase and 10x T4 DNA Ligase Buffer	Thermo Fisher Scientific
Q5 High-Fidelity DNA Polymerase and 5x Q5 Reaction Buffer	NEB
Proteinase K	Roche
RNase A, DNase- and protease-free (10 mg/ml)	Thermo Fisher Scientific
Hatching enzyme	lab made

5.1.8 Antibodies

Primary antibodies used in this thesis are listed in Table 5.9.

Table 5.9: Primary antibodies used in this thesis.

Primary antibody	Species	Concentration	Company
anti-BrdU	rat	1:100	Abcam, ab6326
anti-eGFP	chicken	1:500	Life Technologies, A10262
anti-DsRed	rabbit	1:500	Clontech, 632496
anti-Lcp1	rabbit	1:200	GeneTex, GTX124420-50
anti-pAkt	rabbit	1:200	Cell Signaling, 4060
anti-Pcna	mouse	1:100	Millipore, CBL407
anti-pIgf1r	rabbit	1:100	Abcam, ab39398
anti-Rx2	rabbit	1:500	lab made (Reinhardt et al., 2015)

Secondary antibodies used in this thesis are listed in Table 5.10.

Table 5.10: Secondary antibodies used in this thesis.

Secondary antibody	Species	Concentration	Company
anti-chicken Alexa Fluor 488	donkey	1:750	Jackson, 703-485-155
anti-rabbit Alexa Fluor 488	goat	1:750	Life Technologies, A-11034
anti-rabbit DyLight549	goat	1:750	Jackson, 112-505-144
anti-rabbit Alexa Fluor 647	goat	1:750	Life Technologies, A-21245
anti-mouse Alexa 546	goat	1:750	Life Technologies, A-11030
anti-rat DyLight488	goat	1:750	Jackson, 112-485-143

5.1.9 Kits

Kits used in this thesis are listed in Table 5.11.

Table 5.11: Kits used in this thesis.

Kit	Company
innuPREP PCRpure Kit	Analytik Jena
mMessage mMachine® Sp6 Transcription	Thermo Fisher Scientific
mMessage mMachine® T7 Transcription	Thermo Fisher Scientific
Click-iT® EdU Alexa Fluor® 647 Imaging Kit	Thermo Fisher Scientific
RevertAid First Strand cDNA Synthesis Kit	Thermo Fisher Scientific
MEGAShortScript T7 Kit	Ambion
RNeasy Mini Kit	Qiagen
QIAGEN Plasmid Midi Kit	Qiagen
QIAPrep® Spin Miniprep Kit	Qiagen

5.1.10 Consumables

Consumables used in this thesis are listed in Table 5.12.

Table 5.12: Consumables used in this thesis.

Consumable	Company
Scalpel blades	Roth
Cell saver tips 200 µl	Roth
Cover slips	Roth
Cryosection Superfrost Plus slides	Thermo Fisher Scientific
Filter paper	Whatman
Filter Tips 10 µl, 20 µl, 200 µl, 1.25 ml	Starlab
Folded filters	Sartorius
Gas permeable moisture barrier seal (4ti-0516/96)	4titude
Glass beads	Roth
Glass dishes for microscopy	MatTek
Glass vials	Roth
Injection moulds	homemade
Injection needles GC100F-10	Harvard Apparatus
Latex gloves	Semperguard
Microloader tips	Eppendorf
Micro pestles 0.5/1.5 ml	Laborversand Hartenstein
Micro pestles 1.5/2.0 ml	Eppendorf
Microtome blades C35	Feather
Molding cups	Polysciences
Nitrile gloves	Starlab
Parafilm® M	Bemis
Pasteur pipettes	Sarstedt
PCR stripes	Sarstedt
PCR tubes	Kisker
Petri dishes	Greiner
Pipette tips	Steinbrenner
Reaction tubes 1.5 ml, 2 ml	Sarstedt

Consumable	Company
Sandpaper 1000 grit	Bauhaus
Tissue Freezing Medium	Jung, Leica Microsystems
Tubes 10 ml, 15 ml, 50 ml	Sarstedt
Well plates 6-well, 12-well, 24-well	Böttger, Roth

5.1.11 Equipment

Equipment used in this thesis is listed in Table 5.13.

Table 5.13: Equipment used in this thesis.

Equipment	Company
Bacterial Shaker INNOVA 44	New Brunswick
Camera Nikon DS-Ri1	Nikon
Centrifuges 5417C, 5425, 5430R, 5810R	Eppendorf
Cold light source for stereomicroscope KL 1500 LCD	Schott
Cryostat CM 3050S	Leica
DeNovix DS-11 spectrophotometer	DeNovix
Electrophoresis chambers and combs	homemade and Peqlab
FemtoJet express and Microinjector 5242	Eppendorf
Fish incubators	Heraeus instruments and RuMed
Forceps 5, 55 Inox stainless steel	Dumont
Forceps 110 mm, straight	NeoLab
Freezer -20°C	Liebherr
Freezer -80°C	Thermo Fisher Scientific
Fridge 4°C	Liebherr
Incubator 32°C, 37°C, 60°C	Binder
InjectMan NI2	Eppendorf
Leica TCS SPE	Leica
Leica TCS SP5	Leica
Leica TCS SP8	Leica

Equipment	Company
Microwave	Sharp
Milli-Q water filtration station	Millipore Corporation
Mini-centrifuge	Sarstedt
MS1Minishaker	IKA
Needle puller P-30	Sutter Instrument Co USA
Nikon SMZ18 stereomicroscope	Nikon
Olympus SZX7	Olympus
PCR C100 Touch Thermal Cycler	Bio-Rad
pH-Meter	Sartorius
PipetBoy	Gilson
Pipette 2 µl, 10 µl	Eppendorf
Pipettes 20 µl, 200 µl, 1 ml	Gilson
Power supply Power-PAC Basic	Bio-Rad
PowerPac 300	Bio-Rad
Rotating arm	homemade
Scale	Sartorius
Shakers CAT S 20, DRS-12	NeoLab
Staining box for immunohistochemistry	homemade
Stereomicroscope Zeiss Stemi 2000	Zeiss
Thermocycler	Bio-Rad
Thermomixer Compact	Eppendorf
Thermomixer® F1.5	Eppendorf
UV-Gel Documentation System	Intas
UV table	Vilber Lourmat
Vortex	Scientific Industries
Water bath	GFL
Zeiss Axio Imager M1	Zeiss

5.1.12 Solutions for fish husbandry

Solutions for fish husbandry and fish work used in this thesis are listed in Table 5.14.

Table 5.14: Recipies for solutions for fish husbandry used in this thesis.

Solution	Ingredients	Final concentration
10x ERM (Embryo Rearing Medium)	NaCl	17 mM
	KCl	0.4 mM
	$CaCl_2 \cdot 2\ H_2O$	0.27 mM
	$MgSO_4 \cdot 7\ H_2O$	0.66 mM
	HEPES pH 7.3	17 mM
	pH 7.1	
10x Medaka Hatch Medium	NaCl	17 mM
	KCl	0.4 mM
	$CaCl_2 \cdot 2\ H_2O$	0.27 mM
	$MgSO_4 \cdot 7\ H_2O$	0.66 mM
	HEPES pH 7.3	17 mM
	Methylene blue trihydrate	0.0001 %
	pH 7.1	
20x Tricaine	Tricaine	4 g/l
	$Na_2HPO_4 \cdot 2\ H_2O$	10 g/l
	pH 7-7.5	
32 % PFA stock solution	PFA	500 g
	Millipore H_2O	ad 1562 ml
16 % PFA stock solution	32 % PFA stock	200 ml
	Millipore H_2O	ad 360 ml
	solve at 60°C, adjust to pH	7 with 1 M NaOH
	Millipore H_2O	ad 400 ml, store at 4°C
50x 1-phenyl-2-thiourea (PTU)	N-Phenylthiourea Grade-I 98 %	0.33 g

Solution	Ingredients	Final concentration
stock solution	Millipore H_2O	ad 200 ml
NVP-AEW541	NVP-AEW541	2 mg
stock 10 nM	DMSO	0.455 ml

5.1.13 Solutions for bacterial work

Solutions for bacterial work used in this thesis are listed in Table 5.15.

Table 5.15: Recipes for solutions for bacterial work used in this thesis.

Solution	Ingredients	Final concentration
LB-Bacterial Plates	Bacto-Tryptone	10 g/l
	Yeast extract	5 g/l
	NaCl	10 g/l
	Agar	15 g/l
LB-Medium	Bacto-Tryptone	10 g/l
	Yeast extract	5 g/l
	NaCl	10 g/l
TB-medium	Bacto-Tryptone	12 g/l
	Yeast extract	24 g/l
	Glycerin	0.4 %
	KH_2PO_4	2.13 g/l
	K_2HPO_4	12.54 g/l

5.1.14 Antibiotics

Antibiotics used in this thesis for bacterial selection are listed in Table 5.16.

Table 5.16: Antibiotics for bacterial selection used in this thesis.

Antibiotic	Working concentration	Company
Ampicillin	50 µg/ml	Roth
Kanamycin	100 µg/ml	Roth

5.1.15 Solutions for DNA and RNA work

Solutions for DNA and RNA work used in this thesis are listed in Table 5.17.

Table 5.17: Recipes for solutions for DNA and RNA work used in this thesis.

Solution	Ingredients	Composition
EtBr bath	EtBr (10 mg/ml)	0.02 %
	1x TAE	
Finclip buffer	Tris-HCl pH 8.5	100 mM
	EDTA pH 8	10 mM
	NaCl	200 mM
	SDS	2 %
Finclip buffer with	finclip buffer	95%
Proteinase K	Proteinase K (20 mg/ml)	5 %
Oligo annealing buffer	Tris pH 7.5-8	10 mM
	NaCl	30 mM
P1 buffer	Glucose	50 mM
	Tris-HCl	25 mM
	EDTA	10 mM
	RNase A	100 µg/ml
	pH 8, stored at 4°C	
P2 buffer	NaOH	0.2 M
	SDS	1 %
P3 buffer	KAc	5 M
	pH 5.5, stored at 4°C	
50x Tris-Acetate-EDTA	Tris base	242 g/l
buffer (TAE)	Glacial acetic acid	5.71 %
	EDTA	50 mM
	pH 8.5	
2x RNA loading dye	Bromphenol blue	0.25 %
	Xylene cyanol	0.25 %
	SDS	0.025 %

Solution	Ingredients	Composition
	EDTA pH 8	5 mM
	Formamide	95 %

5.1.16 Solutions for immunohistochemistry

Solutions for immunohistochemistry used in this thesis are listed in Table 5.18.

Table 5.18: Recipes for immunohistochemistry solutions used in this thesis.

Solution	Ingredients	Composition
Bleaching solution	30 % H_2O_2	100 ml
	10 % KOH	50 ml
	1x PTW	ad 1 l
Borax PTW	saturated Borax solution	4 ml
	1x PTW	6 ml
DAPI stock solution	DAPI	10 mg
2 mg/ml	DMSO	ad 5 ml
DiI solution	DiI stain in DMSO	2 mg/ml
HCl nuclear denaturation	2 N HCl	42.5 ml
solution	10x PBS	5 ml
	10 % Triton X-100	0.5 ml
10x Phosphate-buffered	NaCl	70.1 g
saline (PBS)	Na_2HPO_4	49.8 g
	KH_2PO_4	3.4 g
	de-ionised H_2O	ad 1 l, pH 7.3
1x PBS with Tween	10x PBS pH 7.3	100 ml
(PTW)	20 % Tween20	5 ml
	Millipore H_2O	ad 1 l
Saturated Borax solution	$Na_2B_4O_7$	6 g
	Millipore H_2O	ad 100 ml
Sucrose 30%	Sucrose	15 g

Solution	Ingredients	Composition
	1x PTW	ad 50 ml
Whole mount antibody blocking solution	Sheep serum	400 µl
	100 mg/ml BSA solution	100 µl
	DMSO	100 µl
	1x PTW	ad 10 ml

5.1.17 Solutions for *in situ* hybridisation

Solutions for *in situ* hybridisation used in this thesis are listed in Table 5.19.

Table 5.19: Recipes for *in situ* hybridisation solutions used in this thesis.

Solution	Ingredients	Final concentration
20x Saline Sodium citrate buffer (SSC)	NaCl	3 M
	$C_6H_5Na_3O_7 \cdot 2\ H_2O$	300 mM
	pH 7	
4x SSC with Tween (SSCT)	20x SSC	4x
	20 % Tween20	0.1 %
2x SSCT	20x SSC	2x
	20 % Tween20	0.1 %
0.2x SSCT	20x SSC	0.2x
	20 % Tween20	0.1 %
Blocking buffer	Sheep serum	5 %
	in 1x PTW	
Hybridisation Mix	Formamide	50 %
	20x SSC	5x
	Heparin	150 µg/ml
	RNA from torula yeast Type VI	5 mg/ml
	20 % Tween20	0.1 %
Staining buffer	TrisCl pH 9.5	100 mM
	NaCl	100 mM

Solution	Ingredients	Final concentration
	$MgCl_2$	50 mM
	20 % Tween20	0.1 %

5.1.18 Software

Software used in this thesis is listed in Table 5.20.

Table 5.20: Software used in this thesis.

Software	License
Geneious	Biomatters Limited
Microsoft Office	Microsoft
Adobe Illustrator	Adobe
CCTop	(Stemmer et al., 2015)
FileMaker Pro	FileMaker, Inc.
Fiji	(Schindelin et al., 2012)
LAS X	Leica, Inc.
GraphPad Prism	GraphPad Software, Inc.

5.2 Methods

5.2.1 Fish husbandry

Medaka (*Oryzias latipes*) fish used in this thesis were kept as closed stocks in accordance to Tierschutzgesetz 111, Abs. 1, Nr. 1 and with European Union animal welfare guidelines. Fish were maintained in constantly recirculating systems at 28°C on a 14 h light/10 h dark cycle (Tierschutzgesetz 111, Abs. 1, Nr. 1, Haltungserlaubnis AZ35–9185.64 and AZ35–9185.64/BH KIT).

5.2.2 Microinjection into fertilized Medaka eggs

For trans- or mutagenesis, microinjection was performed in medaka embryos. Meganuclease All transgenic lines generated in this thesis were created by microinjection with Meganuclease (I-SceI), and the *ccl25b* mutant line was generated by injection of sgRNAs with *cas9* mRNA. The injection mix recipes used in this thesis are listed in Table 5.21.

Table 5.21: Injection mixes used for Cas9 and plasmid injections.

Cas9 injection	**concentration**	**Plasmid injection**	**concentration**
cas9 mRNA	150 ng/µl	plasmid DNA	10 ng/µl
sgRNAs	15 ng/µl	I-SceI buffer 10x	1.5 µl
RNase-free H_2O	ad 10 µl	I-SceI	1 µl
		H_2O	ad 15 µl

Injections were performed in medaka embryos at 1-cell stage. For this, males were separated from females the night before injections. The next morning, fish were put together for mating and embryos were collected after 30 min. In the meantime, injection plates and injection mix were prepared. A 9 cm petri dish was filled with 1.5 % Agarose/H_2O and an injection mould was placed on top to generate grooves in which embryos were positioned for injection. After the agarose solidified, the mould was removed and the plate was covered with 1x ERM. Embryos were separated with two forceps and sorted into the grooves of the injection plate. Prior to injection, injection needles were pulled from borosilicate glass capillaries with a needle puller. Needles were filled with 2-3 µl injection mix and the needle was opened by scratching over the chorion.

A pressure injector with 80-100 hPa (= P3) and an injection pressure of 450-850 hPa (= P2), dependent on each needle, was used. The needle was inserted through the chorion into the cytoplasm of one-cell stage embryos and a small amount (10 % of the cell volume by visual assessment) was injected. After injections, embryos were raised in 1x ERM or 1x Hatch at 28°C to appropriate stages for further analysis.

5.2.3 BrdU or EdU incorporation

For BrdU incorporation, hatchling fish were incubated in 2.5 mM BrdU dissolved in 1x ERM at 28°C for respective amounts of time. For EdU incorporation, hatchling fish were incubated in 250 µM EdU at 28°C diluted in 1x ERM for respective amounts of time.

5.2.4 Igf1r inhibition

For inhibition of Igf1r, hatchling fish were incubated in 10 µM NVP-AEW541 diluted in 1x ERM at 28°C for 24 h. In a parallel control group, hatchling fish were incubated in 0.001 % DMSO/1x ERM at 28°C for 24 h. Directly afterwards fish were euthanised and fixed for analysis.

5.2.5 Induction of the Cre/lox system

Recombination in *cndp1::Cre^{ERT2}*, Gaudi^{RSG} hatchlings was induced by incubation in 5 µM tamoxifen diluted in 1x ERM at room temperature in the dark overnight and washed with 1x ERM afterwards.

5.2.6 *In vivo* imaging and laser ablations

To inhibit pigmentation of medaka embryos and enable *in vivo* imaging, embryos were raised in 5x PTU/1x ERM from 1 dpf until imaging. For imaging, fish were anesthetised in 1x tricaine/1x ERM and mounted in MatTek dishes in 1 % low melting agarose/1x ERM. Fish were oriented laterally, with the right eye touching the bottom of the dish. *In vivo* imaging and laser ablations were performed on a Leica TCS SP5 equipped with a Spectra Physics Mai Tai® HP DeepSee Ti:Sapphire laser, tunable from 690-1040nm and Leica Hybrid Detectors. An injury was introduced to the retina using a 14x zoom together with the high energy 2-photon laser tuned to 880 nm. Follow-up imaging for GFP detection was performed using the same laser at 880nm and a 40x long distance objective.

5.2.7 Fixation of fish

Fish were first euthanised with 20x tricaine and then fixed in 4 % PFA. For this, fish were washed with 1x PTW and then incubated in 4 % PFA/1x PTW at 4°C at least overnight. Afterwards, fish were washed 5x with 1x PTW to prepare them for cryosections. Alternatively, for long term storage, fish were dehydrated with consecutive dilutions (25 %, 50 %, 75 %, 100 %) of MeOH in 1x PTW for 5 min each and kept in 100 % MeOH at –20°C for *in situ* hybridisation or whole mount staining.

5.2.8 Genotyping of hatchlings

After fish were euthanised with 20x tricaine, the head was cut off with a scalpel and fixed for further processing. The body was transferred to a 1.5 ml Eppendorf tube. 20 µl finclip buffer/Proteinase K mix was added and incubated at 60°C overnight. The next day, two volumes of H_2O were added and contents were mixed by inverting the tube. For Proteinase K inactivation, the tube was incubated at 95°C for 10 min. After centrifugation for 10 min at 10000 rpm and 4°C the supernatant was directly be used for PCR genotyping (2 µl genomic DNA in 25 µl PCR reaction) or stored for later use at 4°C.

5.2.9 Genotyping of adult fish

A piece of the tail fin was cut off with a scalpel and collected in a 1.5 ml Eppendorf tube. 50 µl finclip buffer/Proteinase K mix was added and incubated at 60°C overnight. The next day, two volumes of H_2O were added and contents were mixed by inverting the tube. For Proteinase K inactivation, the tube was incubated at 95°C for 10 min. After centrifugation for 10 min at 10000 rpm and 4°C the supernatant was directly be used for PCR genotyping (2 µl genomic DNA in 25 µl PCR reaction) or stored for later use at 4°C.

5.2.10 Probe synthesis for *in situ* hybridisation

Template DNA plasmids were linearised with NcoI (*igf1ra*, *igf2*, *insrb*), run on a 1 % agarose/TAE gel and purified using the innuPREP PCRpure kit. rNTP mix was prepared according to Table 5.22.

Table 5.22: rNTP mix composition.

Component	Concentration
100 mM ATP	15.4 mM

Component	Concentration
100 mM CTP	15.4 mM
100 mM GTP	15.4 mM
100 mM UTP	10 mM
Millipore H_2O	ad 300 ml

Transcription reactions were prepared according to Table 5.23.

Table 5.23: Transcription reaction for *in situ* hybridisation probe transcription.

Component	Volume per reaction
linearised template	3 µg
100 mM DTT	2 µl
rNTP mix	1.3 µl
10 mM DigUTP	0.7 µl
RiboLock	0.5 µl
10x transcription buffer	2 µl
Sp6 RNA polymerase	2 µl
RNase-free H_2O	ad 20 µl

The mix was incubated for 3 h at 37°C. Afterwards, 1 µl Turbo DNase was added and the mix incubated for another 15 min. RNA purification was performed with the Qiagen RNeasy Mini Kit and eluted 2x with 25 µl H_2O. For quality analysis, 2 µl RNA were mixed with 1 µl H_2O and 3 µl 2x RNA loading dye, incubated for 10 min at 80°C and run on a 1 % Agarose/TAE gel. The remaining transcription product was mixed with 150 µl hybridisation mix, mixed by finger tipping and stored at –20°C.

5.2.11 Whole-mount *in situ* hybridisation

Whole mount *in situ* hybridisation was performed on *Heino* medaka hatchlings. All incubation steps were done at room temperature in tubes on a rotator (to avoid turning tubes overhead) unless stated otherwise. The steps at 65°C were done without rotation in a water bath. All washing steps were done with 1x PTW unless stated otherwise. Fixed hatchlings were rehydrated from 100 % MeOH in successive steps of 75 %, 50 % and 25 % MeOH in 1x

PTW for 5 min each. Then they were washed 2x 5 min each. Next, samples were permeabilised by incubating with 10 µg/ml Proteinase K in 1x PTW for 2 h without shaking. Proteinase K inactivation was performed by rinsing 2x 5 min each with 2 mg/ml glycine in 1x PTW. Additionally, fish were fixed for 20 min in 4 % PFA/1x PTW and washed 5x 5 min each. Samples were then equilibrated by adding room temperature hybridisation mix (hyb-mix) until hatchlings sank to the tube bottom. Pre-hybridisation in hyb-mix was performed at 65°C for 2 h. 10 µl digoxigenin-labelled probe were mixed with 190 µl hyb-mix and denatured for 10 min at 80°C. Directly after, hybridisation was done at 65°C overnight. On the next day, samples were washed with the following buffers heated to 65°C: 2x 30 min with 50 % formamide/2x SSCT, 15 min with 2x SSCT, 2x 30 min with 0.2x SSCT. Then, samples were washed 3x 5 min and blocked at room temperature for 1 h with blocking buffer. Afterwards, incubation was done at 4°C with anti-Digoxigenin-AP Fab fragments (1:2000 dilution) in blocking buffer overnight. The next day, samples were washed 6x 10 min in 6-well plates on a shaker, equilibrated 2x 5 min with pre-staining buffer and 2x 5 min with staining buffer. Next, the staining reaction was done: fish were incubated in 4.5 µl NBT and 3.5 µl BCIP per 1 ml staining buffer without shaking in the dark. Samples were left to develop until blue colour was visible. If overstained, samples were destained with EtHO for 1 h at room temperature, postfixation was done for 20 min at room temperature in 4 % PFA/1x PTW, washed 4x 5 min and processed for cryosections.

5.2.12 Cryosectioning

Fixed fish were washed 3x 10 min with 1x PTW and cryoprotected in 30 % sucrose/1x PTW at 4°C at least overnight. For section quality improvement, samples were incubated for 3-5 more days in a 1:1 mix of 30 % sucrose and tissue freezing medium at 4°C. Hatchlings were mounted in mounting moulds filled with tissue freezing medium, with the head down and the tail up for a transverse section plane. Samples were frozen in liquid nitrogen and left to equilibrate to cryostat temperature for 10 min. Serial sections of 16 µm thickness were obtained on a cryostat, collected on Superfrost Plus slides and dried at 4°C overnight.

5.2.13 Immunohistochemistry on cryosections

The whole staining procedure was performed in homemade, opaque staining boxes with lids. For incubation steps > 10 min, slides were covered with parafilm to avoid evaporation. First, dried sections were rehydrated in 1x PTW for 30 min at room temperature. Then, blocking was performed for 1-2 h with 10 % NGS/1x PTW at room temperature. Slides were washed for 2x 5 min with 1x PTW. Primary antibodies were applied in respective dilutions in 1 % NGS/1x PTW at 4°C overnight. The next day, sections were washed 6x 10 min with 1x PTW. Secondary antibodies were applied in respective dilutions in 1 % NGS/1x PTW together with DAPI (1:500 dilution of 5 mg/ml stock) for 2 h at 37°C. Then, slides were washed for 3x 10 min with 1x PTW. To mount slides, 60 µl of 60 % glycerol/PBS was added, the coverslip was carefully lowered and sealed with nail polish. Slides were stored at 4°C in the dark until imaging.

5.2.14 BrdU and Pcna immunohistochemistry on cryosections

BrdU staining was performed after staining of other antibodies was performed. First, slides were postfixed with 4 % PFA (pH 7) in 1x PTW for 30 min at room temperature. Then, sections were washed 3x 10 min with 1x PTW. Antigen retrieval was performed by incubation of slides with 2N Tris-HCl solution for 90 min at 37°C. Slides were washed 3x 10 min with 1x PTW. Afterwards, pH recovery was performed with a 40 % saturated Borax solution diluted in 1x PTW for 15 min. Then, slides were washed 3x 10 min with 1x PTW. Blocking was performed for 1-2 h with 10 % NGS/1x PTW at room temperature, followed by 2x 5 min washes with 1x PTW. Primary BrdU or Pcna antibodies were applied in the respective dilutions in 1 % NGS/1x PTW at 4°C overnight. The next day, sections were washed 6x 10 min with 1x PTW. Respective secondary antibodies were applied in 1 % NGS/1x PTW for 2 h at 37°C. Then, slides were washed 3x 10 min with 1x PTW before mounting the slides as described in 5.2.13.

5.2.15 EdU staining

EdU staining on cryosections was performed after all other stainings were completed with the Click-iT® EdU Alexa Fluor 647 kit. Sections were washed 3x 5 min with 1x PTW. 75 µl detection mix per slide was prepared according to Table 5.24.

Table 5.24: Recipe for EdU detection mix.

Component	Volume per reaction
10x reaction buffer	6.45 µl
$CuSO_4$	3 µl
10x buffer additive	0.75 µl
Alexa Fluor 647	0.18 µl
H_2O	ad 75 µl

Incubation with detection mix was done for 1 h at room temperature. Afterwards, slides were washed 3x 10 min with 1x PTW and mounted as described in 5.2.13.

5.2.16 Whole-mount immunohistochemistry

All steps were performed in a 6-well plate on a shaker except blocking and antibody incubation, which was performed in 1.5 ml Eppendorf tubes. All washing steps were done with 1x PTW, unless stated otherwise. Juvenile or adult retinae were dissected after bleaching, while hatchling retinae were dissected after the whole staining protocol was completed. Fixed samples were washed for 3x 10 min. To remove pigmentation, samples were bleached with bleaching solution for 0.5-3 h, dependent on age and size of fish, until pigments were gone. Then, samples were washed 2x 5 min before dissecting the retina to remove lens and superficial tissue with sharp forceps. Retinae were washed 2x 5 min, then transferred to glass vials for permeabilisation with pre-cooled acteone at −20°C for 15 min. After rinsing 2x in the vials, retinae were transferred to 6-well plates and washed 2x 5 min. Blocking was done with blocking buffer on a rotator for 2 h. Incubation with primary antibodies (1:200 dilution) was done at least overnight at 4°C in 200 µl blocking buffer. Samples were washed 5x 30 min, before applying the secondary antibodies (1:250 dilution) in 200 µl blocking buffer either overnight at 4°C or for 2 h at 30°C and 350 rpm. Then, samples were washed 5x 30min, hatchling retinae were dissected, and stored in 1% PFA/1x PTW at 4°C until imaging.

5.2.17 DiI injection

For DiI injection, Hatchlings were fixed with 4 % PFA/1x PBS overnight at 4°C. The next day, fish were washed 3x 10 min with 1x PBS. DiI (2 mg/ml

in DMSO) was injected using the setup for microinjections. 2 µl DiI solution was loaded into an injection needle, and fish were positioned in petri dishes with one eye facing towards the needle. Approximately 3–5 injections were performed per eye, distributed around the lens. After injection, hatchlings were washed 2x 5 min with 1x PBS and kept at room temperature in 1x PBS for 2 d. Then, fish were stained with DAPI (1:500 dilution) in 1x PBS for 1 h at room temperature and washed 3x 5 min with 1x PBS. For imaging, hatchlings were mounted with the dorsal part of the head toughing the bottom of the MatTek dish in 1 % low melting agarose/1x PTW and covered with 1x PBS.

5.2.18 Imaging

Sections of *in situ* hybridisations were imaged at the upright Zeiss Axio imager M1 (Plan-Apochromat lenses: 10x/0.45, 20x/0.8; DIC filter). All immunohistochemistry imaging (cryosections and whole mount samples) was performed at the inverted confocal laser scanning microscope Leica TCS SP8 (ACS APO objective lenses: 10x/0.3 dry, 20x/0.75 multi-immersion, 63x/1.3 glycerol; laser lines: 405 nm, 488 nm, 532 nm, 638 nm) equipped with two PMT detectors. For imaging whole mount samples, retinae were mounted in MatTek dishes in 1 % low melting agarose/1x PTW with the CMZ touching the bottom of the dish. The dish was covered with 1x PTW after the agarose had solidified.

Images of whole hatchlings were acquired with a Nikon SMZ18 Stereomicroscope equipped with the camera Nikon DS-Ri1.

5.2.19 Cell cycle quantification

To determine cell cycle length of RPCs, BrdU and EdU were used as described (Das et al., 2009). Hatchlings were incubated 2 h in BrdU, then 30 min in EdU before fixation. Pcna antibody staining was used to label all cycling RPCs. Pcna-, EdU- and BrdU-positive cells as well as only BrdU-positive cells were quantified. Cell cycle length and S phase length were determined according to the following equations: $T_{\text{cell cycle}} = 2\text{h} \cdot (\text{Pcna}^+ \text{ cells/BrdU}^+ \text{ only cells})$; $T_{\text{S phase}} = 2\text{h} \cdot (\text{EdU}^+ \text{ cells/BrdU}^+ \text{ only cells})$. $T_{\text{cell cycle}}$ and $T_{\text{S phase}}$ were determined for individual sections.

5.2.20 Quantification of migration distance and velocity of immune cells

Migration of immune cells was quantified manually with Fiji. In the output file from tracking, velocity and distance were indicated. For the migration distance, all values were summed up per immune cell. The mean of all velocities was calculated for the average velocity of one immune cell.

5.2.21 Image processing and statistical analysis

Images were processed via Fiji image processing software. Statistical analysis and graphical representation of the data were performed using the Prism software package (GraphPad). Bars show mean and standard deviation. Unpaired t-tests were performed to determine statistical significance. The p-value $p < 0.05$ was considered significant and p-values are given in the figure legends. Sample size (n) and number of individuals are mentioned in every figure legend. No statistical methods were used to predetermine sample sizes, but our sample sizes are similar to those generally used in the field. The experimental groups were allocated randomly, and no blinding was done during allocation. The polar plot in Figure 2.18 was done by Erika Tsingos using Python. Figures and illustrations were done with Adobe Illustrator CS6. Quantification of experiments was performed in as stated in Table 5.25.

Table 5.25: Quantification of data presented in the respective figures.

Figure	Data	Quantification in
Figure 2.2	pIGF1R$^+$ cells in CMZ	all Z planes, all sections
Figure 2.3	BrdU$^+$ cells in CMZ	one Z plane, central sections
Figure 2.4	eye diameter/body length	whole animals, both eyes
Figure 2.5	Thickness & number of nuclei	one Z plane, central sections
Figure 2.6	layer thickness	one Z plane, central sections
Figure 2.8	Cell cycle, S-phase, BrdU$^+$ cells in CMZ	3 Z planes (= 6 µm), central sections
Figure 2.11	iArCoS number	whole retinae

Figure	Data	Quantification in
Figure 2.12	$Rx2^+$/$mCherry^+$ cells in CMZ	all Z planes, central sections
Figure 2.13	eye diameter/body length	whole animals, both eyes
Figure 2.14	eye diameter/body length	whole animals, both eyes
Figure 2.15	neuropil area $BrdU^+$ cells in OT	whole animals, one neuropil all Z planes, central sections
Figure 2.18	Phagosome distribution Phagosome number/retina	whole retinae whole retinae
Figure 2.22	migration distance average velocity	retinal sector retinal sector

5.2.22 Polymerase chain reaction (PCR)

PCRs were carried out as described in Table 5.26.

Table 5.26: PCR setup for a 50 µl reaction.

Component	Volume per 50 µl reaction	Final concentration
5x Q5 reaction buffer	10 µl	1x
2.5 mM dNTPs	4 µl	200 µM
10 µM forward primer	1 µl	0.2 µM
10 µM reverse primer	1 µl	0.2 µM
template DNA	variable	< 1 µg
Q5 High-Fidelity DNA Polymerase	0.3 µl	0.012 U/µl
nuclease-free H_2O	ad 50 µl	

PCR programs were chosen as recommended by the manufacturer (NEB). Annealing temperatures were calculated with the NEB Tm calculator (http://tmcalculator.neb.com/#!/main).

5.2.23 Oligonucleotide annealing

Oligonucleotide annealing reactions were performed in a PCR tube. 18 µl H_2O were mixed with 20 µl annealing buffer and 1 µl of each 100 µM oligonucleotide.

The oligonucleotide annealing was done in a PCR cycler with the following program: 5 min at 95°C, ramp down to 70°C, 10 min at 70°C, ramp down to 65°C, 10 min at 65°C, ramp down to 60°C, 10 min at 60°C, ramp down to 10°C. Annealed oligonucleotides were diluted to 0.075 pM with H_2O and ligation reaction was set up as described in Table 5.27 and incubated at room temperature for 1 h.

Table 5.27: Ligation after oligonucleotide annealing reaction.

Component	Volume per 10 µl ligation reaction
10x T4 DNA ligation buffer	1 µl
PEG-4000	1 µl
0.075 pM annealed product	1 µl
linearised vector	0.025 pM
T4 DNA ligase	1 µl
H_2O	ad 10 µl

5.2.24 Agarose gel electrophoresis

DNA samples were mixed with 6x DNA loading dye and loaded into the wells of 1–1.5 % agarose/1x TAE gels in gel chambers filled with 1x TAE. Electrophoresis was carried out with an electric potential difference of 90–130 V for 20–40 min, dependent on the gel and DNA fragment size. Afterwards, the agarose gel was stained in an aqueous TAE/ethidium bromide solution (EtBr bath) for 10–15 min. The stained gels were photographed using a UV light-based ($\lambda = 254$ nm) gel documentation system.

5.2.25 Gel Extraction

DNA bands of interest were identified and cut out of the agarose gel with a scalpel. DNA extraction was performed with the innuPREP PCRpure Kit according to manufacturer's protocol. The DNA was diluted with 15–30 µl pre-warmed H_2O.

5.2.26 DNA restriction

0.5 µl of the respective restriction enzymes, 1x buffer (dependent on the restriction enzymes) and 3–5 µg of DNA were mixed and incubated for at least 1 h at 37°C. For test restriction digests, 5 µl Miniprep were digested

with 0.2 µl restriction enzyme. The products of restriction digests were subsequently analysed by gel electrophoresis.

5.2.27 DNA ligation

For ligation, the optimal amounts of vector and insert were calculated with the following formula: amount of insert = insert size/vector size · 3 (molar ratio of insert/vector) · amount of vector to be used. The reaction was set up as described in Table 5.28 and incubated at room temperature for 1 h.

Table 5.28: Setup of DNA ligation reaction.

Component	Volume per 10 µl ligation reaction
linearised vector	50 ng
insert	according to the formula above
T4 DNA ligase	1 µl
10x T4 DNA ligation buffer	1 µl
H_2O	ad 10 µl

5.2.28 Transformation of chemically competent cells

50 µl MachT1 chemically competent cells were thawed on ice and mixed with up to 5 µl of DNA ligation by pipetting. The solution was incubated for 5–30 min on ice, before a heat shock at 42°C for 45 s was performed. Then, the mix was cooled on ice for 3 min and 300 µl TB medium were added. The tube was incubated for 1 h at 37°C and 200 rpm before spreading it on pre-warmed LB plates containing the respective antibiotic. For blue-white selection, 40 µl X-Gal were evenly spread on pre-warmed LB plates and left to dry before bacteria were plated. Plates were incubated at 37°C overnight, and colonies were used for plasmid preparation.

5.2.29 Plasmid preparation

For small scale plasmid preparation (Miniprep) 2 ml LB medium containing the respective antibiotic were inoculated with single bacterial clones and incubated for at least 5 h at 37°C and 200 rpm. The bacterial culture was centrifuged in 2 ml Eppendorf tubes for 5 min at 14000 rpm. The supernatant was discarded and the pellet resuspended in 250 µl cold P1 buffer. 250 µl P2 buffer were added and tubes inverted to mix contents. Then, 250 µl cold P3 buffer were added and tubes inverted again. Tubes were centrifuged for 10

min at 14000 rpm and supernatant was transferred to a new 1.5 ml Eppendorf tube. 500 µl 2-Propanol were added, contents were thoroughly mixed and centrifuged for 10 min at 14000 rpm. The supernatant was discarded and the pellet was washed with 500 µl EtOH (70 %) and centrifuged for 5 min at 14000 rpm. The supernatant was discarded and the pellet left to dry before dissolving it in 50 µl H_2O.

For large scale plasmid preparation ("Big Mini") using the QIAprep Spin Miniprep Kit, 20 ml LB medium containing the respective antibiotic were inoculated with single bacterial clones and incubated at 37°C and 200 rpm overnight. Purification of plasmid DNA was performed according to manufacturer's instructions with the following changes: two 2 ml Eppendorf tubes were used per plasmid and centrifuged 2x each with 2 ml bacterial culture (equals 8 ml bacterial culture per plasmid preparation). Later, the supernatants of both tubes were merged onto the same spin column. The DNA was eluted with 50 µl H_2O.

For large scale plasmid preparations (Midiprep) 50 ml LB medium with the respective antibiotic were inoculated with single bacterial clones or 100 µl of a single clone-derived bacterial culture and incubated at 37°C and 200 rpm overnight. Purification of plasmid DNA was performed using the Plasmid Midi Kit according to manufacturer's instructions with the following changes: all centrifugation steps were performed at 4000 rpm, increasing the duration of centrifugation steps accordingly. After addition of P3, the centrifugation step was replaced by filtration of the solution with filter paper. The pellet was resuspended in 80 µl TE first, then diluted to 1 µg/µl with TE and stored at –20°C.

5.2.30 Preparation of sgRNAs

Design of sgRNAs was done with CCTop (Stemmer et al., 2015). Cloning of sgRNA templates was performed as described (Stemmer et al., 2015). Template plasmid was digested with DraI overnight at 37°C, bands were separated by gel electrophoresis and the 300 bp band was purified with the innuPREP PCRpure Kit. Transcription of sgRNAs was done with the MEGAShortScript T7 Kit and purified with the RNeasy Mini Kit, according to manufacturers' protocols. RNA quality was checked with a test gel and the concentration adjusted to 150 ng/µl.

5.2.31 Preparation of cDNA

Total RNA was isolated from 6 wildtype and 6 *ccl25b*$^{-/-}$ hatchlings by lysis in Trizol and chloroform extraction following the manufacturer's protocol. Precipitation of RNA was performed with isopropanol and resuspended in nuclease-free H_2O. Reverse transcription of RNA into cDNA was done with RevertAid First Strand cDNA Synthesis Kit after DNAse digestion and inactivation according to manufacturer's instructions. RT-PCR was performed using the primers JW6725 and JW8643. PCR products were analysed on a 1 % agarose gel, extracted and sent for sequencing.

Contributions

The immune part (2.2) was done in collaboration with Katharina Lust. Experiments presented in this thesis were performed by me, but conceptualization, discussion and analysis was a shared effort.
The graphical representation of data in the polar plot in Figure 2.18B was done by Erika Tsingos.
In collaboration with Karl-Heinz Körtje and Leica, the *in vivo* time-lapse movie of one *ccr9a::eGFP*, *ccl25b::H2B-RFP* hatchling was acquired (Figure 2.19).

Acknowledgements

First and foremost, I want to thank you, Jochen, for offering me the opportunity to do the PhD in your lab. I know this sounds lame, and everyone probably writes similar stuff, but this offer literally changed my life. I was not sure what to do after finishing the master, and there you were with this "easy" option, so I decided to take it as long as it was making me happy. You saw potential in me where I didn't even know I had any, and for mentoring me and shaping me to become the scientist and person that I am now I will forever be grateful! I learned so much, grew up, met amazing friends, became me, all while being part of your lab. As a supervisor, I love that you not only challenged me scientifically, but that you genuinely cared about me and my well-being. I couldn't have come to a better place for the PhD and would totally do it again.

I want to thank Prof. Dr. Jan Lohmann for being my second supervisor, providing a fresh perspective in my TACs and for valuable feedback on my project.

Lázaro, I want to thank you for always having an open door for me. I loved our little random conversations about life, but I especially value the feedback and input you gave me during my PhD. Your somehow always knew when I was sad or stressed or lost my motivation and came to talk to me then and changed my perspective. Thank you so much for your scientific as well as emotional support!

I would like to thank Dr. Annika Guse for being in my committee and for being an inspiring female scientist.

I want to thank you, Steffen, for always being super excited about everything, basically. First in my master thesis defence, then in my third TAC and all the moments in between, but also in the impromptu career advice session that we had. I appreciate your honesty and sensitivity in approaching this topic and broadening my thinking.

To all (past and present) 5th floor people: I can't thank you enough for generating such a welcoming, friendly and supportive environment. Doing a PhD is a challenge, but it was made so much easier and enjoyable by having you as colleagues and friends. I especially want to thank Tanja, for all the support, excellent advice on all technical things and for patiently answering

all my questions. Frederike, thank you so much for making the bureaucracy as easy as possible for us and all the help with filling out incomprehensible forms.
I was lucky to be adopted into Bay 4 when I started in the lab. I had so much fun with you, and I have found such great friends in you. Eva, thank you for being my first supervisor, for teaching me a practical, pragmatic approach to experimenting and for being even more impatient than me! I admire your ability to juggle everything in your life, being an amazing mother, an awesome friend and a scientist. Alicia, I love you for being always there for me, for putting up with me even when we are annoyed with each other, and for unconditionally accepting me and being happy for me. Isa, you were not part of Bay 4, but I regard you as an honourable member nonetheless. You were supervising me for my first lab rotation in the 5th floor universe, and I had so much fun and learnt a lot which made me want to become part of it.
To all my other friends that I made during the master and PhD: I am so glad that I met you and that you are part of my life, I really do hope it stays that way!
Katha (die Wissenschaftlerin), dir kann ich gar nicht genug danken. Du hast mich die ersten zwei Jahre meines PhDs - inoffiziell - betreut, und ich habe so viel von dir gelernt. Für all die Sachen die du mir beigebracht hast, die Anforderungen die du an mich als Wissenschaftlerin stellst, die Ergebnisse und Experimente die du mit mir diskutierst bin ich dir so dankbar, weil mich das so viel weitergebracht hat. Außerdem bewundere ich deine Leidenschaft für die Wissenschaft, auch wenn ich im Gegensatz zu dir nicht unbedingt beim Frühstück die neueste Nature-Ausgabe lesen muss.
Katha (meine Katha), ich bin so froh dich gefunden zu haben. Du bist die großartigste Person die ich kenne, und bei dir fühle ich mich zuhause. Ich möchte dir für deine Unterstützung, deine Motivation und deinen Enthusiasmus, mit dem du mich oft ansteckst, danken, ohne dich wäre der PhD sehr viel anstrengender, langweiliger und schwieriger gewesen.
Als letztes möchte ich meiner Familie und insbesondere meinen Eltern danken: ihr seid die allerbesten, ich bin euch so dankbar dass ihr immer für mich da seid, mich in allem unterstützt und mich bedingungslos akzeptiert. Danke!

References

Aghaallaei, N., Bajoghli, B., Schwarz, H., Schorpp, M., and Boehm, T. (2010). Characterization of mononuclear phagocytic cells in medaka fish transgenic for a cxcr3a:gfp reporter. Proceedings of the National Academy of Sciences *107*, 18079–18084.

Ahmad, I., Tang, L., and Pham, H. (2000). Identification of Neural Progenitors in the Adult Mammalian Eye. Biochemical and Biophysical Research Communications *270*, 517–521.

Alberts, B., Johnson, A., Lewis, J., Morgan, D., Raff, M., Roberts, K., Walter, P., and Horstmann, C. (2017). Angeborene und adaptive Immunsysteme. In Molekularbiologie Der Zelle, (John Wiley & Sons, Incorporated), pp. 1475–1528.

Alunni, A., Hermel, J.-M., Heuzé, A., Bourrat, F., Jamen, F., and Joly, J.-S. (2010). Evidence for neural stem cells in the Medaka optic tectum proliferation zones. Devel Neurobio *70*, 693–713.

Ansai, S., and Kinoshita, M. (2014). Targeted mutagenesis using CRISPR/Cas system in medaka. Biology Open *3*, 362–371.

Arunachalam, M., Raja, M., Vijayakumar, C., Malaiammal, P., and Mayden, R.L. (2013). Natural History of Zebrafish (Danio rerio) in India. Zebrafish *10*, 1–14.

Asensio, V.C., and Campbell, I.L. (1999). Chemokines in the CNS: Plurifunctional mediators in diverse states. Trends in Neurosciences *22*, 504–512.

Ayaso, E., Nolan, C.M., and Byrnes, L. (2002). Zebrafish insulin-like growth factor-I receptor: molecular cloning and developmental expression. Molecular and Cellular Endocrinology *191*, 137–148.

Åberg, M.A.I., Åberg, N.D., Hedbäcker, H., Oscarsson, J., and Eriksson, P.S. (2000). Peripheral Infusion of IGF-I Selectively Induces Neurogenesis in the Adult Rat Hippocampus. Journal of Neuroscience *20*, 2896–2903.

Baader, C. (2016). Epidermal growth factor receptor signalling-related component expression in retina and brain of *Oryzias latipes*. Universität Heidelberg.

Bacon, K., Baggiolini, M., Broxmeyer, H., Horuk, R., Lindley, I., Mantovani, A., Matsushima, K., Murphy, P., Nomiyama, H., Oppenheim, J., et al. (2002). Chemokine/Chemokine Receptor Nomenclature. Journal of Interferon & Cytokine Research *22*, 1067–1068.

Bajoghli, B., Aghaallaei, N., Hess, I., Rode, I., Netuschil, N., Tay, B.-H., Venkatesh, B., Yu, J.-K., Kaltenbach, S.L., Holland, N.D., et al. (2009). Evolution of Genetic Networks Underlying the Emergence of Thymopoiesis in Vertebrates. Cell *138*, 186–197.

Bajoghli, B., Kuri, P., Inoue, D., Aghaallaei, N., Hanelt, M., Thumberger, T., Rauzi, M., Wittbrodt, J., and Leptin, M. (2015). Noninvasive In Toto Imaging of the Thymus Reveals Heterogeneous Migratory Behavior of Developing T Cells. J Immunol *195*, 2177–2186.

Barbieri, M., Bonafè, M., Franceschi, C., and Paolisso, G. (2003). Insulin/IGF-I-signaling pathway: an evolutionarily conserved mechanism of longevity from yeast to humans. American Journal of Physiology-Endocrinology and Metabolism *285*, E1064–E1071.

Bendall, S.C., Stewart, M.H., Menendez, P., George, D., Vijayaragavan, K., Werbowetski-Ogilvie, T., Ramos-Mejia, V., Rouleau, A., Yang, J., Bossé, M., et al. (2007). IGF and FGF cooperatively establish the regulatory stem cell niche of pluripotent human cells in vitro. Nature *448*, 1015–1021.

Bernardos, R.L., Barthel, L.K., Meyers, J.R., and Raymond, P.A. (2007). Late-Stage Neuronal Progenitors in the Retina Are Radial Muller Glia That Function as Retinal Stem Cells. Journal of Neuroscience *27*, 7028–7040.

Boehm, T. (2011). Design principles of adaptive immune systems. Nature Reviews Immunology *11*, 307–317.

Boucher, S.E., and Hitchcock, P.F. (1998a). Insulin-related growth factors stimulate proliferation of retinal progenitors in the goldfish. J. Comp. Neurol. *394*, 386–394.

Boucher, S.E.M., and Hitchcock, P.F. (1998b). Insulin-like growth factor-I binds in the inner plexiform layer and circumferential germinal zone in the retina of the goldfish. J. Comp. Neurol. *394*, 395–401.

Boya, J., Calvo, J., and Carbonell, A.L. (1987). Appearance of Microglial Cells in the Postnatal Rat Retina. Archivum Histologicum Japonicum *50*, 223–228.

Breit, A., Miek, L., Schredelseker, J., Geibel, M., Merrow, M., and Gudermann, T. (2018). Insulin-like growth factor-1 acts as a zeitgeber on hypothalamic circadian clock gene expression via glycogen synthase kinase-3β signaling. The Journal of Biological Chemistry *293*, 17278–17290.

Carboni, J.M., Lee, A.V., Hadsell, D.L., Rowley, B.R., Lee, F.Y., Bol, D.K., Camuso, A.E., Gottardis, M., Greer, A.F., Ho, C.P., et al. (2005). Tumor Development by Transgenic Expression of a Constitutively Active Insulin-Like Growth Factor I Receptor. Cancer Res *65*, 3781–3788.

Caruso, M.A., and Sheridan, M.A. (2011). New insights into the signaling system and function of insulin in fish. General and Comparative Endocrinology *173*, 227–247.

Caves, E.M., Sutton, T.T., and Johnsen, S. (2017). Visual acuity in ray-finned fishes correlates with eye size and habitat. Journal of Experimental Biology *220*, 1586–1596.

Centanin, L., and Wittbrodt, J. (2014). Retinal neurogenesis. Development *141*, 241–244.

Centanin, L., Ander, J.J., Hoeckendorf, B., Lust, K., Kellner, T., Kraemer, I., Urbany, C., Hasel, E., Harris, W.A., Simons, B.D., et al. (2014). Exclusive multipotency and preferential asymmetric divisions in post-embryonic neural stem cells of the fish retina. Development *141*, 3472–3482.

Centanin, L., Hoeckendorf, B., and Wittbrodt, J. (2011). Fate restriction and multipotency in retinal stem cells. Cell Stem Cell *9*, 553–562.

Cepko, C.L., Austin, C.P., Yang, X., Alexiades, M., and Ezzeddine, D. (1996). Cell fate determination in the vertebrate retina. Proceedings of the National Academy of Sciences *93*, 589–595.

Chablais, F., and Jazwinska, A. (2010). IGF signaling between blastema and wound epidermis is required for fin regeneration. Development *137*, 871–879.

Chakrabarti, R., Celià-Terrassa, T., Kumar, S., Hang, X., Wei, Y., Choudhury, A., Hwang, J., Peng, J., Nixon, B., Grady, J.J., et al. (2018). Notch ligand Dll1 mediates cross-talk between mammary stem cells and the macrophageal niche. Science (New York, N.Y.) *360*, eaan4153.

Chaudhari, A., Gupta, R., Patel, S., Velingkaar, N., and Kondratov, R. (2017). Cryptochromes regulate IGF-1 production and signaling through control of JAK2-dependent STAT5B phosphorylation. Molecular Biology of the Cell *28*, 834–842.

Chell, J.M., and Brand, A.H. (2010). Nutrition-responsive glia control exit of neural stem cells from quiescence. Cell *143*, 1161–1173.

Chiu, J.F., Mack, A.F., and Fernald, R.D. (1995). Daily rhythm of cell proliferation in the teleost retina. Brain Research *673*, 119–125.

Choi, W.-Y., Gemberling, M., Wang, J., Holdway, J.E., Shen, M.-C., Karlstrom, R.O., and Poss, K.D. (2013). In vivo monitoring of cardiomyocyte proliferation to identify chemical modifiers of heart regeneration. Development *140*, 660–666.

Chow, A., Lucas, D., Hidalgo, A., Méndez-Ferrer, S., Hashimoto, D., Scheiermann, C., Battista, M., Leboeuf, M., Prophete, C., van Rooijen, N., et al. (2011). Bone marrow CD169 + macrophages promote the retention of hematopoietic stem and progenitor cells in the mesenchymal stem cell niche. J Exp Med *208*, 261–271.

Collett, T.S., and Land, M.F. (1975). Visual control of flight behaviour in the hoverfly, Syritta pipiens L. Journal of Comparative Physiology *99*, 1–66.

Collin, S.P., and Partridge, J.C. (1996). Fish Vision - Retinal specializations in the eyes of deep-sea teleosts. J Fish Biology *49*, 157–174.

Conedera, F.M., Pousa, A.M.Q., Mercader, N., Tschopp, M., and Enzmann, V. (2019). Retinal microglia signaling affects Müller cell behavior in the zebrafish following laser injury induction. Glia *67*, 1150–1166.

Conner, C., Ackerman, K.M., Lahne, M., Hobgood, J.S., and Hyde, D.R. (2014). Repressing notch signaling and expressing TNFα are sufficient to mimic retinal regeneration by inducing Müller glial proliferation to generate committed progenitor cells. J. Neurosci. *34*, 14403–14419.

Craig, S.E.L., Calinescu, A.-A., and Hitchcock, P.F. (2008). Identification of the molecular signatures integral to regenerating photoreceptors in the retina of the zebra fish. J Ocul Biol Dis Inform *1*, 73–84.

D'Ercole, A.J., Applewhite, G.T., and Underwood, L.E. (1980). Evidence that somatomedin is synthesized by multiple tissues in the fetus. Developmental Biology *75*, 315–328.

Dai, X., Zhang, W., Zhuo, Z., He, J., and Yin, Z. (2015). Neuroendocrine regulation of somatic growth in fishes. Sci. China Life Sci. *58*, 137–147.

Darmaillacq, A.-S., Chichery, R., Poirier, R., and Dickel, L. (2004). Effect of early feeding experience on subsequent prey preference by cuttlefish, Sepia officinalis. Dev. Psychobiol. *45*, 239–244.

Darwish, S.T., Mohalal, M.E., Helal, M.M., and El-Sayyad, H.I.H. (2015). Structural and functional analysis of ocular regions of five marine teleost fishes (Hippocampus hippocampus, Sardina pilchardus, Gobius niger, Mullus barbatus & Solea solea). Egyptian Journal of Basic and Applied Sciences *2*, 159–166.

Das, G., Choi, Y., Sicinski, P., and Levine, E.M. (2009). Cyclin D1 fine-tunes the neurogenic output of embryonic retinal progenitor cells. Neural Development *4*, 1–23.

Das, R., and Dobens, L.L. (2015). Conservation of gene and tissue networks regulating insulin signalling in flies and vertebrates. Biochemical Society Transactions *43*, 1057–1062.

Davis, B.M., Salinas-Navarro, M., Cordeiro, M.F., Moons, L., and Groef, L.D. (2017). Characterizing microglia activation: A spatial statistics approach to maximize information extraction. Scientific Reports *7*, 1–12.

de Busserolles, F., Fitzpatrick, J.L., Marshall, N.J., and Collin, S.P. (2014). The influence of photoreceptor size and distribution on optical sensitivity in the eyes of lanternfishes (Myctophidae). PLoS ONE *9*, e99957.

de Busserolles, F., Fitzpatrick, J.L., Paxton, J.R., Marshall, N.J., and Collin, S.P. (2013). Eye-size variability in deep-sea lanternfishes (Myctophidae): an ecological and phylogenetic study. PLoS ONE *8*, e58519.

DeVries, M.E., Kelvin, A.A., Xu, L., Ran, L., Robinson, J., and Kelvin, D.J. (2006). Defining the Origins and Evolution of the Chemokine/Chemokine Receptor System. J Immunol *176*, 401–415.

Diaz-Aparicio, I., Beccari, S., Abiega, O., and Sierra, A. (2016). Clearing the corpses: regulatory mechanisms, novel tools, and therapeutic potential of harnessing microglial phagocytosis in the diseased brain. Neural Regen Res *11*, 1533–1539.

Eggeler, F. (2017). Ccl25 chemokines and Ccr9 receptors in the retinal stem cell niche of medaka. Universität Heidelberg.

Eivers, E., McCarthy, K., Glynn, C., Nolan, C.M., and Byrnes, L. (2004). Insulin-like growth factor (IGF) signalling is required for early dorso-anterior development of the zebrafish embryo. Int. J. Dev. Biol. *48*, 1131–1140.

El-Brolosy, M.A., Kontarakis, Z., Rossi, A., Kuenne, C., Günther, S., Fukuda, N., Kikhi, K., Boezio, G.L.M., Takacs, C.M., Lai, S.-L., et al. (2019). Genetic compensation triggered by mutant mRNA degradation. Nature *568*, 193–197.

Engeszer, R.E., Patterson, L.B., Rao, A.A., and Parichy, D.M. (2007). Zebrafish in The Wild: A Review of Natural History And New Notes from The Field. Zebrafish *4*, 21–40.

Fekete, D.M., Perez-Miguelsanz, J., Ryder, E.F., and Cepko, C.L. (1994). Clonal Analysis in the Chicken Retina Reveals Tangential Dispersion of Clonally Related Cells. Developmental Biology *166*, 666–682.

Fischer, A.J., and Reh, T.A. (2000). Identification of a proliferating marginal zone of retinal progenitors in postnatal chickens. Developmental Biology *220*, 197–210.

Fischer, A.J., Bosse, J.L., and El-Hodiri, H.M. (2013). The ciliary marginal zone (CMZ) in development and regeneration of the vertebrate eye. Experimental Eye Research *116*, 199–204.

Freund, C., Ward-van Oostwaard, D., Monshouwer-Kloots, J., van den Brink, S., van Rooijen, M., Xu, X., Zweigerdt, R., Mummery, C., and Passier, R. (2007). Insulin Redirects Differentiation from Cardiogenic Mesoderm and Endoderm to Neuroectoderm in Differentiating Human Embryonic Stem Cells. Stem Cells *26*, 724–733.

Grabher, C., and Wittbrodt, J. (2007). Meganuclease and transposon mediated transgenesis in medaka. Genome Biol. *8*, S10.1–S10.7.

Gyda, M., Wolman, M., Lorent, K., and Granato, M. (2012). The tumor suppressor gene retinoblastoma-1 is required for retinotectal development and visual function in zebrafish. PLoS Genet *8*, e1003106.

Hall, Z.J., and Tropepe, V. (2018). Visual experience facilitates BDNF-dependent adaptive recruitment of new neurons in the postembryonic optic tectum. Journal of Neuroscience *38*, 1962–1917.

Hasel, E.M. (2017). Egfr signaling in *Oryzias latipes* - Characterization of inducible oncogene gain-of-function and receptor loss-of-function Medaka lines. Universität Heidelberg.

He, J., Zhang, G., Almeida, A.D., Cayouette, M., Simons, B.D., and Harris, W.A. (2012). How Variable Clones Build an Invariant Retina. Neuron *75*, 786–798.

Herbomel, P., Thisse, B., and Thisse, C. (1999). Ontogeny and behaviour of early macrophages in the zebrafish embryo. Development *126*, 3735–3745.

Herbomel, P., Thisse, B., and Thisse, C. (2001). Zebrafish Early Macrophages Colonize Cephalic Mesenchyme and Developing Brain, Retina, and Epidermis through a M-CSF Receptor-Dependent Invasive Process. Developmental Biology *238*, 274–288.

Hess, I., and Boehm, T. (2012). Intravital Imaging of Thymopoiesis Reveals Dynamic Lympho-Epithelial Interactions. Immunity *36*, 298–309.

Hollyfield, J.G. (1971). Differential growth of the neural retina in Xenopus laevis larvae. Developmental Biology *24*, 264–286.

Holstein, T.W. (2012). The Evolution of the Wnt Pathway. Cold Spring Harbor Perspectives in Biology *4*, a007922–a007922.

Holt, C.E., Bertsch, T.W., Ellis, H.M., and Harris, W.A. (1988). Cellular determination in the xenopus retina is independent of lineage and birth date. Neuron *1*, 15–26.

Hong, C.J., Park, H., and Yu, S.-W. (2016). Autophagy for the quality control of adult hippocampal neural stem cells. Brain Research *1649*, 166–172.

Hoopes, B.C., Rimbault, M., Liebers, D., Ostrander, E.A., and Sutter, N.B. (2012). The insulin-like growth factor 1 receptor (IGF1R) contributes to reduced size in dogs. Mamm Genome *23*, 780–790.

Huang, Y., Harrison, M.R., Osorio, A., Kim, J., Baugh, A., Duan, C., Sucov, H.M., and Lien, C.-L. (2013). Igf Signaling is Required for Cardiomyocyte Proliferation during Zebrafish Heart Development and Regeneration. PLoS ONE *8*, e67266.

Huangfu, D., and Anderson, K.V. (2006). Signaling from Smo to Ci/Gli: conservation and divergence of Hedgehog pathways from Drosophila to vertebrates. Development *133*, 3–14.

Hume, D.A., Perry, H., and Gordon, S. (1983). Immunohistochemical localization of a macrophage-specific antigen in developing mouse retina: phagocytosis of dying neurons and differentiation of microglial cells to form a regular array in the plexiform layers. J Cell Biol *97*, 253–257.

Ishtiaq Ahmed, A.S., Xiong, F., Pang, S.-C., He, M.-D., Waters, M.J., Zhu, Z.-Y., and Sun, Y.-H. (2011). Activation of GH signaling and GH-independent stimulation of growth in zebrafish by introduction of a constitutively activated GHR construct. Transgenic Res *20*, 557–567.

Johns, P.R., and Easter, S.S. (1977). Growth of the adult goldfish eye. II. Increase in retinal cell number. J. Comp. Neurol. *176*, 331–341.

Jones, S.L., Wang, J., Turck, C.W., and Brown, E.J. (1998). A role for the actin-bundling protein l-plastin in the regulation of leukocyte integrin function. Proceedings of the National Academy of Sciences *95*, 9331–9336.

Ju, B., Chen, W., Orr, B.A., Spitsbergen, J.M., Jia, S., Eden, C.J., Henson, H.E., and Taylor, M.R. (2015). Oncogenic KRAS promotes malignant brain tumors in zebrafish. Molecular Cancer *14*, 18–11.

Junnila, R.K., List, E.O., Berryman, D.E., Murrey, J.W., and Kopchick, J.J. (2013). The GH/IGF-1 axis in ageing and longevity. Nature Reviews Endocrinology *9*, 366–376.

Kaletsky, R., and Murphy, C.T. (2010). The role of insulin/IGF-like signaling in C. elegans longevity and aging. Disease Models & Mechanisms *3*, 415–419.

Kapp, F.G., Perlin, J.R., Hagedorn, E.J., Gansner, J.M., Schwarz, D.E., O'Connell, L.A., Johnson, N.S., Amemiya, C., Fisher, D.E., Wölfle, U., et al. (2018). Protection from UV light is an evolutionarily conserved feature of the haematopoietic niche. Nature *558*, 445–448.

Kirchmaier, S., Naruse, K., Wittbrodt, J., and Loosli, F. (2015). The genomic and genetic toolbox of the teleost medaka (Oryzias latipes). Genetics *199*, 905–918.

Kizil, C., Dudczig, S., Kyritsis, N., Machate, A., Blaesche, J., Kroehne, V., and Brand, M. (2012). The chemokine receptor cxcr5 regulates the regenerative neurogenesis response in the adult zebrafish brain. Neural Development *7*, 27–39.

Klimova, L., and Kozmik, Z. (2014). Stage-dependent requirement of neuroretinal Pax6 for lens and retina development. Development *141*, 1292–1302.

Kobayashi, I., Katakura, F., and Moritomo, T. (2016). Isolation and characterization of hematopoietic stem cells in teleost fish. Developmental and Comparative Immunology *58*, 86–94.

Kraft, P., Evangelista, C., Dacke, M., Labhart, T., and Srinivasan, M.V. (2011). Honeybee navigation: following routes using polarized-light cues. Philosophical Transactions of the Royal Society B: Biological Sciences *366*, 703–708.

Kubota, R., Hokoc, J.N., Moshiri, A., McGuire, C., and Reh, T.A. (2002). A comparative study of neurogenesis in the retinal ciliary marginal zone of homeothermic vertebrates. Developmental Brain Research *134*, 31–41.

Kyritsis, N., Kizil, C., Zocher, S., Kroehne, V., Kaslin, J., Freudenreich, D., Iltzsche, A., and Brand, M. (2012). Acute Inflammation Initiates the Regenerative Response in the Adult Zebrafish Brain. Science *338*, 1353–1356.

Lahne, M., Piekos, S.M., O'Neill, J., Ackerman, K.M., and Hyde, D.R. (2019). Photo-regulation of rod precursor cell proliferation. Experimental Eye Research *178*, 148–159.

Laviola, L., Natalicchio, A., and Giorgino, F. (2007). The IGF-I Signaling Pathway. Current Pharmaceutical Design *13*, 663–669.

Lenkowski, J.R., and Raymond, P.A. (2014). Müller glia: Stem cells for generation and regeneration of retinal neurons in teleost fish. Progress in Retinal and Eye Research *40*, 94–123.

Li, J., Chu, L., Sun, X., Liu, Y., and Cheng, C.H.K. (2015). IGFs Mediate the Action of LH on Oocyte Maturation in Zebrafish. Molecular Endocrinology *29*, 373–383.

Li, J., Liu, Z., Wang, D., and Cheng, C.H.K. (2011). Insulin-like growth factor 3 is involved in oocyte maturation in zebrafish. Biology of Reproduction *84*, 476–486.

Li, J., Wu, P., Liu, Y., Wang, D., and Cheng, C.H.K. (2014). Temporal and spatial expression of the four Igf ligands and two Igf type 1 receptors in zebrafish during early embryonic development. Gene Expression Patterns *15*, 104–111.

Ling, E.A. (1982). A Light Microscopic Demonstration of Amoeboid Microglia and Microglial Cells in the Retina of Rats of Various Ages. Archivum Histologicum Japonicum *45*, 37–44.

Lischik, C. (2019). Combining *in vivo* imaging and mechanistic approaches to investigate Wnt regulation of retinal stem cells. Universität Heidelberg.

Livet, J., Weissman, T.A., Kang, H., Draft, R.W., Lu, J., Bennis, R.A., Sanes, J.R., and Lichtman, J.W. (2007). Transgenic strategies for combinatorial expression of fluorescent proteins in the nervous system. Nature *450*, 56–62.

Loosli, F., Köster, R.W., Carl, M., Kühnlein, R., Henrich, T., Mücke, M., Krone, A., and Wittbrodt, J. (2000). A genetic screen for mutations affecting embryonic development in medaka fish (Oryzias latipes). Mechanisms of Development *97*, 133–139.

Lust, K. (2017). The regenerative potential of Müller glia cells in the medaka retina. Universität Heidelberg.

Lust, K., and Wittbrodt, J. (2018). Activating the regenerative potential of Müller glia cells in a regeneration-deficient retina. eLife *7*, 7028.

Lust, K., Sinn, R., Pérez Saturnino, A., Centanin, L., and Wittbrodt, J. (2016). *De novo* neurogenesis by targeted expression of *atoh7* to Müller glia cells. Development *143*, 1874–1883.

Lustig, A., Ketter-Katz, H., and Katzir, G. (2012). Visually Guided Avoidance in the Chameleon (Chamaeleo chameleon): Response Patterns and Lateralization. PLoS ONE *7*, e37875.

Mack, A.F., and Fernald, R.D. (1993). Regulation of cell division and rod differentiation in the teleost retina. Developmental Brain Research *76*, 183–187.

Mack, A.F., Balt, S.L., and Fernald, R.D. (1995). Localization and expression of insulin-like growth factor in the teleost retina. Visual Neuroscience *12*, 457–461.

Mantovani, A., Sica, A., Sozzani, S., Allavena, P., Vecchi, A., and Locati, M. (2004). The chemokine system in diverse forms of macrophage activation and polarization. Trends in Immunology *25*, 677–686.

Martins, R.R., Ellis, P.S., MacDonald, R.B., Richardson, R.J., and Henriques, C.M. (2019). Resident Immunity in Tissue Repair and Maintenance: The Zebrafish Model Coming of Age. Frontiers in Cell and Developmental Biology *7*, 12.

Maures, T., Chan, S.J., Xu, B., Sun, H., Ding, J., and Duan, C. (2002). Structural, biochemical, and expression analysis of two distinct insulin-like growth factor I receptors and their ligands in zebrafish. Endocrinology *143*, 1858–1871.

Mayrhofer, M., Gourain, V., Reischl, M., Affaticati, P., Jenett, A., Joly, J.-S., Benelli, M., Demichelis, F., Poliani, P.L., Sieger, D., et al. (2017). A novel brain tumour model in zebrafish reveals the role of YAP activation in MAPK- and PI3K-induced malignant growth. Disease Models & Mechanisms *10*, 15–28.

McClure, M.M., McIntyre, P.B., and McCune, A.R. (2006). Notes on the natural diet and habitat of eight danionin fishes, including the zebrafish Danio rerio. J Fish Biology *69*, 553–570.

McCormick, S.D., Kelley, K.M., Young, G., Nishioka, R.S., and Bern, H.A. (1992). Stimulation of coho salmon growth by insulin-like growth factor I. General and Comparative Endocrinology *86*, 398–406.

McMenamin, P.G., Saban, D.R., and Dando, S.J. (2019). Immune cells in the retina and choroid: Two different tissue environments that require different defenses and surveillance. Progress in Retinal and Eye Research *70*, 85–98.

Mellough, C.B., Collin, J., Khazim, M., White, K., Sernagor, E., Steel, D.H.W., and Lako, M. (2015). IGF-1 Signaling Plays an Important Role in the Formation of Three-Dimensional Laminated Neural Retina and Other Ocular Structures From Human Embryonic Stem Cells. Stem Cells *33*, 2416–2430.

Mitchell, D.M., Lovel, A.G., and Stenkamp, D.L. (2018). Dynamic changes in microglial and macrophage characteristics during degeneration and regeneration of the zebrafish retina. Journal of Neuroinflammation *15*, 163–183.

Mitchell, D.M., Sun, C., Hunter, S.S., New, D.D., and Stenkamp, D.L. (2019). Regeneration associated transcriptional signature of retinal microglia and macrophages. Scientific Reports *9*, 4768.

Morris, V.B., Wylie, C.C., and Miles, V.J. (1976). The growth of the chick retina after hatching. The Anatomical Record *184*, 111–113.

Moshiri, A., and Reh, T.A. (2004). Persistent Progenitors at the Retinal Margin of ptc+/- Mice. Journal of Neuroscience *24*, 229–237.

Möller, E.K. (2017). Modulation of the Wnt pathway at single-cell level uncovers diverging functional domains in the ciliary marginal zone of medaka. Universität Heidelberg.

Naik, S., Larsen, S.B., Cowley, C.J., and Fuchs, E. (2018). Two to Tango: Dialog between Immunity and Stem Cells in Health and Disease. Cell *175*, 908–920.

Nässel, D.R., Liu, Y., and Luo, J. (2015). Insulin/IGF signaling and its regulation in Drosophila. General and Comparative Endocrinology *221*, 255–266.

Nelson, J.S., Grande, T.C., and Wilson, M.V.H. (2016). Fishes of the World (Hoboken, NJ, USA: John Wiley & Sons, Inc).

Nguyen, A.T., Emelyanov, A., Koh, C.H.V., Spitsbergen, J.M., Parinov, S., and Gong, Z. (2012). An inducible kras V12 transgenic zebrafish model for liver tumorigenesis and chemical drug screening. Disease Models & Mechanisms *5*, 63–72.

Nguyen, V., Deschet, K., Henrich, T., Godet, E., Joly, J.-S., Wittbrodt, J., Chourrout, D., and Bourrat, F. (1999). Morphogenesis of the optic tectum in the medaka (Oryzias latipes): A morphological and molecular study, with special emphasis on cell proliferation. Journal of Comparative Neurology *413*, 385–404.

Nieto-Estévez, V., Defterali, Ç., and Vicario-Abejón, C. (2016). IGF-I: A Key Growth Factor that Regulates Neurogenesis and Synaptogenesis from Embryonic to Adult Stages of the Brain. Front. Neurosci. *10*, 52.

Nimmerjahn, A., Kirchhoff, F., and Helmchen, F. (2005). Resting Microglial Cells Are Highly Dynamic Surveillants of Brain Parenchyma in Vivo. Science *308*, 1314–1318.

Nóbrega, R.H., Morais, R.D.V. de S., Crespo, D., de Waal, P.P., de França, L.R., Schulz, R.W., and Bogerd, J. (2015). Fsh Stimulates Spermatogonial Proliferation and Differentiation in Zebrafish via Igf3. Endocrinology *156*, 3804–3817.

Otteson, D.C., Cirenza, P.F., and Hitchcock, P.F. (2002). Persistent neurogenesis in the teleost retina: Evidence for regulation by the growth-hormone/insulin-like growth factor-I axis. Mechanisms of Development *117*, 137–149.

Otteson, D.C., and Hitchcock, P.F. (2003). Stem cells in the teleost retina: Persistent neurogenesis and injury-induced regeneration. Vision Research *43*, 927–936.

Otteson, D.C., D'Costa, A.R., and Hitchcock, P.F. (2001). Putative Stem Cells and the Lineage of Rod Photoreceptors in the Mature Retina of the Goldfish. Developmental Biology *232*, 62–76.

Pankhurst, N.W. (1989). The relationship of ocular morphology to feeding modes and activity periods in shallow marine teleosts from New Zealand. Environmental Biology of Fishes *26*, 201–211.

Park, S.W., Davison, J.M., Rhee, J., Hruban, R.H., Maitra, A., and Leach, S.D. (2008). Oncogenic KRAS Induces Progenitor Cell Expansion and Malignant Transformation in Zebrafish Exocrine Pancreas. Gastroenterology *134*, 2080–2090.

Peatman, E., and Liu, Z. (2007). Evolution of CC chemokines in teleost fish: A case study in gene duplication and implications for immune diversity. Immunogenetics *59*, 613–623.

Perez, L.N., Lorena, J., Costa, C.M., Araujo, M.S., Frota-Lima, G.N., Matos-Rodrigues, G.E., Martins, R.A.P., Mattox, G.M.T., and Schneider, P.N. (2017). Eye development in the four-eyed fish Anableps anableps: cranial and retinal adaptations to simultaneous aerial and aquatic vision. Proc. Biol. Sci. *284*, 20170157.

Perron, M., Kanekar, S., Vetter, M.L., and Harris, W.A. (1998). The genetic sequence of retinal development in the ciliary margin of the Xenopus eye. Developmental Biology *199*, 185–200.

Pertseva, M.N., and Shpakov, A.O. (2002). Conservatism of the insulin signaling system in evolution of invertebrate and vertebrate animals. Journal of Evolutionary Biochemistry and Physiology *38*, 547–561.

Peterson, C., Carney, G.E., Taylor, B.J., and White, K. (2002). reaper is required for neuroblast apoptosis during Drosophila development. Development *129*, 1467–1476.

Pérez Saturnino, A., Lust, K., and Wittbrodt, J. (2018). Notch signalling patterns retinal composition by regulating atoh7 during post-embryonic growth. Development (Cambridge, England) *145*, dev169698.

Pittendrigh, C.S. (1993). Temporal organization: reflections of a Darwinian clock-watcher. Annu. Rev. Physiol. *55*, 16–54.

Pozios, K.C., Ding, J., Degger, B., Upton, Z., and Duan, C. (2001). IGFs stimulate zebrafish cell proliferation by activating MAP kinase and PI3-kinase-signaling pathways. American Journal of Physiology Regulatory, Integrative and Comparative Physiology *280*, R1230–R1239.

Puche, J.E., and Castilla-Cortázar, I. (2012). Human conditions of insulin-like growth factor-I (IGF-I) deficiency. Journal of Translational Medicine *10*, 224–253.

Purcell, M.K., Smith, K.D., Hood, L., Winton, J.R., and Roach, J.C. (2006). Conservation of Toll-Like Receptor Signaling Pathways in Teleost Fish. Comparative Biochemistry and Physiology Part D: Genomics and Proteomics *1*, 77–88.

Radaelli, G., Domeneghini, C., Arrighi, S., Bosi, G., Patruno, M., and Funkenstein, B. (2003a). Localization of IGF-I, IGF-I receptor, and IGFBP-2 in developing Umbrina cirrosa (Pisces: Osteichthyes). General and Comparative Endocrinology *130*, 232–244.

Radaelli, G., Patruno, M., Maccatrozzo, L., and Funkenstein, B. (2003b). Expression and cellular localization of insulin-like growth factor-II protein and mRNA in Sparus aurata during development. The Journal of Endocrinology *178*, 285–299.

Rathnasamy, G., Foulds, W.S., Ling, E.-A., and Kaur, C. (2019). Retinal microglia – A key player in healthy and diseased retina. Progress in Neurobiology *173*, 18–40.

Ravi, V., and Venkatesh, B. (2018). The Divergent Genomes of Teleosts. Annu. Rev. Anim. Biosci. *6*, 47–68.

Raymond Johns, P. (1977). Growth of the adult goldfish eye. III: Source of the new retinal cells. J. Comp. Neurol. *176*, 343–357.

Raymond, P.A., and Easter, S.S. (1983). Postembryonic growth of the optic tectum in goldfish. I. Location of germinal cells and numbers of neurons produced. Journal of Neuroscience *3*, 1077–1091.

Raymond, P.A., Easter, S.S., Burnham, J.A., and Powers, M.K. (1983). Postembryonic growth of the optic tectum in goldfish. II. Modulation of cell proliferation by retinal fiber input. Journal of Neuroscience *3*, 1092–1099.

Raymond, P.A., Barthel, L.K., Bernardos, R.L., and Perkowski, J.J. (2006). Molecular characterization of retinal stem cells and their niches in adult zebrafish. BMC Dev Biol *6*, 36–53.

Reinecke, M., Schmid, A., Ermatinger, R., and Loffing-cueni, D. (1997). Insulin-Like Growth Factor I in the Teleost. *138*, 3613–3619.

Reinhardt, R., Centanin, L., Tavhelidse, T., Inoue, D., Wittbrodt, B., Concordet, J.-P., Martinez-Morales, J.-R., and Wittbrodt, J. (2015). Sox2, Tlx, Gli3, and Her9 converge on Rx2 to define retinal stem cells in vivo. Embo J. *34*, 1572–1588.

Riera Romo, M., Pérez-Mart i nez, D., and Castillo Ferrer, C. (2016). Innate immunity in vertebrates: An overview. Immunology *148*, 125–139.

Ritchey, E.R., Zelinka, C.P., Tang, J., Liu, J., and Fischer, A.J. (2012). The combination of IGF1 and FGF2 and the induction of excessive ocular growth and extreme myopia. Experimental Eye Research *99*, 1–16.

Said, El, O. (2016). Characterization of the CCL25 chemokine and its CCR9 receptor in the medaka retina. Universität Heidelberg.

Sarma, Das, S., Chatterjee, K., Dinda, H., Chatterjee, D., and Sarma, Das, J. (2013). Cytomorphological and Cytochemical Identification of Microglia. ISRN Immunology *2013*, 205431.

Schindelin, J., Arganda-Carreras, I., Frise, E., Kaynig, V., Longair, M., Pietzsch, T., Preibisch, S., Rueden, C., Saalfeld, S., Schmid, B., et al. (2012). Fiji: An open-source platform for biological-image analysis. Nat Meth *9*, 676–682.

Schlueter, P.J., Peng, G., Westerfield, M., and Duan, C. (2007a). Insulin-like growth factor signaling regulates zebrafish embryonic growth and development by promoting cell survival and cell cycle progression. Cell Death Differ *14*, 1095–1105.

Schlueter, P.J., Royer, T., Farah, M.H., Laser, B., Chan, S.J., Steiner, D.F., and Duan, C. (2006). Gene duplication and functional divergence of the zebrafish insulin-like growth factor 1 receptors. The FASEB Journal *20*, 1230–1232.

Schlueter, P.J., Sang, X., Duan, C., and Wood, A.W. (2007b). Insulin-like growth factor receptor 1b is required for zebrafish primordial germ cell migration and survival. Developmental Biology *305*, 377–387.

Sehgal, A., Donaldson, D.S., Pridans, C., Sauter, K.A., Hume, D.A., and Mabbott, N.A. (2018). The role of CSF1R-dependent macrophages in control of the intestinal stem-cell niche. Nature Communications *9*, 1272–1289.

Sierra, A., Encinas, J.M., Deudero, J.J.P., Chancey, J.H., Enikolopov, G., Overstreet-Wadiche, L.S., Tsirka, S.E., and Maletic-Savatic, M. (2010). Microglia shape adult hippocampal neurogenesis through apoptosis-coupled phagocytosis. Cell Stem Cell *7*, 483–495.

Sokol, C.L., and Luster, A.D. (2015). The chemokine system in innate immunity. Cold Spring Harbor Perspectives in Biology *7*, a016303.

Solozobova, V., and Blattner, C. (2011). p53 in stem cells. World J Biol Chem *2*, 202–214.

Song, H., Wang, D., De Jesus Perez, F., Xie, R., Liu, Z., Chen, C.-C., Yu, M., Yuan, L., Fernald, R.D., and Zhao, S. (2017). Rhythmic expressed clock regulates the transcription of proliferating cellular nuclear antigen in teleost retina. Experimental Eye Research *160*, 21–30.

Soteriou, D., and Fuchs, Y. (2018). A matter of life and death: stem cell survival in tissue regeneration and tumour formation. Nat Rev Cancer *18*, 187–201.

Soules, K.A., and Link, B.A. (2005). Morphogenesis of the anterior segment in the zebrafish eye. BMC Dev Biol *5*, 12–28.

Spence, J.R., Mayhew, C.N., Rankin, S.A., Kuhar, M.F., Vallance, J.E., Tolle, K., Hoskins, E.E., Kalinichenko, V.V., Wells, S.I., Zorn, A.M., et al. (2011). Directed differentiation of human pluripotent stem cells into intestinal tissue in vitro. Nature *470*, 105–109.

Spivakov, M., Auer, T.O., Peravali, R., Dunham, I., Dolle, D., Fujiyama, A., Toyoda, A., Aizu, T., Minakuchi, Y., Loosli, F., et al. (2014). Genomic and Phenotypic Characterization of a Wild Medaka Population: Towards the Establishment of an Isogenic Population Genetic Resource in Fish. G3: Genes, Genomes, Genetics *4*, 433–445.

Stemmer, M., Thumberger, T., del Sol Keyer, M., Wittbrodt, J., and Mateo, J.L. (2015). CCTop: An Intuitive, Flexible and Reliable CRISPR/Cas9 Target Prediction Tool. PLoS ONE *10*, e0124633.

Storer, N.Y., White, R.M., Uong, A., Price, E., Nielsen, G.P., Langenau, D.M., and Zon, L.I. (2013). Zebrafish rhabdomyosarcoma reflects the developmental stage of oncogene expression during myogenesis. Development *140*, 3040–3050.

Straznicky, K., and Gaze, R.M. (1971). The growth of the retina in Xenopus laevis: an autoradiographic study. Journal of Embryology and Experimental Morphology *26*, 67–79.

Sugiyama, T., Kohara, H., Noda, M., and Nagasawa, T. (2006). Maintenance of the Hematopoietic Stem Cell Pool by CXCL12-CXCR4 Chemokine Signaling in Bone Marrow Stromal Cell Niches. Immunity *25*, 977–988.

Sutter, N.B., Bustamante, C.D., Chase, K., Gray, M.M., Zhao, K., Zhu, L., Padhukasahasram, B., Karlins, E., Davis, S., Jones, P.G., et al. (2007). A Single IGF1 Allele Is a Major Determinant of Small Size in Dogs. Science *316*, 112–115.

Svensson, M., and Agace, W.W. (2006). Role of CCL25/CCR9 in immune homeostasis and disease. Expert Review of Clinical Immunology *2*, 759–773.

Tropepe, V., Coles, B.L.K., Chiasson, B.J., Horsford, D.J., Elia, A.J., McInnes, R.R., and van der Kooy, D. (2000). Retinal Stem Cells in the Adult Mammalian Eye. Science *287*, 2032–2036.

Tsingos, E., Höckendorf, B., Sütterlin, T., Kirchmaier, S., Grabe, N., Centanin, L., and Wittbrodt, J. (2019). Retinal stem cells modulate proliferative parameters to coordinate post-embryonic morphogenesis in the eye of fish. eLife *8*, 3470.

Turner, D.L., Snyder, E.Y., and Cepko, C.L. (1990). Lineage-independent determination of cell type in the embryonic mouse retina. Neuron *4*, 833–845.

van der Heijden, M., Zimberlin, C.D., Nicholson, A.M., Colak, S., Kemp, R., Meijer, S.L., Medema, J.P., Greten, F.R., Jansen, M., Winton, D.J., et al. (2016). Bcl-2 is a critical mediator of intestinal transformation. Nature Communications *7*, 10916.

Vicari, A.P., Figueroa, D.J., Hedrick, J.A., Foster, J.S., Singh, K.P., Menon, S., Copeland, N.G., Gilbert, D.J., Jenkins, N.A., Bacon, K.B., et al. (1997). TECK: A novel CC chemokine specifically expressed by thymic dendritic cells and potentially involved in T cell development. Immunity *7*, 291–301.

Villani, A., Benjaminsen, J., Moritz, C., Henke, K., Hartmann, J., Norlin, N., Richter, K., Schieber, N.L., Franke, T., Schwab, Y., et al. (2019). Clearance by Microglia Depends on Packaging of Phagosomes into a Unique Cellular Compartment. Developmental Cell *49*, 77–88.e77.

Vincent, A.M., and Feldman, E.L. (2002). Control of cell survival by IGF signaling pathways. Growth Hormone & IGF Research *12*, 193–197.

Volff, J.-N. (2005). Genome evolution and biodiversity in teleost fish. Heredity *94*, 280–294.

Wagner, H.J., Fröhlich, E., Negishi, K., and Collin, S.P. (1998). The eyes of deep-sea fish. II: Functional morphology of the retina. Progress in Retinal and Eye Research *17*, 637–685.

Wan, J., Zhao, X.-F., Vojtek, A., and Goldman, D. (2014). Retinal Injury, Growth Factors, and Cytokines Converge on β-Catenin and pStat3 Signaling to Stimulate Retina Regeneration. Cell Reports *9*, 285–297.

Wan, Y., Almeida, A.D., Rulands, S., Chalour, N., Muresan, L., Wu, Y., Simons, B.D., He, J., and Harris, W. (2016). The ciliary marginal zone of the zebrafish retina: clonal and time-lapse analysis of a continuously growing tissue. Development (Cambridge, England) *143*, 1099–1107.

Wang, D.-S., Jiao, B., Hu, C., Huang, X., Liu, Z., and Cheng, C.H.K. (2008). Discovery of a gonad-specific IGF subtype in teleost. Biochemical and Biophysical Research Communications *367*, 336–341.

Wang, L., Schulz, T.C., Sherrer, E.S., Dauphin, D.S., Shin, S., Nelson, A.M., Ware, C.B., Zhan, M., Song, C.-Z., Chen, X., et al. (2007). Self-renewal of human embryonic stem cells requires insulin-like growth factor-1 receptor and ERBB2 receptor signaling. Blood *110*, 4111–4119.

Wang, S., Wang, X., Wu, Y., and Han, C. (2015). IGF-1R Signaling Is Essential for the Proliferation of Cultured Mouse Spermatogonial Stem Cells by Promoting the G2/M Progression of the Cell Cycle. Stem Cells and Development *24*, 471–483.

Wetts, R., and Fraser, S. (1988). Multipotent precursors can give rise to all major cell types of the frog retina. Science *239*, 1142–1145.

White, D.T., Sengupta, S., Saxena, M.T., Xu, Q., Hanes, J., Ding, D., Ji, H., and Mumm, J.S. (2017). Immunomodulation-accelerated neuronal regeneration following selective rod photoreceptor cell ablation in the zebrafish retina. Proceedings of the National Academy of Sciences *114*, E3719–E3728.

White, K., Grether, M., Abrams, J., Young, L., Farrell, K., and Steller, H. (1994). Genetic control of programmed cell death in Drosophila. Science *264*, 677–683.

Wittbrodt, J., Shima, A., and Schartl, M. (2002). Medaka - a model organism from the far East. Nat Rev Genet *3*, 53–64.

Wong, L.L., and Rapaport, D.H. (2009). Defining retinal progenitor cell competence in Xenopus laevis by clonal analysis. Development *136*, 1707–1715.

Wood, A.W., Duan, C., and Bern, H.A. (2005). Insulin-Like Growth Factor Signaling in Fish. International Review of Cytology *243*, 215–285.

Wurbel, M.-A., Malissen, M., Guy-Grand, D., Malissen, B., and Campbell, J.J. (2007). Impaired Accumulation of Antigen-Specific CD8 Lymphocytes in Chemokine CCL25-Deficient Intestinal Epithelium and Lamina Propria. J Immunol *178*, 7598–7606.

Wurbel, M.-A., Nussenzweig, M.C., Richelme, M., Carrier, A., Malissen, B., Malissen, M., Guy-Grand, D., and Mettre, E. (2001). Mice lacking the CCR9 CC-chemokine receptor show a mild impairment of early T- and B-cell development and a reduction in T-cell receptor γδ+ gut intraepithelial lymphocytes. Blood *98*, 2626–2632.

Xue, X.Y., and Harris, W.A. (2012). Using myc genes to search for stem cells in the ciliary margin of the Xenopus retina. Devel Neurobio *72*, 475–490.

Zaballos, Á., Gutiérrez, J., Varona, R., Ardav i n, C., and Márquez, G. (1999). Cutting Edge: Identification of the Orphan Chemokine Receptor GPR-9-6 as CCR9, the Receptor for the Chemokine TECK. The Journal of Immunology *162*, 5671LP–5675.

Zapata, A. (1979). Ultrastructural study of the teleost fish kidney. Developmental and Comparative Immunology *3*, 55–65.

Zapata, A., and Amemiya, C.T. (2000). Phylogeny of Lower Vertebrates and Their Immunological Structures. In Origin and Evolution of the Vertebrate Immune System. Current Topics in Microbiology and Immunology, Vol 248, L. Du Pasquier, and G.W. Litman, eds. (Springer, Berlin, Heidelberg), pp. 67–107.

Ziegler, A.N., Levison, S.W., and Wood, T.L. (2015). Insulin and IGF receptor signalling in neural-stem-cell homeostasis. Nature Reviews Endocrinology *11*, 161–170.

Zlotnik, A., and Yoshie, O. (2012). The Chemokine Superfamily Revisited. Immunity *36*, 705–716.

Zou, S., Kamei, H., Modi, Z., and Duan, C. (2009). Zebrafish IGF genes: gene duplication, conservation and divergence, and novel roles in midline and notochord development. PLoS ONE *4*, e7026.

Zygar, C.A., Colbert, S., Yang, D., and Fernald, R.D. (2005). IGF-1 produced by cone photoreceptors regulates rod progenitor proliferation in the teleost retina. Developmental Brain Research *154*, 91–100.

Declaration

Herewith I declare that I prepared the PhD Thesis "Mechanisms of growth control in the postembryonic medaka retina" on my own and with no other sources and aids than quoted.

Heidelberg, 2019

List of Figures

List of Tables